USE OF CFRP OVERLAYS TO REPAIR FATIGUE DAMAGE IN STEEL BRIDGE GIRDERS AND COMPONENTS

BY

Regan E. Gangel

Submitted to the graduate degree program in Civil, Architectural, and Environmental Engineering and the Graduate Faculty of the University of Kansas in partial fulfillment of the requirements for the degree of Master's of Science.

Committee members:

____
Co- Chairperson Dr. Caroline Bennett

____
Co- Chairperson Dr. Adolfo Matamoros

____
Dr. Stanley Rolfe

____
Dr. Ron Barrett- Gonzalez

Date defended: January 9, 2011

The Thesis Committee for Regan E. Gangel
certifies that this is the approved Version of the following thesis:

USE OF CFRP OVERLAYS TO REPAIR FATIGUE DAMAGE IN STEEL BRIDGE GIRDERS AND COMPONENTS

____
Co- Chairperson Dr. Caroline Bennett

____
Co- Chairperson Dr. Adolfo Matamoros

____
Dr. Stanley Rolfe

____
Dr. Ron Barrett- Gonzalez

Date approved: ________________

EXECUTIVE SUMMARY

Fatigue damage in steel girder bridges built prior to the mid-1980s is common due to distortion-induced fatigue. Different repair techniques have been developed and implemented to retrofit bridges of this era with existing fatigue damage. An experimental and analytical evaluation was conducted on the use of Carbon Fiber Reinforced Polymer (CFRP) as an alternative repair technique. Experimental testing was conducted on component specimens tested under pure tension loading conditions. Comparisons between specimens were based on the axial stiffness of the repaired specimen, a method commonly used in the Aerospace Engineering field. The analytical evaluation comprised of a suite of Finite Element models. A simplified steel girder section was modeled with two main objectives. The first was to evaluate the effect of bending and cross-frame forces on fatigue-crack location. The second was to compare the use of CFRP overlays as a repair technique to two techniques currently being used; drilling of crack-stop holes and attachment of steel splice plates. The intention of this research was to test the use of CFRP as a repair technique and validate its use for further testing more applicable to actual field conditions.

This thesis is organized into two primary parts. The first, entitled "Use of CFRP Overlays to Repair Fatigue Damage in Steel Plates under Tension Loading" details the experimental testing on component specimens. The second, entitled "Evaluation of Fatigue Damage Repair Measures in Welded Steel Plate Bridge Girders" details the analytical evaluation of different repair techniques and loading conditions. Procedural appendices have also been included to aid in future research in involving the testing of CFRP overlays. These appendices include the manufacture and attachment procedures of CFRP developed at the University of Kansas, an operational manual of sorts for the two testing machines used to complete Part 1 of this study, and the manufacture and attachment procedure of clamps used to control de-bonding of the CFRP overlays.

ACKNOWLEDGEMENTS

It is with great admiration that I acknowledge those who contributed to the successful completion of this study and thesis. Neither would have been possible without the guidance, support, and expertise of Drs. Caroline Bennett, Adolfo Matamoros, Stanley Rolfe, and Ron Barrett. In addition, I would like to thank my colleagues for their instruction and assistance, especially Amanda Hartman, Temple Richardson, Gary Simmons, Nathan Hickey, and Say Hak Bun. I would also like to thank Jim Weaver for his valuable assistance during the experimental testing of this study. This thesis was also made possible with the support of the University of Kansas Transportation Research Institute (KU TRI) and Transportation Pooled Fund Study TPF-T(189) funded by the department of transportation of the following states: California, Illinois, Iowa, Kansas, Louisiana, New Jersey, New York, Oregon, Pennsylvania, Tennessee, Washington State, Wisconsin, and Wyoming. Finally, I would like to thank my family for their encouragement, patience, and support.

TABLE OF CONTENTS

PART 1: USE OF CFRP OVERLAYS TO REPAIR FATIGUE DAMAGE IN STEEL PLATES UNDER TENSION LOADING

PART 2: EVALUATION OF FATIGUE DAMAGE REPAIR MEASURES IN WELDED STEEL PLATE BRIDGE GIRDERS

LIST OF TABLES

PART 1: USE OF CFRP OVERLAYS TO REPAIR FATIGUE DAMAGE IN STEEL PLATES UNDER TENSION LOADING

PART 2: EVALUATION OF FATIGUE DAMAGE REPAIR MEASURES IN WELDED STEEL PLATE BRIDGE GIRDERS

LIST OF FIGURES

PART 1: USE OF CFRP OVERLAYS TO REPAIR FATIGUE DAMAGE IN STEEL PLATES UNDER TENSION LOADING

PART 2: EVALUATION OF FATIGUE DAMAGE REPAIR MEASURES IN WELDED STEEL PLATE BRIDGE GIRDERS

Appendix A: Manufacture and Attachment of CFRP Doublers

Appendix B: Procedural Documentation for MTS Testing Machine

Appendix C: Procedural Documentation for INSTRON Testing Machine

Appendix D: A Detailed Look at Web Gap Stresses

List of Acronyms and Symbols

Acronym/Symbol	Description
AASHTO	American Association of State Highway and Traffic Officials
ASTM	American Society for Testing and Materials
CFRP	Carbon Fiber Reinforced Polymer
CSH	Crack-Stop Hole
FE	Finite Element
FRP	Fiber Reinforced Polymer
HSS	Hot Spot Stress
KDOT	Kansas Department of Transportation
KU TRI	University of Kansas Transportation Research Institute
LRFD	Load and Resistance Factor Design
S-N	Stress-Number of cycles
A	Material property constant (Barsom and Rolfe 1999, tabled), MPa^3 (ksi^3)
A_{st}	Net cross section of steel less area of drilled hole, mm^2 ($in.^2$)
a_{avg}	Average crack length, mm (in.)
b	Finite width of plate, mm (in.)
da	Change in crack length, mm (in.)
dN	Change in number of cycles, (~)
E_{FRP}	Modulus of elasticity of FRP, GPa (ksi)
E_s	Modulus of elasticity of steel, GPa (ksi)
$F_{actuator}$	Force from actuator applied during experimental testing, kN (kip)
ΔK	Stress intensity factor range, MPa $mm^{-1/2}$ (ksi $in^{-1/2}$)
K	Stiffness, kN/mm (kip/in)
K_{max}	Maximum stiffness, kN/mm (kip/in)
m	Material property constant (Barsom and Rolfe 1999, tabled), (~)
N	Number of cycles, (~)
Q	Flaw-shape parameter, (~)
SR	Ratio of axial stiffness of FRP to that of steel, Stiffness Ratio
R	Radius of drilled hole, mm (in.)
t_{FRP}	Thickness of FRP, mm (in.)
t_S	Thickness of steel, mm (in.)
δL	Change in load applied by actuator, kN (kip)
δP	Change in position of actuator, mm (in.)
$\Delta\sigma$	Stress range, MPa (ksi)
$\Delta\sigma_{st}$	Testing stress range based on nominal steel cross-section, MPa (ksi)
P	Notch tip radius, mm (in.)
σ_{ys}	Yield strength, MPa (ksi)

PART 1:

USE OF CFRP OVERLAYS TO REPAIR FATIGUE DAMAGE IN STEEL PLATES UNDER TENSION LOADING

Use of CFRP Overlays to Repair Fatigue Damage in Steel Plates under Tension Loading

Fatih Alemdar[1]

Regan Gangel[2]

Adolfo Matamoros[3], A.M. ASCE

Caroline Bennett[4], A.M. ASCE

Ron Barrett-Gonzalez[5]

Stan Rolfe[6], P.E., Hon. M. ASCE

Abstract

Fiber reinforced polymer (FRP) overlays have been successfully used in the aerospace industry to repair fatigue damage in aluminum plate. With this success there is potential for use of similar FRP overlays to repair fatigue damage in aging steel bridge structures. This study investigates the effectiveness of repairing fatigue damage in steel plate with adhesively bonded carbon fiber reinforced polymer (CFRP) overlays. A total of 15 steel plate specimens with pre-existing fatigue cracks were repaired with varying thicknesses of CFRP overlays to evaluate the effect of the ratio of axial stiffness of the composite to that of the underlying steel, *SR*, on increased fatigue life and decreased applied stress. The results showed that increasing the axial stiffness ratio from 0 to 0.4 could increase the fatigue life by a factor of 10 for the most extreme conditions, and with an optimal axial stiffness ratio infinite fatigue life may be reached. Fatigue life of the steel specimens in this study was found to be dependent on both axial stiffness and applied stress range. Results from Finite Element Analyses validated the use of axial stiffness as a design parameter and correlated to the experimental results discussed.

[1] Fatih Alemdar, Graduate Research Assistant, University of Kansas, 1530 W. 15th St., Lawrence KS, 66045
[2] Regan Gangel, Graduate Research Assistant, University of Kansas, 1530 W. 15th St., Lawrence KS, 66045
[3] Adolfo Matamoros, PhD, Associate Professor, University of Kansas, 1530 W. 15th St., Lawrence KS, 66045
[4] Caroline Bennett, PhD, Assistant Professor, University of Kansas, 1530 W. 15th St., Lawrence KS, 66045
[5] Ron Barrett, PhD, Associate Professor, University of Kansas, 1530 W. 15th St., Lawrence KS, 66045
[6] Stan Rolfe, P.E., PhD, A.P. Learned Professor, University of Kansas, 1530 W. 15th St., Lawrence KS, 66045

Introduction

A significant number of aging steel bridge structures experience structural problems due to fatigue cracks. Currently available methods used to repair fatigue cracks in steel structures include drilling of crack-stop holes, crack grinding and (re-)welding, ultrasonic impact treatment at weld toes, and/or attachment of steel splice plates.

Drilling crack-stop holes removes the sharp end of a crack and reduces the localized stress that drives crack propagation (Barsom and Rolfe 1999). However, fatigue cracks in steel bridge structures are most often found near complicated connection geometries and the diameter of a crack-stop hole needed to arrest further crack propagation is usually impossible or impractical to drill. This leads to the drilling of undersized crack-stop holes, re-initiation of the fatigue crack, and continued damage to the structure (Roddis and Zhao 2001). Other repair techniques have similar drawbacks. Grinding the fatigue crack and re-welding the area introduces another fatigue sensitive detail and is unlikely to be a long-term fix (Dexter 2004).

One repair technique that has been used by the Kansas Department of Transportation (KDOT) in cases where fatigue cracks have propagated significantly into girder webs is to retrofit the web with a full-depth bolted steel splice at the location of cracking. The intent of the splice is to provide an alternate load path around the damaged web, and it is designed for the full shear demand at that web location. Attaching full-depth splice plates to the damaged web does reduce the stress in the fatigue sensitive area (Roddis and Zhao 2001), however, there is potential that with a full-depth steel splice plate covering the damaged region of a girder any additional crack propagation may be hidden from view and go unnoticed. In a worst-case scenario, cracking could propagate into a tension flange and result in loss of load-carrying capacity for that girder. For this worst-case scenario, there is significant cost associated with implementing this repair technique.

A more localized repair utilizing CFRP materials could result in a more cost-effective and inspectable repair. One potential embodiment of this type of repair is a pair of CFRP overlay elements, one bonded to each face of the steel web over the crack with an epoxy resin layer. The CFRP overlays would not need to extend the full-depth of the web; instead, they could “patch” the region over the crack. However, before the potential of any such specific repair geometry can be effectively investigated, fundamental questions must be answered concerning the effectiveness of CFRP overlays in extending the fatigue life of steel plate loaded in tension with a pre-existing fatigue crack. The aim of the research described in this article is to provide fundamental information concerning basic proportions (thicknesses) of CFRP overlays relative to the steel to which they are bonded to effectively slow or halt fatigue crack propagation in the steel under various stress demands. The effect of bond thickness and modulus of elasticity of CFRP on the reduction in stress at critical locations was also evaluated.

Background

A significant amount of research on the use of composite materials has been carried out in the field of aerospace engineering to address fatigue problems in the fuselages of airplanes (Mall and Conley 2009; Umamaheswar and Singh 1999; Schubbe and Mall 1999; Naboulsi and Mall 1996; Lee and Lee 2004; Liu, Xiao, et al. 2009). The most recent research performed on this topic in the aerospace field has focused on the use of fiber reinforced polymer (FRP) patches to repair fatigue damage in aluminum plates. These studies have shown that FRP plates can reduce the stress demand in a vulnerable element or connection significantly if properly proportioned and bonded to the steel substrate. An experimental study by Mall and Conley (2009) reported that bonding a boron fiber reinforced polymer overlay to only one side of an aluminum specimen increased the fatigue crack propagation life between four and 10 times with respect to the propagation life of an untreated specimen. Wang et al. (2002) also found an increase in fatigue crack propagation life on the order of 10 times in aluminum plates repaired with FRP patches.

One of the most important concerns when implementing this repair method is to achieve adequate bond between the steel and the composite overlay. Voids or imperfections in the layer of resin used to attach the composite overlay to the underlying metal can lead to the formation and propagation of fatigue cracks within the resin. This can eventually cause debonding of the overlay, rendering the repair ineffective.

In the aerospace field a commonly used parameter for proportioning composite patches for the purpose of repairing fatigue damage is the ratio of axial stiffness of the composite patch to the axial stiffness of the plate (Sabelkin et al. 2006). For steel substrate, the ratio is defined as:

$$SR = E_{FRP}\, t_{FRP} / E_s\, t_s \qquad (1)$$

where SR is the stiffness ratio, E_{FRP} is the modulus of elasticity of the FRP, t_{FRP} is the thickness of the FRP patch, E_s is the modulus of the steel, and t_s is the thickness of the steel plate. The SR

parameter is used to determine thickness of FRP needed to repair fatigue-damaged steel plates by assuming that the driving force is redistributed in proportion to the relative axial stiffness of the two materials. For aerospace structures the recommended stiffness ratio is 1.0 (Schubbe et al. 2009). Schubbe et al. (1999) performed experimental tests on aluminum plates that were repaired with a bonded composite patch and found that as the stiffness ratio between the repair and steel plate increased, so did the fatigue life of both thin and thick plates. Stiffness ratios of 1.0 and 1.3 were evaluated in that study.

Although the use of CFRP is not widely implemented in steel structures yet, several studies have investigated their use to repair fatigue-related damage. Tavakkolizadeh and Saadatmanesh (2003) studied the effectiveness of unidirectional CFRP sheets to improve the fatigue strength of S127x4.5 steel girders with pre-existing notch cracks. The authors reported that the fatigue-crack propagation life of the specimens with CFRP sheets was extended by a factor of approximately three compared with that of control specimens. Liu, Al-Mahaidi, et al. (2009) studied the tensile fatigue behavior of notched steel plates strengthened with single-ply CFRP patches. Results showed that single-sided repair extended the fatigue-crack propagation life of the specimen by a factor ranging between 2.2 and 2.7, whereas a double sided repair extended the fatigue-crack propagation life by a factor ranging between 4.7 and 7.9. Roy et al. (2009) performed a study using the same type of materials and procedure used by Liu et al. (2009), but focused the study on the single sided repair because of the inherent asymmetry. Roy et al. (2009) reported that the fatigue-crack propagation life was increased by a factor of 2.2 compared with that of the control specimens. Both Liu et al. (2009) and Roy et al. (2009) showed similar increases in fatigue-crack propagation life of steel plates repaired with single-sided CFRP patches.

Kaan et al. (2012) studied the behavior of un-cracked plate-coverplate connections repaired with CFRP overlays. Results showed that specimen behavior, according to the AASHTO design specifications, could be improved from a fatigue design Category E’ detail to fatigue design Category B’ or B detail. In this study, increased fatigue crack initiation life was a direct result of maintaining adequate bond.

Analytical modeling of CFRP repairs using the Finite Element (FE) method is also an important technique when developing efficient retrofit schemes for steel structures. Researchers (Liu, Xiao, et al. 2009; Lee and Lee 2004) have shown good agreement between the change in stress demand estimated using FE models and experimentally observed changes in fatigue-crack propagation life. In FE models that include a layer of resin between the CFRP overlay and the underlying metal, the potential for debonding can be assessed by comparing the stress demand in the resin with a limiting value. This approach was also adopted in the FE simulations conducted in this study.

Objective and Scope

The overall objective of the research described in this paper was to determine the effectiveness of carbon fiber reinforced polymer (CFRP) overlays to repair existing fatigue damage in steel plate tested under cyclic tensile load. This overall objective was addressed in four parts through a scope of study that included both experimental and analytical components. First, fifteen steel plate specimens were repaired with varying thicknesses of CFRP overlays to evaluate the effect of the axial stiffness ratio, *SR*, on fatigue crack propagation life and effective stress range. Second, relationships between the stiffness of the CFRP overlays and steel substrate were identified such that future CFRP repair techniques can be proportioned to effectively slow or halt fatigue crack propagation in the steel substrate. Third, the effect of bond layer thickness and CFRP overlay thickness on the reduction in Hot Spot Stress (HSS) was evaluated using FE models. Finally, the effect of axial stiffness determined using the FE method was compared to its effect determined from experimental results. FE simulations and experimental testing were performed on identical specimens with dimensions as shown in Fig 1.

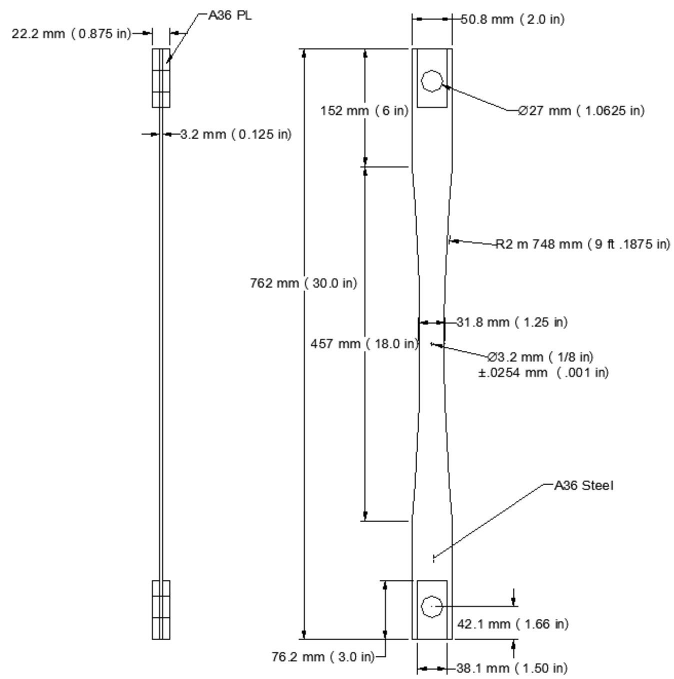

(a)

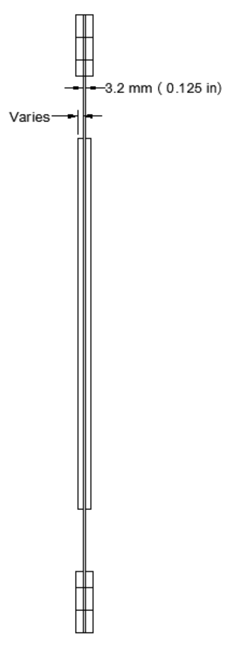

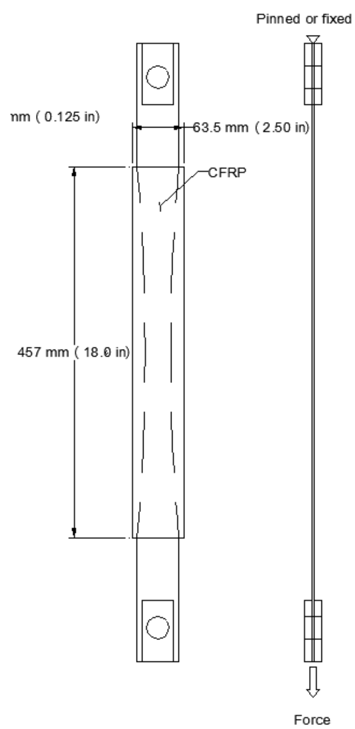

(b) **(c)**

Figure 1 : Tension specimen: (a) 3 mm ($^{1}/_{8}$ in.) bare steel (b) specimen with CFRP overlay attached (c) boundary and loading conditions imposed on the FE model and experimental test.

Finite Element Simulations

When considering the use of CFRP overlays as a fatigue repair technique on steel plate, there are numerous parameters that could affect the success of the repair. A parametric study was completed to investigate the decrease in HSS of specimens repaired with varying modulus of elasticity of the CFRP and thickness of the CFRP, both which alter the stiffness ratio of the system. The effects of bond layer properties on peel and shear stresses were also evaluated.

Modeling Methodology

Finite element simulations of the tensile specimens tested during the experimental program (Fig. 1) were carried out using the commercially-available finite element analysis software ABAQUS version 6.8.2 (Simulia 2009). A base FE model consisted of the steel specimen with a modulus of elasticity of 200 GPa (29,000 ksi). It was repaired with a 6 mm ($^{1}/_{4}$ in.) thick, 458 mm (18 in.) long CFRP overlay with a modulus of elasticity of 83 GPa (12,000 ksi). This CFRP overlay was attached to each side of the specimen with a 0.6 mm (25 mil) thick resin interface layer with a modulus of elasticity of 2 GPa (300 ksi). Only one parameter was altered from the base model within each parametric model.

FE models were developed using linear elastic material models and meshes were assembled using 8-node brick elements. The mesh density was defined such that elements would be 0.30 mm (0.01 in.) within a region 51 mm (2.0 in.) from the center hole, and 2.5 mm (0.1 in.) in all other parts of the specimen. Interfaces between the steel, resin, and composite parts of the model were defined using tie constraints. Motion was restrained at one end of the model while the other end was free to move only in the vertical direction (Fig. 1c). Two 10.5 kN (2.35 kip) concentrated loads were applied in the vertical direction at the unrestrained end, one on each face of the model. This load corresponds to a nominal testing stress range of 221 MPa (32 ksi), based upon the steel net section area.

Comparisons were performed on the basis of the Hot Spot Stress (HSS). In this paper, HSS was defined as the stress at a distance half the thickness of the steel plate away from the point of peak stress, which occurred at the edge of the hole (Marquis and Kaehoenen 1995). Hot Spot Stress analysis was used as an indicator of stress range, and consequently, as a measure of the effectiveness of various composite overlay configurations. This technique has been used in other finite element modeling investigations aimed at examping fatigue performance and behavior (Hassel 2011; Kaan et al. 2012; Hartman et al 2010).

Effect of the Modulus of Elasticity of the CFRP

From the base model, six models were developed to investigate the effect of the modulus of elasticity of the CFRP on stress imposed on the steel specimen. The modulus of elasticity of the CFRP, which was varied between 27 GPa (3,860 ksi) and 138 GPa (20,000 ksi), in increments of 28 GPa (4,000 ksi). The effect of CFRP modulus of elasticity on Hot Spot Stress in the steel specimen is shown in Fig 2. The point corresponding to a modulus of elasticity of zero represents results from the analysis of the specimen without an overlay. The relationship between the modulus of elasticity of the CFRP overlay and HSS was parabolic in nature and inversely proportional, indicating that there was a significant advantage associated with using an overlay, even if the modulus of elasticity of the composite material was relatively low. As Fig. 2 shows, HSS dropped by 58% with the introduction of an overlay with a very low modulus (26,600 MPa, 3,860 ksi) when compared with the unreinforced case. This data also shows that increasing the modulus of elasticity of the CFRP material exhibits diminishing returns, which is important to consider when determining optimal configuration of the overlay. Increasing the modulus of elasticity of the CFRP by a factor of five, from 26,000 MPa (3,860 ksi) to 138,000 MPa (20,000 ksi), led to a reduction in HSS by a factor of approximately three. If infinite fatigue or propagation life can be achieved with a relatively inexpensive overlay, there is no economic incentive for using stiffer, and often much more expensive, fibers.

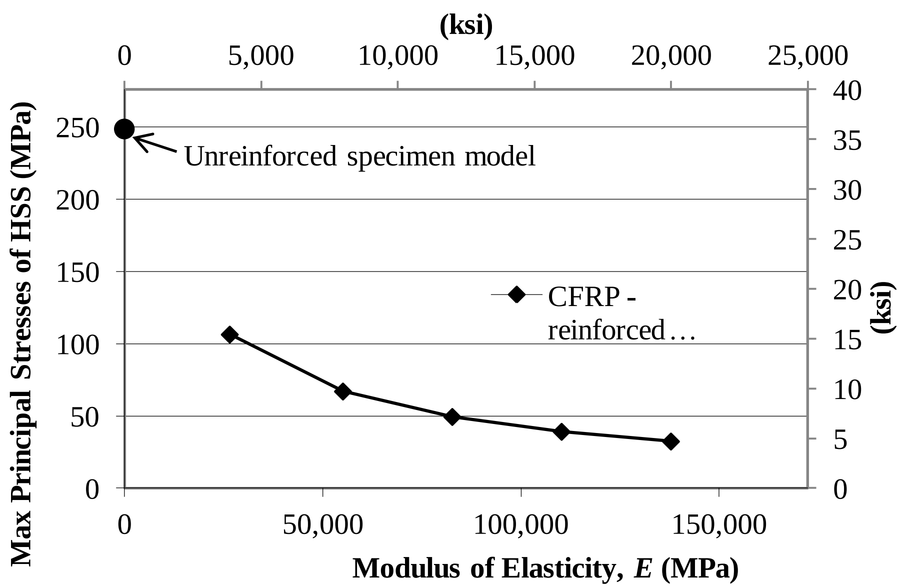

Figure 2 : Effect of stiffness of the CFRP overlays on maximum principal Hot Spot Stresses in the steel specimen

Effect of the Thickness of the CFRP Overlay

The effect of the CFRP overlay thickness on HSS was evaluated using five FE models. The CFRP overlay thickness on each side of the steel plate was varied using values of 1.6, 2.4, 3.2, 6.4, and 12.7 mm (1/16, 3/32, 1/8, 1/4, and 1/2 in.). HSS results are presented in Fig. 3. The relationship between the CFRP overlay thickness and the maximum principal HSS was found to be inversely proportional and parabolic. The addition of the thinnest CFRP tested, 1.6 mm (1/16 in.) decreased the maximum principal HSS by a factor of two when compared to an un-reinforced specimen. Similar to the behavior found when the CFRP modulus of elasticity was varied; increasing the thickness of the overlay exhibited diminishing returns, with the largest change in HSS observed between the unreinforced case and the case in which a 1.6-mm (63-mil) thick overlay was utilized.

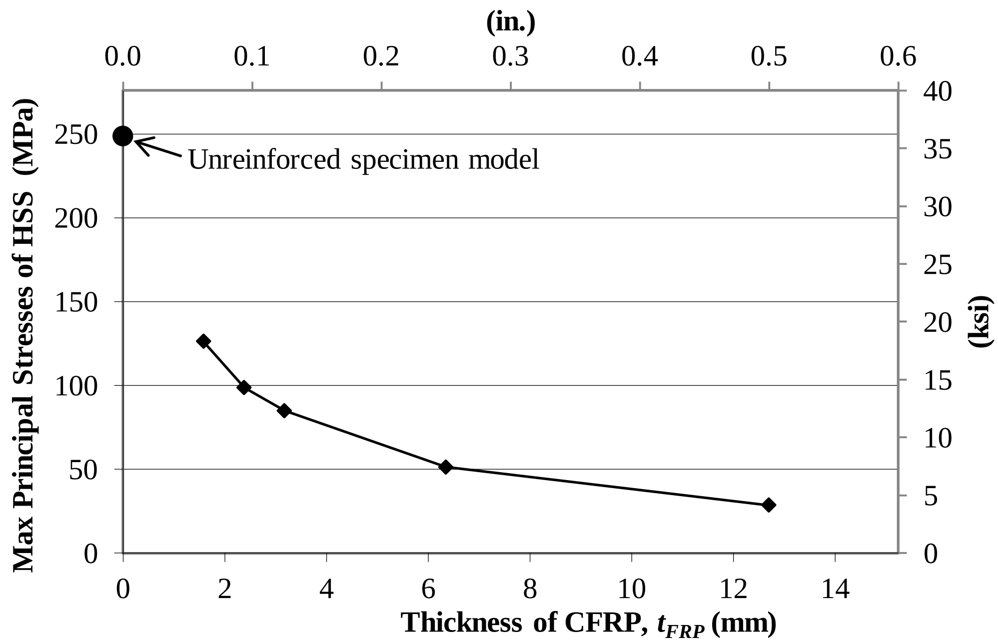

Figure 3 : Effect of CFRP overlay thickness on maximum principal Hot Spot Stresses in the steel specimen

Ratio of Overlay Axial Stiffness to Steel Axial Stiffness

As discussed in the Introduction, one of the design parameters referenced in the literature for proportioning FRP patches is the ratio of axial stiffness of the composite patch to the axial stiffness of the underlying plate (Eq. 1). As Eq. 1 shows, this ratio may be modified by changing the modulus of elasticity of the FRP, thickness of the FRP, or both. The results presented in

Figs. 2 and 3 were used to derive two curves showing the effect of the stiffness ratio *SR* on the maximum principal HSS in the steel substrate (Fig. 4). For each curve, one of the two parameters (modulus of elasticity of the FRP or thickness of the overlay) was varied while maintaining the other constant. All other parameters were equivalent to that of the base model.

The results presented in Fig. 4 show that changing the stiffness ratio, *SR*, by changing the modulus of elasticity of the CFRP had consistent results with changing *SR* by altering overlay thickness. There was a common trend, in that sequential increments in the thickness of the overlay and the modulus of elasticity of the CFRP resulted in similar reductions on the HSS. Therefore, how the axial stiffness parameter was changed did not significantly affect the amount of stress reduction.

What did affect the reduction in HSS was the increase in stiffness ratio. A stiffness ratio of approximately 0.41 decreased the maximum principal HSS by a factor of two when compared to an unreinforced specimen. Increasing the *SR* by a factor of 8 to approximately 3.3 only decreased the maximum principal HSS by a factor of 5. For these specimens modeled with a 221 MPa (32 ksi) testing stress range, a stiffness ratio of 1.0 seems to be optimal, as shown in Fig. 4. Stiffness ratios greater than 1.0 show diminishing returns in HSS reduction.

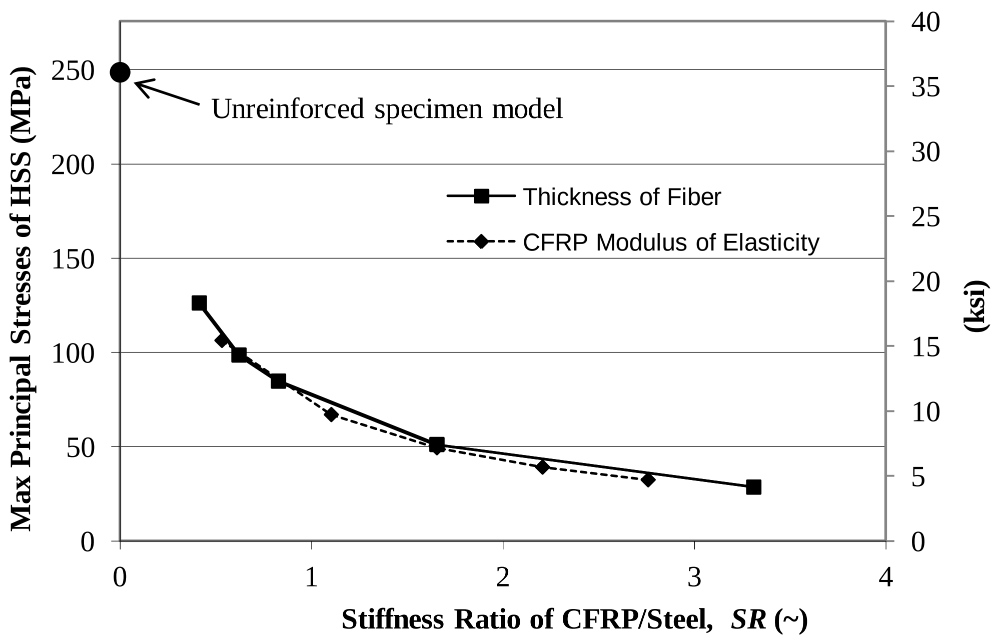

Figure 4 : Effect of stiffness ratio on maximum principal Hot Spot Stress in the steel

Effect of Thickness of Bond Layer

One of the parameters often neglected in FE simulations of retrofit measures with composite overlays is the flexibility inherent to the adhesive resin used to bond the overlay to the metal substrate. In most analyses found in the literature (Sabelkin et al. 2006; Liu, Xiao, et al. 2009; Mall and Conley 2009), it was assumed that the thickness of such a layer was very small, and that there was perfect bond between the composite and the substrate. Explicit modeling of this layer provides an indication of the average shear demand on the resin and the tensile demand on the resin-steel interface, which can be used to gage the potential for debonding. Because the shear and tensile demands on the resin are affected by the thickness of the resin layer, this is an important parameter to consider in terms of fatigue and fatigue crack propagation life.

Five different models were defined to investigate the effect of the thickness of the interface bond layer between the CFRP overlay and the steel substrate. The interface layer thickness was varied from 0.6 mm (20 mils) to 5 mm (200 mils). Results discussed by Alemdar (2011) found that the maximum principal HSS was not affected by the thickness of the interface layer. However, another important design consideration is the effect of the interface layer thickness on the stress demand at the resin layer itself. This is important because maintaining bond between the composite and the steel is critical to the successful performance of the retrofit scheme, and higher stress demands increase the probability of fatigue failure at the interface. Fig. 5 shows the stress demand along the resin layer for a model with a layer thickness of 0.6 mm (20 mil). As Fig. 5 presents, the shear and peel stress (out of plane stress) demands are relatively low along most of the interface. Stress demands are greatest at both ends of the interface, and this is the location considered to be the most susceptible to fatigue failure.

Figure 6 presents the variation of peak shear and peel stresses as a function of the thickness of the resin layer. The results show that increasing the interface layer thickness from 0.6 mm (20 mil) to 5.0 mm (200 mil) caused a reduction in peak shear demand by approximately 66%. Figure 6 also presents that the same increase in the thickness of the interface layer led to a reduction in peak peel stresses by approximately 40%. The trend observed for the peel stress was different from that observed for the shear stress in that the lowest peel stress demand was observed when an interface thickness of 2.5 mm (100 mil) was used, and any further increases in the thickness of the interface layer led to an increase in the peel stress. Figures 5 and 6 show that although the thickness of the interface layer may not be relevant to fatigue-crack propagation life due to the negligible effect on the stress range, it is a very important parameter in terms of the bond performance of the interface layer under cyclic loading.

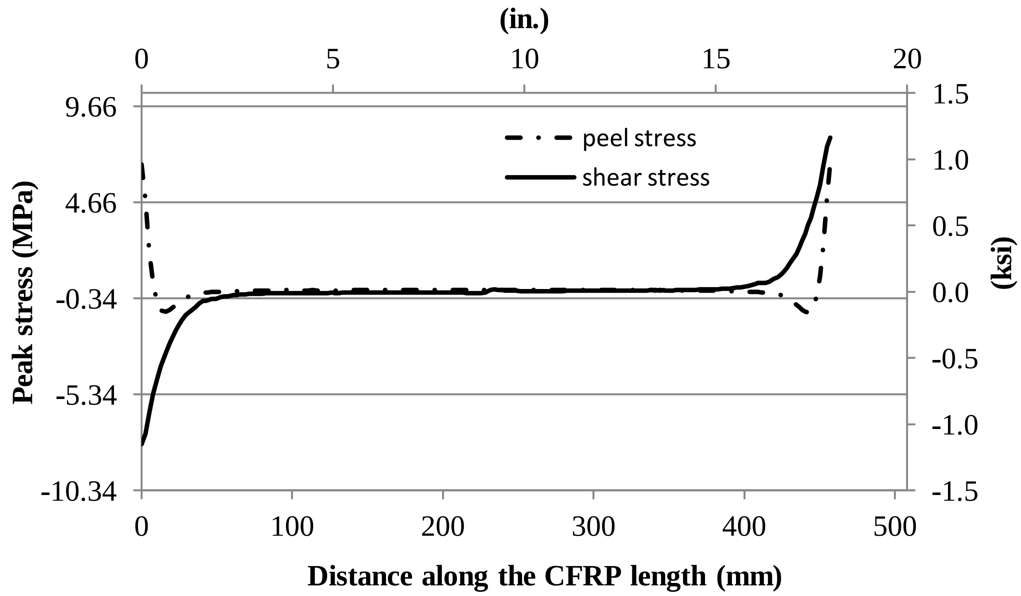

Figure 5: Peak stresses along CFRP overlay on resin layer end of hole

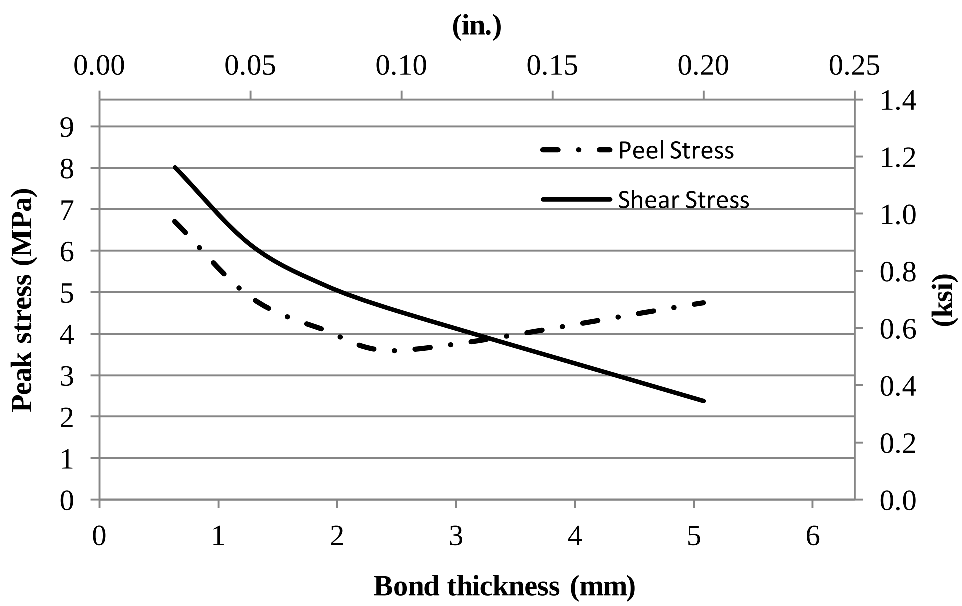

Figure 6: Peak stresses demand on CFRP layer as a function of resin layer thickness

Experimental Program

The primary goal of the experimental program was to evaluate the effect of stiffness ratio on fatigue-crack propagation life of steel specimens with pre-existing fatigue cracks repaired using CFRP overlays under cyclic loading. Fatigue cracks were propagated on each side of the drilled and reamed hole, shown in Fig.1, until either of the cracks reached a length of approximately 7 mm (0.3 in.), the initial crack length. Crack propagation of the initial crack was completed under low and varying stress ranges to control opening of the crack and yielding at the edge of the specimen. Once the initial crack length was reached, each specimen was repaired using CFRP overlays. In total, 15 specimens were tested. The text matrix for the experimental program is summarized in Table 1.

Table 1: Specimen test matrix

Specimen Designation	Specimen Thickness mm (in.)	CFRP Overlay Thickness mm (in.)	Stress Range MPa (ksi)
F15	3 ($^{1}/_{8}$)	1.6 ($^{1}/_{16}$)	263 (38)
F3	3 ($^{1}/_{8}$)	1.6 ($^{1}/_{16}$)	221 (32)
F6	3 ($^{1}/_{8}$)	1.6 ($^{1}/_{16}$)	166 (24)
Pick12	3 ($^{1}/_{8}$)	2.4 ($^{3}/_{32}$)	221 (32)
Pick11	3 ($^{1}/_{8}$)	3.2 ($^{1}/_{8}$)	263 (38)
F14	3 ($^{1}/_{8}$)	3.2 ($^{1}/_{8}$)	221 (32)
F2	3 ($^{1}/_{8}$)	3.2 ($^{1}/_{8}$)	166 (24)
Pick10	3 ($^{1}/_{8}$)	6.4 ($^{1}/_{4}$)	263 (38)
Pick13	3 ($^{1}/_{8}$)	6.4 ($^{1}/_{4}$)	221 (32)
Pick7	3 ($^{1}/_{8}$)	6.4 ($^{1}/_{4}$)	166 (24)
F27	3 ($^{1}/_{8}$)	12.8 ($^{1}/_{2}$)	221 (32)
F4-25	6 ($^{1}/_{4}$)	1.6 ($^{1}/_{16}$)	221 (32)
F4-21	6 ($^{1}/_{4}$)	3.2 ($^{1}/_{8}$)	221 (32)
F4-23	6 ($^{1}/_{4}$)	6.4 ($^{1}/_{4}$)	221 (32)
F4-20	6 ($^{1}/_{4}$)	12.8 ($^{1}/_{2}$)	221 (32)

Of the four parameters in Eq. 1 that could have been varied to alter the stiffness ratio, two were investigated in this study: the thickness of the CFRP overlay and the thickness of the steel plate. Testing was conducted at varying stress ranges, 166 MPa (24 ksi), 221 MPa (32 ksi) and 263 MPa (38 ksi), to evaluate the role this played in determining an optimal stiffness ratio for CFRP overlay repair.

Measured material properties are presented in Table 2. Coupon tests (ASTM 2000) from single-layered specimens showed that the modulus of elasticity of the CFRP was approximately 83 GPa (12,000 ksi). Liu et al. (2009) observed in their experiments that after the second layer of CFRP the strain demand quickly dropped; therefore, the modulus of elasticity of the composite used for the computer simulations was selected to be between measured values for one and three layers. The modulus of elasticity of the 9412 Hysol resin was also measured using coupon tests (Table 2) performed as prescribed by ASTM (2000). The measured modulus of elasticity of the Hysol resin was 2.1 GPa (300 ksi).

Table 2: Measured material properties

Continuous CFRP

No. of Layers in Coupon	No. of Coupons	Avg. Modulus of Elasticity *GPa (ksi)*	Standard Deviation *GPa (ksi)*
1	3	85.8 (12,440)	10.0 (1,450)
3	4	75.3 (10,930)	10.9 (1,580)
5	3	61.7 (8,940)	0.3 (42.0)

9412 Hysol Resin

Coupon Thickness *mm (in.)*	No. of Coupons	Avg. Modulus of Elasticity *GPa (ksi)*	Standard Deviation *GPa (ksi)*
6 (0.25)	6	2.1 (303)	0.2 (25)

Specimen Dimensions

The specimens were fabricated using grade A36 steel and were either 3 mm ($^1/_8$ in.) or 6 mm ($^1/_4$ in.) thick. For specimens with a thickness of 3 mm ($^1/_8$ in.) the measured average yield strength was 319 MPa (46 ksi), and the measured tensile strength was 381 MPa (55 ksi) (Crain 2010). For specimens with a thickness of 6 mm ($^1/_4$ in.) the measured average yield strength was 335 MPa (48 ksi), and the measured tensile strength was 495 MPa (72 ksi) (Crain 2010).

Specimen dimensions for 3 mm ($^1/_8$ in.) thick specimens are shown in Fig. 1. There are three significant dimension changes between the 6 mm ($^1/_4$ in.) thick specimens and the dimensions shown in Fig. 1. First, the width at each end measures 63.5 mm (2.5 in.) instead of 60.8 mm (2.0 in.). Second, the width at the reduced net sections measures 44.5 mm (1.75 in.) instead of 31.8 mm (1.25 in.). Third, the diameter of the drilled and reamed hole is equal to the thickness of the specimen, 6mm ($^1/_4$ in.). Each specimen had a drilled and reamed hole at the center of the specimen with a diameter equal to the thickness. Both sides of the hole had pre-existing fatigue cracks of approximately 7.6 mm (0.3 in) to standardize initial crack length and to decrease testing time. These initial fatigue cracks were created by loading the specimens under repeated cycles at stress ranges varying from 166 MPa (24 ksi) to 263 MPa (38 ksi).

Fabrication of the Multi-Layered CFRP Overlays

The multi-layered CFRP overlays were pre-fabricated and subsequently attached to the steel specimens, described in the following. Each CFRP overlay consisted of single layers of CFRP bi-directional pre-impregnated carbon fiber ply. Scotch-Weld Epoxy adhesive (1838 B/A Green) was used between certain layers to ensure that there was a sufficient amount of resin to prevent voids from occurring between resin layers during the curing process. Table 3 summarizes the number of carbon fiber plies and Scotch Weld Epoxy adhesive layers used in each CFRP overlay.

Table 3 : Fabrication of multi-layered CFRP overlays

Overlay Thickness mm (in.)	Single Carbon Fiber Plies	Scotch Weld Epoxy adhesive	Placement of Adhesive
1.6 ($^1/_{16}$)	2	1	After 1st ply
2.4 ($^3/_{32}$)	3	1	After 2rd ply
3.2 ($^1/_8$)	4	2	After 2rd ply
6.4 ($^1/_4$)	8	3	After 3rd and 5th ply
12.8 ($^1/_2$)	16	4	After 4th, 8th, and 12th ply

The thickness of the overlay was controlled during the fabrication process by using a mold consisting of aluminum plates placed between bolted steel plates. The fabrication process is described in the following. First, the pre-impregnated CFRP plies were cut to dimensions of approximately 457 x 152 mm (18 x 6 in.), which was double the size of the overlays. The CFRP sheets were placed on the bottom steel plate of the mold, and were added one layer at a time. A single sheet of Scotch-Weld Epoxy adhesive (1838 B/A Green) resin with the same dimensions was added according to Table 3. The CFRP was surrounded by an aluminum spacer with a thickness equal to that of the desired overlay thickness. Due to voids in the interfaces between layers of CFRP plies, the total thickness of the overlay was greater than the intended target thickness after all of the CFRP plies were placed in the mold. The top steel plate of the mold was then placed on top of the CFRP stack, and pressure was applied by tightening the bolts around the perimeter of the mold to reach the target thickness. The overlay was then placed in the oven for curing. The curing oven was preheated to a temperature of 175 C (347 *F)*. The CFRP overlays were cured inside the metal mold for three hours, and subsequently allowed to cure for 48 hours. After the curing process was completed, the CFRP overlays were taken out of the metal molds and cut to final dimensions of 457 x 64 mm (18 x 2.5 in.) using a diamond saw. Sand paper (grade 400) was used to smooth the edges of the CFRP.

Surface preparation and bonding

Maintaining bond under cyclic loading is critical to the successful performance of the repair methods discussed in this paper. In studies performed on aluminum plate, bonding is an elaborate process including grit blasting of the surface, applying and curing a hydrolyzed silane solution, and treating with a corrosion inhibiting primer (Sabelkin et al 2006). In this study, surface preparation of the steel and bonding of the CFRP overlays was performed using simpler techniques than those used in the aerospace industry so that repairs would be more representative of the kind of work that can be performed under field conditions on bridge structures. To develop adequate bond, the steel surface was prepared by a process of abrading and cleaning. Abrading consisted of roughening of the surface with a hand grinder to achieve a surface roughness of approximately 0.8 mm (30 mils). After abrading, cleaning of the surface was performed using acetone and methanol.

The CFRP overlays were attached to the steel specimen using Hysol® 9412 epoxy resin, which has a nominal shear strength of 28 MPa (4 ksi) (Hysol® 2001). The thickness of the Hysol® layer was 0.6 mm (24 mil), maintained during fabrication by using six spacers evenly distributed throughout the interface. Drafting tape surrounding the steel plate was used to prevent leaking of the Hysol® resin. Hysol® resin was poured inside the taped-off area, and pressure was applied using grips to maintain the thickness of the interface layer at 0.6 mm (24 mils). After two days of curing the interface bond layer, final preparation was performed by cleaning the specimen of remnant resin using a chisel and a heat gun.

Test procedure

A cyclic tensile load was applied at the ends of the specimen using an MTS closed-loop servo-controlled loading system. The stress range applied to the steel specimen, $\Delta\sigma_{st,}$ was determined based on the following equation:

$$\Delta\sigma_{st} = \frac{F_{actuator}}{A_{net,st}} \qquad (2)$$

where $F_{actuator}$ is the force or load produced by the actuator, and $A_{net,st}$ is the nominal net cross sectional area of the steel at the reduced cross-section less the area of the drilled hole.

These values, although not representative of the peak stress demand, were adopted to simplify the comparison between various specimens. The ratio of minimum to maximum stress was maintained constant at $R = 0.1$. The rate of fatigue crack propagation was evaluated at three different stress ranges, 262 MPa (38 ksi), 221 MPa (32 ksi) and 166 MPa (24 ksi).

Testing was continuous and CFRP overlays remained bonded to the steel specimens throughout testing so that that any cumulative damage to the interface layer due to fatigue could be directly accounted for within the test results. Testing was terminated once the specimens reached failure or run-out. Failure of these specimens was defined as fatigue crack propagation completely through the width of the specimen; however, because of the bonded CFRP overlays, crack propagation and failure could not be tracked visually. Instead, failure was indicated by a drastic decrease in the percent change in stiffness of the system. The percent change in stiffness was calculated using the following equation:

$$\%\text{ change in } K = [(\delta L/\delta P) - K_{max}] / K_{max} \qquad (3)$$

where K is the stiffness of the combined steel and CFRP overlays, L is the load placed on the specimen, P is the position reading from the testing machine, and K_{max} is the maximum stiffness recorded during testing. Run-out was defined as exceeding the AASHTO S-N curve for Category A detail at the corresponding nominal stress range (AASHTO 2010).

Experimental Results

Fatigue Crack Propagation Life

For each specimen, the fatigue-crack propagation life of the steel substrate from an initial crack length of 7.6 mm (0.3 in) to complete failure in the steel was determined. The monitored change in stiffness was used as an indicator of crack and failure. Under load control, any change in stiffness would be a direct result of an increase in the extension of the specimen, indicative of failure. An increase in compliance could be caused by loss of bond, damage in the composite overlays, or a reduction in the net cross sectional area of the steel specimen. Because the composite overlays showed no signs of damage or distress before failure, except for specimen F4-20, which will be discussed later, it is hypothesized that a gradual increases in compliance was caused primarily by the reduction of the net cross sectional area of the steel specimen. Significant increase in compliance would then indicate propagation of the fatigue crack through the entire cross section of the specimen leading to 100% of the load being transferred through the composite overlays. This new load path caused a rapid increase in the damage to the overlays in the vicinity of the fatigue crack and to local loss of bond, leading to a large increase in compliance (or increase in the percent change in stiffness) in comparison to that observed during propagation of the crack through the steel. The number of cycles at which a significant change in compliance was observed, as shown in Figs. 7-10, was adopted as the fatigue propagation life for the specimen. Upon the conclusion of testing, the CFRP overlays were removed to inspect the steel specimen to confirm that the fatigue crack had in fact propagated through the entire net section of the steel. This was true of all specimens presented in Figs. 7-10.

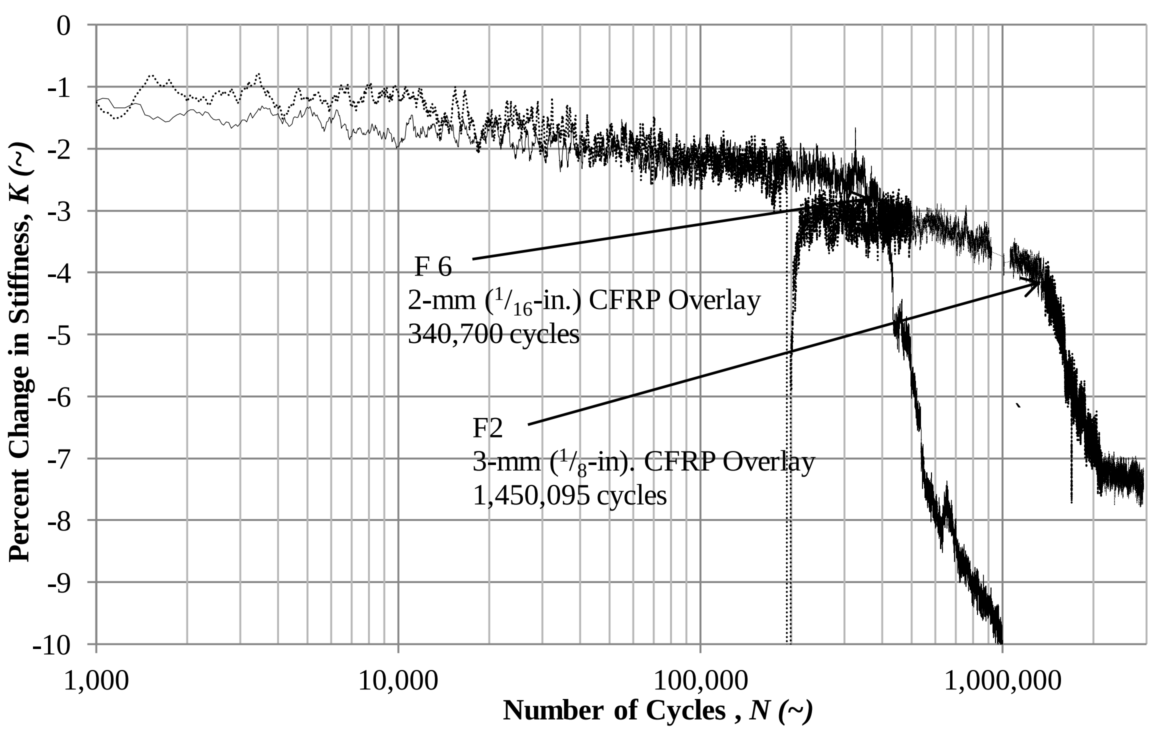

Figure 7: Percent change in stiffness of 3 mm ($^1/_8$ in.) thick specimens tested at 166 MPa (24 ksi)

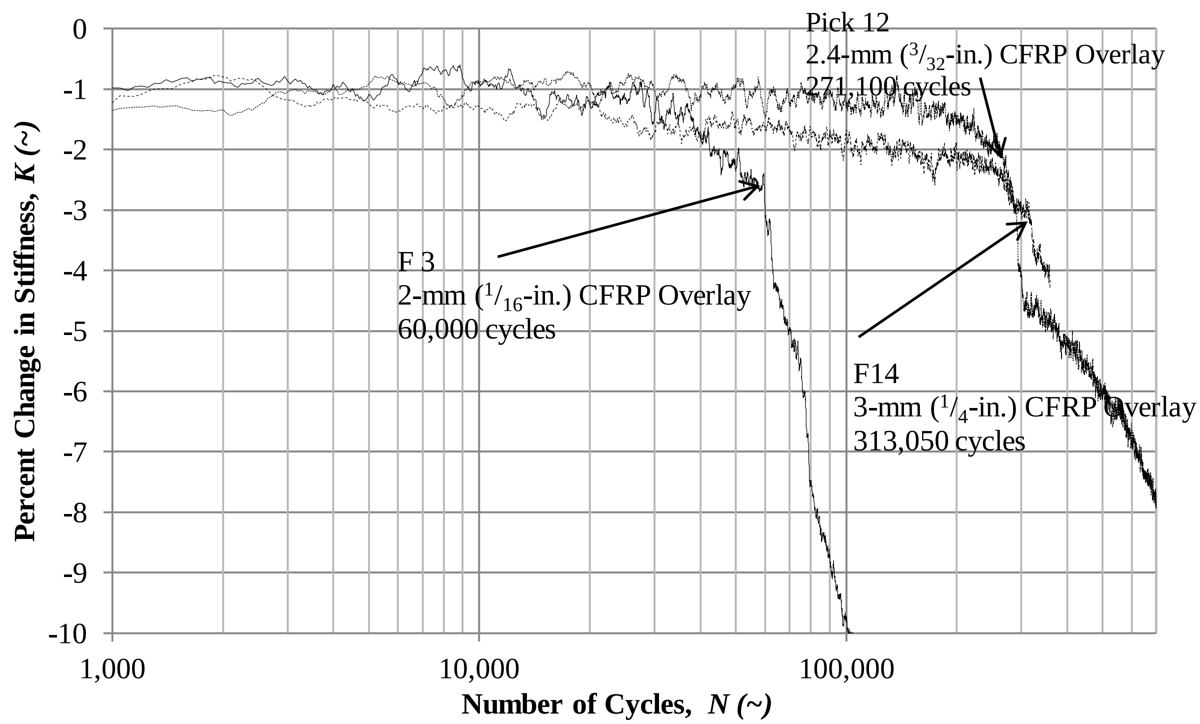

Figure 8: Percent change in stiffness of 3 mm ($^1/_8$ in.) thick specimens tested at 221 MPa (32 ksi)

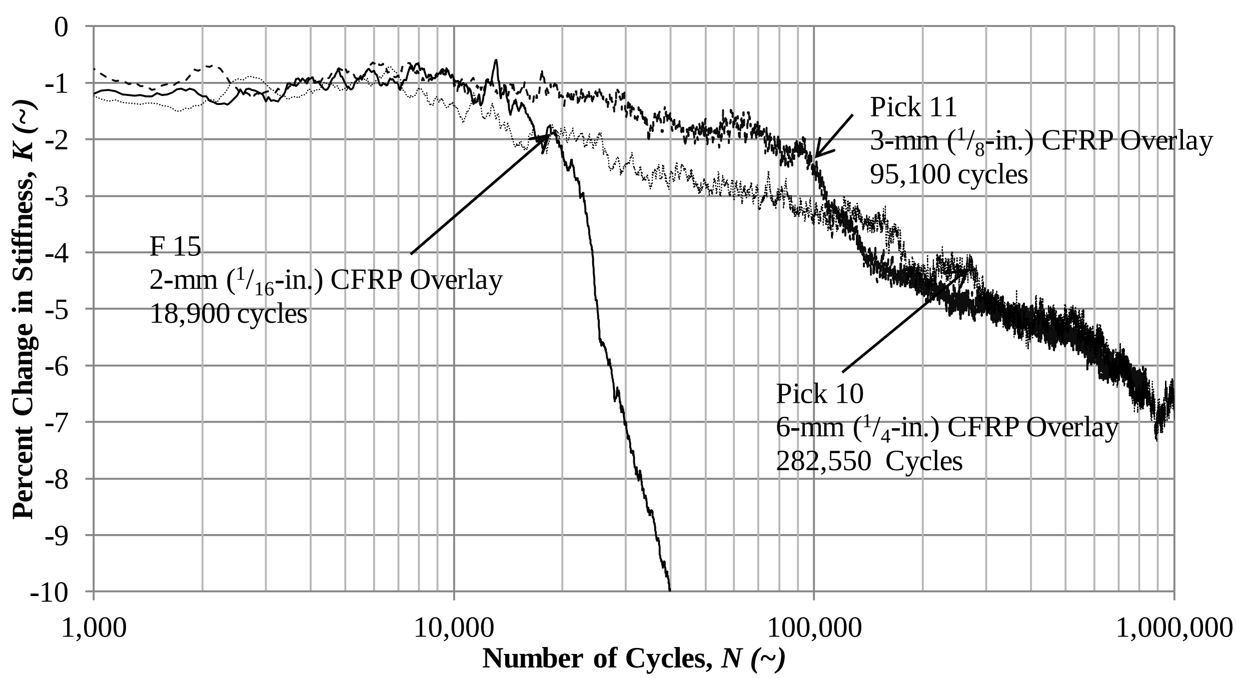

Figure 9: Percent change in stiffness of 3 mm ($^1/_8$ in.) thick specimens tested at 263 MPa (38 ksi)

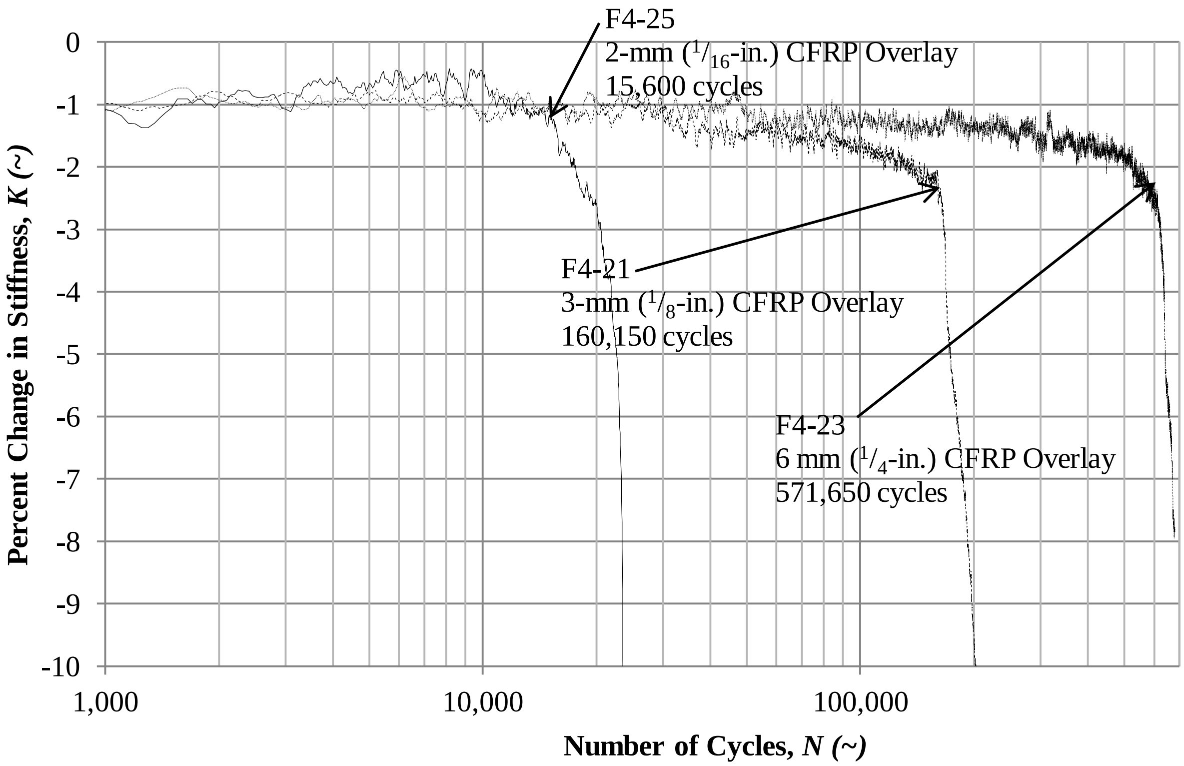

Figure 10: Percent change in stiffness of 6 mm ($^1/_4$ in.) thick specimens tested at 221 MPa (32 ksi)

Specimens Pick 13, Pick 7, F27, and F4-20 were not included in Figs. 7-10. For these specimens, a significant change in compliance was never observed. After the number of cycles exceeded the AASHTO S-N curve for Category A detail at the corresponding nominal stress range (AASHTO 2010) the test was terminated and deemed a run-out. The stress reduction in the steel due to the alternate load path provided by the CFRP overlay was sufficient to drive the demand below the fatigue crack propagation threshold (Barsom and Rolfe 1999) as shown in Figs. 11 and 12. S-N curves for various fatigue categories in the AASHTO-LRFD Bridge Design Specifications (AASHTO 2010) are presented for reference. After the number of cycles associated with infinite fatigue life or finite fatigue life of a Category A detail in the AASHTO-LRFD Bridge Design Specifications was surpassed in these three specimens, the composite overlays were removed for inspection and it was confirmed that the fatigue crack had not propagated fully through the steel cross section.

The number cycles to failure for each specimen are summarized in Table 4.

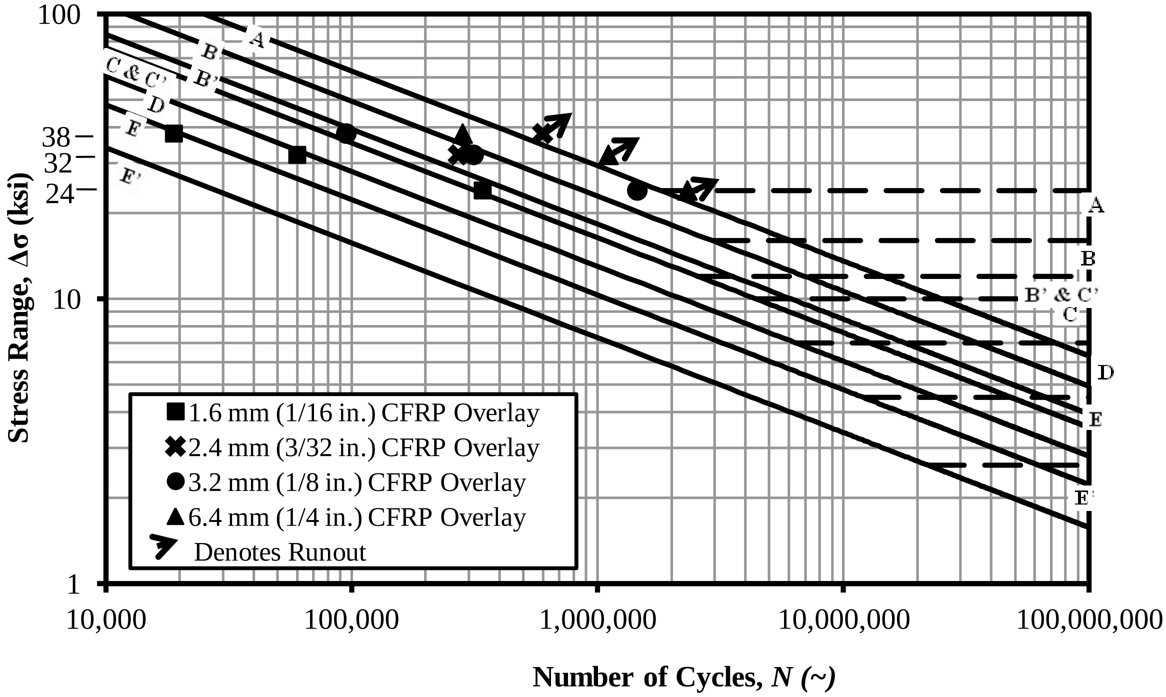

Figure 11: S-N diagram for 3 mm ($^{1}/_{8}$ in.) thick specimens showing fatigue-crack propagation life

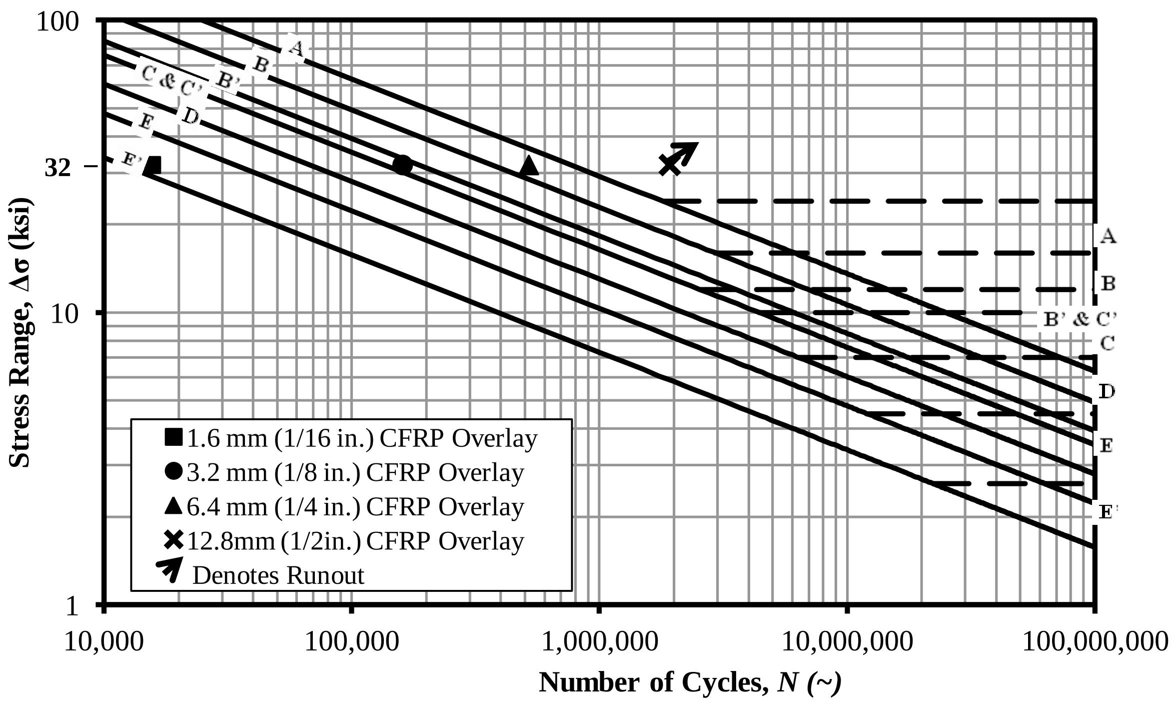

Figure 12: S-N diagram for 6 mm ($^{1}/_{4}$ in.) thick specimens showing fatigue-crack propagation life

Table 4: Fatigue crack propagation life of CFRP repaired steel specimens

Specimen Designation	Fatigue Crack Propagation Life
F15	18,900
F3	60,000
F6	340,700
Pick 12	271,100
Pick 11	95,100
F14	313,050
F2	1,450,095
Pick 10	282,550
Pick 13	Run-Out
Pick 7	Run-Out
F27	Run-Out
F4-25	15,600
F4-21	160,150
F4-23	571,650
F4-20	Run-Out

Effect of Stiffness Ratio

The fatigue-crack propagation lives determined above were compared on the basis of the axial stiffness ratio. The axial stiffness ratio (Eq. 1) was determined for each specimen based on a modulus of elasticity of CFRP, E_{FRP}, equal to 83 GPa (12,000 ksi) regardless of overlay thickness, the measured thickness of the steel, t_s, and CFRP overlay thickness used ,t_{FRP}, and the modulus of elasticity of steel, E_s (200 GPa, 29,000 ksi). Fig. 14 shows the fatigue-crack propagation life of each specimen vs. the stiffness ratio, *SR*. For specimens that reached run-out, the number of cycles to failure was extrapolated using accepted models of theoretical crack propagation presented by Barsom and Rolfe (1999).

Fig. 13 shows that the effect of the stiffness ratio is dependent on the applied stress range. For a specific stiffness ratio, as the stress range at which the specimen was tested increased the fatigue life decreased, as expected. However, this trend was not proportional. A much greater improvement was observed when the stress range decreased from 221 MPa (32 ksi) to 166 MPa (24 ksi) than when the stress range decreased from 263 MPa (38 ksi) to 221 MPa (32 ksi).

Fig. 13 also shows a relationship between propagation life and the stiffness ratio that may be approximated as bilinear. For all specimens, the fatigue-crack propagation life increased as the stiffness ratio increased. For each stress range there was a stiffness ratio at which the slope of the curve had a sudden increase, trending towards infinity. Past this point, small increases in the stiffness ratio resulted in propagation lives that vastly exceeded the limits of run-out discussed above (AASHTO 2010). It is clear from Fig.13 that the critical stiffness ratio at which each set of data trended towards infinity increased with stress range. The critical stiffness ratios for specimens tested at stress ranges of 166 MPa (24 ksi), 221 MPa (32 ksi), and 263 MPa (38 ksi) ksi were approximately 0.8, 1.0, and 1.6, respectively, regardless of specimen thickness. These results indicate that as the stress range increases, the stiffness ratio must be increased to achieve infinite fatigue life.

Because the critical width of the 6 mm (¼ in.) thick specimens differed from that of the 3 mm ($^{1}/_{8}$ in.) thick specimens, failure of the former specimens was taken as the number of cycles at which the crack reached a length of 14 mm ($^{9}/_{16}$ in.). Therefore, the propagation life used in the comparisons corresponds to the same crack growth for all specimens, regardless of specimen thickness, allowing a direct comparison between the two. A direct comparison between the 3 mm ($^{1}/_{8}$ in.) thick and the 6 mm (¼ in.) thick specimens tested at 221 MPa (32 ksi) (Fig. 13) shows that for the same stiffness ratio the thicker specimen had the greater propagation life. However, both specimens had approximately the same critical stiffness ratio.

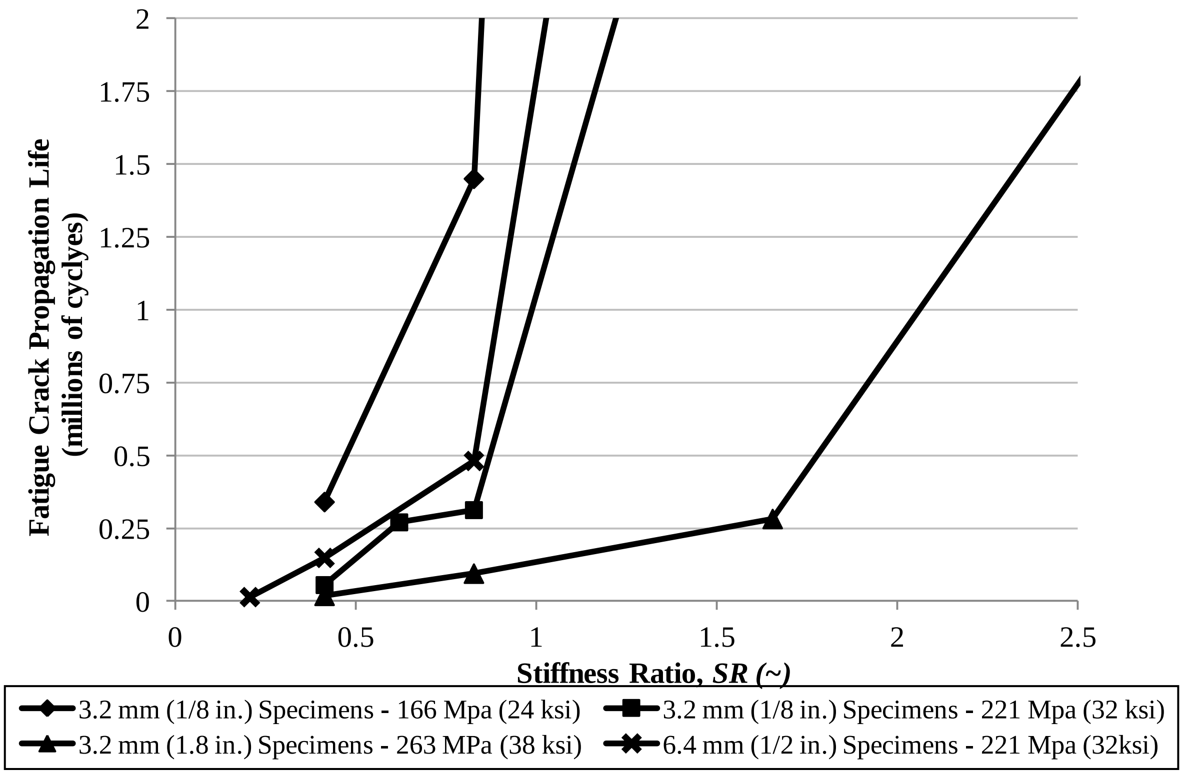

Figure 13: Fatigue-crack propagation life for all specimens treated with CFRP overlays and an initial crack length of 7 mm (0.3 in.)

Given the relatively large initial crack size of 7.6 mm (0.3 in.) relative to the remaining steel net section, control specimens were not tested in this study as the fatigue life would have been quite low in the unreinforced condition. However, theoretical crack propagation lives for un-retrofitted specimens were determined using the following equation presented by Barsom and Rolfe (1999):

$$\frac{da}{dN} = A(\Delta K)^m \qquad (4)$$

where A and m are properties constant for a material, ΔK is the stress intensity factor range, and da is the change in crack length. Because fatigue cracks extended from a round hole on a plate with a finite width, ΔK was calculated using the following equation (Barsom and Rolfe 1999):

$$\Delta K = \Delta\sigma\sqrt{\frac{\pi \times a_{avg}}{Q}} \times f\left(\frac{a}{r}\right) x f\left(\frac{a}{b}\right) \qquad (5)$$

where $\Delta\sigma$ is the applied testing stress range, a_{avg} is the average crack length between incremental calculation steps, Q is the flaw-shape parameter (taken as 1.0 in this case), $f(a/r)$ is a function of the radius of the drilled hole to crack length, and $f(a/b)$ is a function of the crack length to finite width of the tensile specimen.

With the calculation of ΔK from Eq. 5, the theoretical number of cycles to failure of an un-retrofitted specimen can be found from Eq. 4 if the change in crack length (*da)* is set as the distance from an initial crack length of 7.6 mm (0.3 in.) to the edge of the specimen. The results of this theoretical fatigue crack propagation life for un-retrofitted specimens are shown in Table 5 under a stiffness ratio of 0.0 according to Eq. 1.

Once the theoretical fatigue crack propagation life of un-retrofitted specimens was determined, from an initial crack length of 7.6 mm (0.3 in.), they were compared to the fatigue crack propagation lives of CFRP repaired specimens presented in Table 4. Table 5 also shows the factor of increase in fatigue crack propagation life between specimens repaired with CFRP overlays and un-retrofitted specimens.

Table 5: Theoretical fatigue life of un-retrofitted specimen and comparative Increase in Fatigue Life of CFRP repaired specimens

		3 mm ($^1/_8$ in.) steel specimens			6 mm ($^1/_4$ in.) steel specimens			
		Stress Range			Stress Range			
	Stiffness Ratio	166 MPa (24 ksi)	221 MPa (32 ksi)	263 MPa (38 ksi)	166 MPa (24 ksi)	221 MPa (32 ksi)	263 MPa (38 ksi)	Description
(a)	0	6,891	2,907	1,736	10,423	4,397	2,625	Theoretical fatigue crack propagation life (cycles) calculated using Equations 3 and 4
(b)	0.21	--	--	--	--	3	--	Increase in fatigue life from theoretical values (5a) to measured values (Table 4)
	0.41	49.4	19.2	10.9	--	34	--	
	0.62	--	93.3	--	--	--	--	
	0.83	210.4	107.7	54.8	--	109.5	--	
	1.66	run-out	run-out	162.8	--	run-out	--	
	3.31	--	--	run-out	--	--	--	

Table 5 also shows that the applied stress range plays a crucial role in the level of fatigue life improvement that may be achieved through use of a CFRP retrofit. When the stress range is decreased 16 %, from 263 MPa (38 ksi) to 221 (32 ksi), the factor of increase of fatigue crack propagation life is approximately doubled at a stiffness ratio of both 0.41 and 0.83. The same is true when the applied stress range was deceased form 221 MPa (32 ksi) to 166 MPa (24 ksi).

Although this means a CFRP overlay repair will be more effective at a lower stress range, the improvements seen at very high stress ranges are still promising. For a specimen with a thickness of 6 mm ($^1/_4$ in.) tested at a stress range of 221 MPa (32 ksi), the smallest stiffness ratio tested of 0.21 increased the fatigue life by a factor of 3 when compared to the theoretical fatigue crack propagation life of an un-retrofitted specimen. At 263 MPa (38 ksi), a stiffness ratio of 0.41, the fatigue life of the specimen with the same thickness increased by a factor of 10.9. For specimens with a thickness of 3 mm ($^1/_8$ in.), increasing the stiffness ratio to 1.66 at 263 MPa (38 ksi) increased the fatigue life by a factor of 162 when compared to an un-retrofitted specimen. Drastic increases in fatigue crack propagation life can be attributed to the reduced applied stress imposed on the steel. Using the relationships from Eq. 4 and 5, it was determined what stress range corresponded to the fatigue crack propagation lives presented in Table 4. For example, specimen F15 was tested at a stress range of 263 MPa (38 ksi) based on the measured cross-section of the steel; however, the experimental fatigue crack propagation life presented in Table

4 corresponds to an effective applied stress range of approximately 118 MPa (17 ksi) based on the measured cross-section of the steel. Fig. 14 presents the effective stress ranges for all steel tensile specimens based on their calculated stiffness ratio. The reductions in stress follow the same patterns determined during the FE analysis and shown in Fig. 4. Both Fig. 4 and Fig. 14 show a relationship between stiffness ratio and stress reduction that is parabolic and inversely related in nature. Each Fig. also shows the most drastic decrease is stress between the un-retrofitted and the lowest evaluated stiffness ratio.

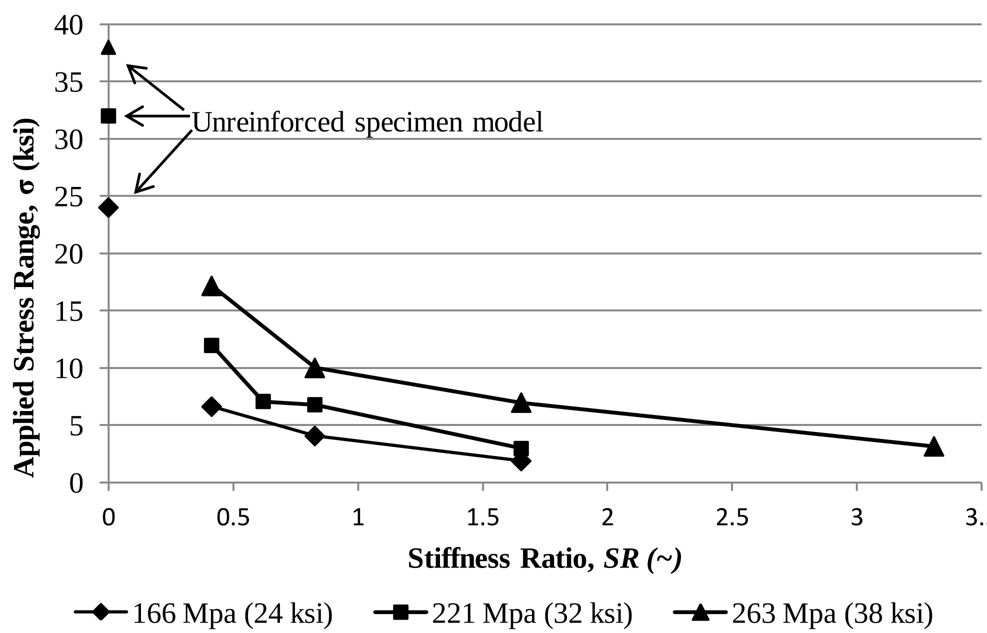

Figure 14: Equivalent applied stress of all specimens treated with CFRP overlays and an initial crack length of 7 mm (0.3 in.)

Specimen Debond Behavior

Of the 15 specimens tested with initial crack lengths of 0.3 in., only one specimen, F4-20, experienced partial debonding between the steel and CFRP overlays. This specimen represented the thickest steel plate tested, combined with the thickest CFRP overlay tested. This suggests that the combination of very thick components led to independent behavior in terms of deformation, instead of system deformation. It is hypothesized that this behavior resulted in fatigue crack initiation in the resin layer at the bottom and top of the CFRP overlay, and subsequent crack propagation towards the center of the length of the overlay. The fatigue crack in the bond layer was noticed at a length of approximately 38 mm (1.5 in.). At this point, a steel collar consisting of two steel plates bolted around each end of the specimen was attached to prevent further debonding. The debonding never approached the region of the fatigue crack in the steel since it was arrested with the steel collar installation; therefore, the results from this specimen are presented as comparable to the others in the study.

Conclusions

Results of an experimental and analytical study examining the use of CFRP overlays to repair fatigue cracks in steel plates has resulted in the following conclusions:

- Experimental results showed that as the stress range was increased, a greater stiffness ratio was required for the fatigue crack propagation life to tend towards infinity. At 166 MPa (24 ksi), 221 MPa (32 ksi), and 263 MPa (38 ksi) the number of cycles to failure tended towards infinity at stiffness ratios of 0.8, 1.0, and 1.6, respectively.
- Both FE analysis and experimental results showed diminishing returns for stress reduction as the stiffness ratio increased past an optimal ratio. The optimal stiffness ratio of 1.0 at a stress range of 221 MPa (32ksi) was confirmed by both methods.
- Experimental results showed that bonding of pre-fabricated multi-layered CFRP overlays increased the theoretical fatigue crack propagation life of un-retrofitted steel specimens by at least three times and up to 162 times before experimental specimens reached run-out.
- The observed increase in fatigue-crack propagation life matched or was significantly higher than values ranging between 3 and 10 reported in previous studies on aluminum plates, steel plates, and steel beams. The main difference between the overlays used in this study and those used in other studies found in the literature is that the stiffness ratio *SR* was significantly higher in this study when compared to previous literature.

Implications of the fundamental research described herein are significant. Research presented within this article has shown that use of CFRP overlays to repair cracks in steel members can be a highly effective means of reducing the stress demand and greatly prolonging the fatigue-crack propagation life of steel substrate. This work has provided a basis for proportioning CFRP overlays for effectiveness in halting/slowing fatigue crack propagation, based upon nominal stress range and the stiffness ratio between the overlay and the steel.

Future research is advised to better understand the demands upon and the behavior of CFRP overlays bonded to steel substrate. Topics that should be studied include: testing thicker steel plates representative of bridge girder webs and investigating wide steel plates with a bonded overlay element of dissimilar (smaller) width.

References

AASHTO (2010). “AASHTO-LRFD Bridge Design Specifications: 5^{th}." *American Association of State Highway and Transportation Officials (AASHTO)*, Washington D.C.

Alemdar, F. (2011). "Repair of bridge steel girders damaged by distortion-induced fatigue," thesis, presented to University of Kansas, at Lawrence, KS, in partial fulfillment of the requirments for the degree of Doctor of Philosophy in Civil Engineering.

ASTM D3039/D3039M-08, "Standard Test Method for Tensile Properties of Polymer Matrix Composite Materials," American Society for Testing and Materials, West Conshocken, PA, 2008.

Barsom, J.M., and Rolfe, S.T. (1999). “Fatigue and fracture behavior of welded components.” Fracture and Fatigue Control in Structures, 3rd ed., (10), American Society for Testing and Materials, West Conshohocken, PA, 35-53.

Crain, J. (2010). "Fatigue enhancement of undersized, drilled crack-stop holes," thesis, presented to University of Kansas, at Lawrence, KS, in partial fulfillment of the requirements for the degree of Mater of Science in Civil Engineering.

Dexter, R.J. (2004). "Sign, Signal, and Light Support Structures and Manural for Repair of Fatigue Cracks*."* Third Annual Bridge Workshop: Fatigue and Fracture. March 5, 2004.

Hassel, H.L. (2011). "An analytical evaluation of distortion-indiced fatigue in steel bridges," thesis, presented to University of Kansas, at Lawrence, KS, in partial fulfilment of the requirements for the degree of Master of Science in Civil Engineering.

Hysol® 9412, Loctite 9412 Hysol Epoxy Adhesive, 2001, http://www.henkelna.com.

Kaan, B.N., Alemdar, F., Bennett, C.R., Matamoros, A., Barrett-Gonzalez, R., and Rolfe, S. (2012). "Fatigue enchancement of welded details in steel bridges using CFRP overlay elements". *Journal of Composites for Construction,* in press.

Lee, W. Y., and Lee, J.J. (2004). "Successive 3D FE analysis technique for characterization of fatigue crack growth behavior in composite-repaired aluminum plate." *Composite Structures,* 66(1-4), 513-520.

Liu, H. B., Al-Mahaidi, R., and Zhao, X.L. (2009). "Experimental study of fatigue crack growth behaviour in adhesively reinforced steel structures." *Composite Structures,* 90(1), 12-20.

Liu, H. B., Xiao, Z. G., Zhao, X. L., and Al-Mahaidi, R. (2009). "Prediction of fatigue life for CFRP-strengthened steel plates." *Thin-Walled Structures,* 47(10), 1069-1077.

Mall, S., and Conley, D.S. (2009). "Modeling and validation of composite patch repair to cracked thick and thin metallic panels." *Composites Part A: Applied Science and Manufacturing,* 40(9), 1331-1339.

Marquis, G., and Kahonen, A. (1995). "Fatigue testing and analysis using the hot spot method." Technical Research Centre of Finland.

Naboulsi, S., and Mall, S. (1996). "Modeling of a cracked metallic structure with bonded composite patch using the three layer technique." *Composite Structures*, 35(3), 295-308.

Roddis, W. M., and Zhao, Y. (2001). "Out-of-Plane Fatigue Cracking in Welded Steel Bridges: why it happened and how it will be reapired." *Welding Inovation*, 27(2) , 2-7

Roy, M., Lang, C., & May, I. (2009). "Modelling composite repairs to cracked metal structures." *Proceedings of the Institution of Civil Engineers (ICE)-Structures and Building*s, 162(2), 107-113.

Sabelkin, V., Mall, S., and Avram J. B. (2006). "Fatigue crack growth analysis of stiffened cracked panel repaired with bonded composite patch." *Engineering Fracture Mechanics,* 73(11), 1553-1567.

Schubbe, J.J., and Mall, S. (1999). "Modeling of cracked thick metallic structure with bonded composite patch repair using three-layer technique." *Composite Structures,* 45(3), 185-193.

Simulia. (2009). ABAQUS FEA Version 6.10-2. Providence, RI. http://www.simulia.com.

Tavakkolizadeh, M., and Saadatmanesh, H. (2003). "Fatigue strength of steel girders strengthened with carbon fiber reinforced polymer patch." *Journal of Structural Engineering,* 129(2), 186-196.

Umamaheswar, T.V.R.S., and Singh, R. (1999). "Modelling of a patch repair to a thin cracked sheet." *Engineering Fracture Mechanics,* 62(2), 267-289.

PART 2:

Evaluation of Fatigue Damage Repair Measures in Welded Steel Plate Bridge Girders

Evaluation of Fatigue Damage Repair Measures in Welded Steel Plate Bridge Girders

Abstract

Fatigue damage is a common problem in steel girder bridges built prior to the mid-1980s. The location in which damage is likely to occur and the type of damage pattern are affected by the bridge geometry and loading conditions. In this study the propensity for damage under the combined effects of girder bending and cross-frame loading, as well as the pattern of damage that is to be expected were evaluated by performing a suite of finite element analyses.

After fatigue damage is detected, some repair or retrofit method must be implemented to prevent further fatigue crack propagation and protect the structural integrity of the bridge. Three repair methods were evaluated to determine the reduction in stress demand that each method produced at two critical locations. The three methods evaluated were: (1) drilling of crack-stop holes at crack tips, (2) attachment of bolted full-depth splice plates to the damaged web, (3) and attachment of adhesively bonded CFRP overlays reinforced by bolted steel cover plates. Results of finite element analyses show that while both the full-depth steel splice plates and CFRP assemblage showed large reductions in stress, the later outperformed the other repaired methods and had the best potential for preventing further fatigue crack growth.

Introduction

Problem Statement

Steel girder bridges built prior to the mid-1980s were commonly designed without positive attachment between connection stiffeners and the tension flange (Hassel 2011). Unfortunately an outcome of this detailing practice was the fabrication of a large number of connections likely to develop distortion-induced fatigue damage in this region of the girder web, known as the *web gap*. Fatigue cracks in the web gap region are common in bridges of this era, requiring some repair or retrofit measure. AASHTO has since rectified this issue in new bridge construction by specifying that all connection stiffeners be welded or bolted to both the top and bottom flange of the girder if they are subsequently attached to a diaphragm, cross-frame, or floorbeam (AASHTO 2010). Implementing this type of connectivity in existing bridges would likely prevent further fatigue damage, but a bolted retrofit requires the removal of part of the bridge deck to make attachment to the top flange.

Because removal of the bridge deck can be costly in terms of the retrofit itself and traffic interruptions it causes, a repair or retrofit not involving its removal is preferred. Two such methods are the drilling of a crack-stop hole at the tip of fatigue cracks and attaching steel splice plates over the damaged region (Dexter 2004). Crack-stop holes have been shown to prevent crack re-initiation in plates with notches subjected to direct tension. Equations to determine the diameter of the crack-stop hole needed to prevent further crack growth have been developed based on tensile fatigue tests. One such equation, Eq. 1, was proposed by Barsom and Rolfe (1999):

$$\frac{\Delta K}{\sqrt{\rho}} < 10\sqrt{\sigma_{ys}} \qquad \text{Eq. 1}$$

which can be rearranged as:

$$\rho > \left(\frac{\Delta K}{10\sqrt{\sigma_{ys}}}\right)^2 \qquad \text{Eq. 2}$$

where ΔK is the stress-intensity factor range, σ_{ys} is the yield strength of the material, and ρ is the notch tip radius.

Equation 2 indicates that the hole diameter required to prevent crack re-initiation is proportional to the stress intensity factor range and inversely proportional to the yield strength of the steel. One of the main drawbacks of this repair method is that expressions such as Eq. 2 were based on experimental data from specimens subjected to fracture Mode 1 displacements (Barsom and Rolfe 1999), while the stress fields in web gap regions are much more complex and impose mixed fracture mode displacements. The other drawback of using crack-stop holes is that often times the calculated diameter of the hole needed to prevent crack re-initiation is rather large, or large relative to the available space in the web gap region, making it impossible or impractical to implement. Undersized holes will prevent fatigue crack propagation temporarily but often lead to re-initiation and further growth. Crack re-initiation is a major concern because it will require additional repairs and threaten the structural integrity of the member and potentially the bridge.

Retrofitting a bridge with full-depth steel splice plates over the damaged area stiffens the cracked girder web and restores the properties of the web to pre-cracked conditions (Roddis and Zhao 2001). The main drawback for bridge engineers is that this type of repair covers the crack, making it difficult to inspect existing cracks for propagation or initiation of new cracks without removal of the entire splice during inspection. Given these limitations, an alternative method to repair fatigue damage was investigated and their expected performance compared with that of existing repair and retrofit measures.

Objective

The first objective of this study was to evaluate various combinations of bending and out-of-plane load demands on the magnitude and orientation of the stress field in the web gap region of steel girders. High-resolution computer simulations were carried out to investigate the effect of loading conditions on the location and type of fatigue damage most likely to occur in steel bridge girders.

The second objective of the study was to evaluate the performance of three different repair methods for girders with large cracks caused by distortion-induced fatigue. Effectiveness of the repair methods was quantified on the basis of the computed reduction in stress demand with respect to companion models of unrepaired girders with a simulated crack. The three repair methods evaluated were: (1) drilling crack-stop holes of varying diameter at the crack tips, (2) attaching bolted splice plates over the full depth of the girder, and (3) attaching a repair assemblage consisting of bonded carbon fiber reinforced polymer (CFRP) overlays reinforced with bolted steel cover plates. High-resolution finite element models of a simply-supported, full-depth steel bridge girder were used to investigate both objectives.

Background

Fatigue Crack Locations

Fatigue damage caused by distortion-induced fatigue in welded plate girder bridges is most often observed in the web, between transversely welded structural components (floor beams, diaphragms, or cross-frames) and an adjacent flange (Fisher 1984). Within this web gap region there are three types of cracks that are most commonly found. They are: (1) a horizontal crack oriented parallel to the web-to-flange weld along the weld toe, designated as Type 1, (2) a horse shoe shaped crack originating in the web gap region and propagating outward into the web, designated as Type 2, and (3) a vertical crack originating in the web gap region following the weld toe of the stiffener-to-web weld, designated as Type 3 (Fisher 1984). The crack type designations, shown in Fig. 1, will be used throughout this study.

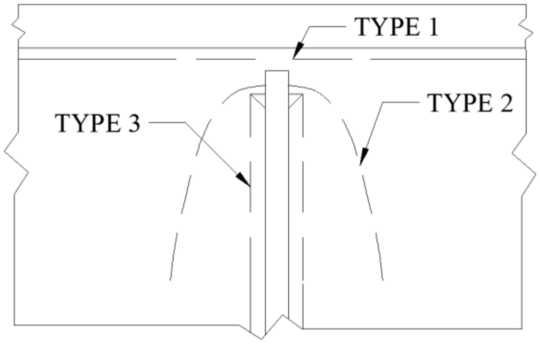

Figure 1: Typical fatigue crack locations and types

A case study of a Kansas Department of Transportation (KDOT) bridge constructed in 1977 found cracks of Type 1 and 2 in the web gap adjacent to the top flange in positive and negative flexure (Roddis and Zhao 2003). Cracking near the top flange was attributed to the composite action of the slab, which restrains rotation in the top flange of the girder but not in the bottom flange. The bridge studied was a two-girder non-skewed bridge (Roddis and Zhao 2003). Two other non-skewed bridges evaluated for fatigue damage, the Belle Fourche River Bridge and Chamberlin Bridge over the Missouri river (Fisher 1984), also had the majority of fatigue damage occur in the positive moment region, in the web gap adjacent to the compression flange. The fatigue cracks were recorded as through-thickness cracks. (Fisher 1984).

Type 2 cracks have also been found to propagate deep into the web of steel girder bridges, as was observed in a Maryland highway bridge investigated by Zhou and Biegalski (2010). This skewed continuous steel girder bridge had web fractures initiating near the tension flange and extending the entire depth of the web. Fatigue cracks of this magnitude are not common, but do occur and pose a serious threat to the structural integrity of a bridge.

Parametric studies completed at the University of Kansas investigated the likely regions where fatigue damage would occur in bridges with varying skew angle and cross frame placement (Hartman et al. 2010; Hassel 2011). It was found that in all bridge configurations studied, fatigue cracks were most likely to form in the positive moment region (Hartman et al. 2010). Reports of fatigue cracks mainly in the negative moment region have been documented (Khalil et al. 1998). The study by Hartman et al. (2010) found that fatigue cracks in the negative moment region are more likely to occur if the bridge is skewed. Hartman et al. (2010) also concluded that fatigue cracking was most likely to occur in the top web gap region of the exterior girder when the cross frames were placed parallel to skew. This behavior was found to change when skewed and staggered cross-frames were used, in which case the critical crack location moved from the top to the bottom web gap (Hassel 2011).

Common Fatigue Repair Techniques

When cracking is discovered in welded steel girder bridges, the fatigue detail is most often retrofitted to prevent further propagation and possible failure. Currently, one of the most common retrofit or repair technique is drilling a hole at the tip of the fatigue crack in the girder web. The radius of this crack-stop hole theoretically needed to prevent crack re-initiation can be calculated using Eq. 1.

In many instances, because of the crack location and the geometric constraints in the web gap region, it is not physically possible to drill a hole with the diameter calculated using Eq. 1. The only alternative is to drill an undersized crack-stop hole, which will likely lead to the re-initiation of cracks and the need for drilling more crack-stop holes. Even when a relatively large crack-stop hole is drilled, crack re-initiation is still probable. Zhou and Biegalski (2010) investigated the use of a 51 mm (2.0 in.) crack stop-holes along predicted fatigue crack paths using the Finite Element method. They found that implementing this crack-stop hole along the expected fracture path increased the web flexibility and produced high stresses in the surrounding area under both in-plane and out-of-plane girder loading (Zhou and Biegalski 2010).

A repair technique used when large fatigue cracks propagate deep into the girder web is bolting steel cover plates to both sides of the web over the cracked region. This type of repair creates an alternate load path through the web, lowering the stress demand at the tip of the fatigue crack, prolonging the fatigue life of the girder (Roddis and Zhao 2001). The drawback to this repair method is that the steel plate covers the entire depth of the web. If any further crack propagation does occur, it will go unnoticed during inspections unless the entire retrofit is removed, or the crack propagates outside the footprint of the retrofit.

Carbon Fiber Reinforced Polymer Overlays

There has been a significant amount of research on the use of fiber reinforced polymer (FRP) overlays to repair fatigue damage in aircraft fuselages (Mall and Conley 2009; Umamaheswar and Singh 1999; Schubbe and Mall 1999; Naboulsi and Mall 1996; Lee and Lee 2004; Liu, Xiao, et al. 2009) and aluminum plate (Mall and Conley 2009;Denney and Mall 1997, Sabelkin et al. 2006). In a study conducted by Mall and Conley (2009), the fatigue life of 6-mm

($^{1}/_{4}$-in.) thick aluminum plate was extended by a factor of four compared with that of an unrepaired plate. A comparable study by Denney and Mall (1997) found that the fatigue life of 1-mm (0.04-in.) thick aluminum plate was extended by a factor of 10 compared with that of an unrepaired plate. Currently, adhesively bonded FRPs are used in the repair of fuselages and structural components of airplanes (Sabelkin et al. 2006).

The positive results generated by research in the aerospace industry have spurred the use of FRP overlays to repair fatigue damage in steel plates. The most commonly used composite material in research investigating the repair of fatigue damage in steel plates is carbon fiber reinforced polymer (CFRP). CFRP overlays have the advantage that the coefficient of thermal expansion of carbon closely matches that of steel. Materials with similar coefficients of thermal expansion produce a more effective repair, whereas a mismatch in coefficients of thermal expansion could cause the opening of a fatigue crack and subsequent reduction in fatigue life (Sabelkin et al. 2007).

Lui et al. (2009) found that the fatigue life of steel plates could be increased by a factor of 7.9 when repaired with adhesively bonded CFRP overlays. They also found that the fatigue life was greatly increased when the CFRP overlays were attached to both sides of the steel plate when compared with a single-sided repair technique, because the stiffening of only one side introduced out-of-plane bending stresses.

Parametric Analysis of Factors Effecting Susceptibility to Fatigue Damage

Under normal loading conditions, bridge girders are subjected to both out-of-plane forces from cross-frames and in-plane bending from gravity loads. The effect of various combinations of these two types of loads were studied using Finite Element models to determine if either load increased the stress demand in the web gap regions where fatigue cracking is likely to occur or caused the location of the critical stress demand in the web gap region to change. The angle between the out-of-plane cross-frame force and the horizontal was varied between 0 and 45 degrees, simulating X-type cross frames with various girder spacing. The gravity load producing in-plane bending was varied to create a longitudinal bending stress in the top flange ranging between 35 and 138 MPa (5 and 20 ksi), to simulate cross-frame locations at various stations along the girder length.

Girder Section Geometry

The effects of in-plane bending and cross frame loading were studied on a single 3.0-m (10.0-ft) wide by 1524-mm (60-in.) deep steel girder section, shown in Fig. 2 and 3. The simply-supported girder was comprised of a web, top and bottom flanges, and a single connection stiffener welded to the web at mid-span on what will be referred to as the interior side the web. The opposite side of the web is referred to as the fascia side of the web. In this simplified girder model no bridge deck was included. The depth of this section was chosen to represent a reasonable girder depth for a multi-girder highway overpass. The length of the girder section was chosen to be twice the girder depth. The connection stiffener welded at mid-span was truncated 6 mm (1.4 in.) from the face of each adjacent flange. A 25-mm (1.0-in.) clip produced a web gap region of 35 mm (1.38 in.). At each end of the girder a 13-mm (1/2-in.) thick steel transverse stiffener was attached over the entire depth of the girder, shown in Fig. 2 but removed from Fig. 3. The end stiffeners were attached to both the top and bottom flange and the entire depth of the web. All girder dimensions are shown in Fig. 2 and 3.

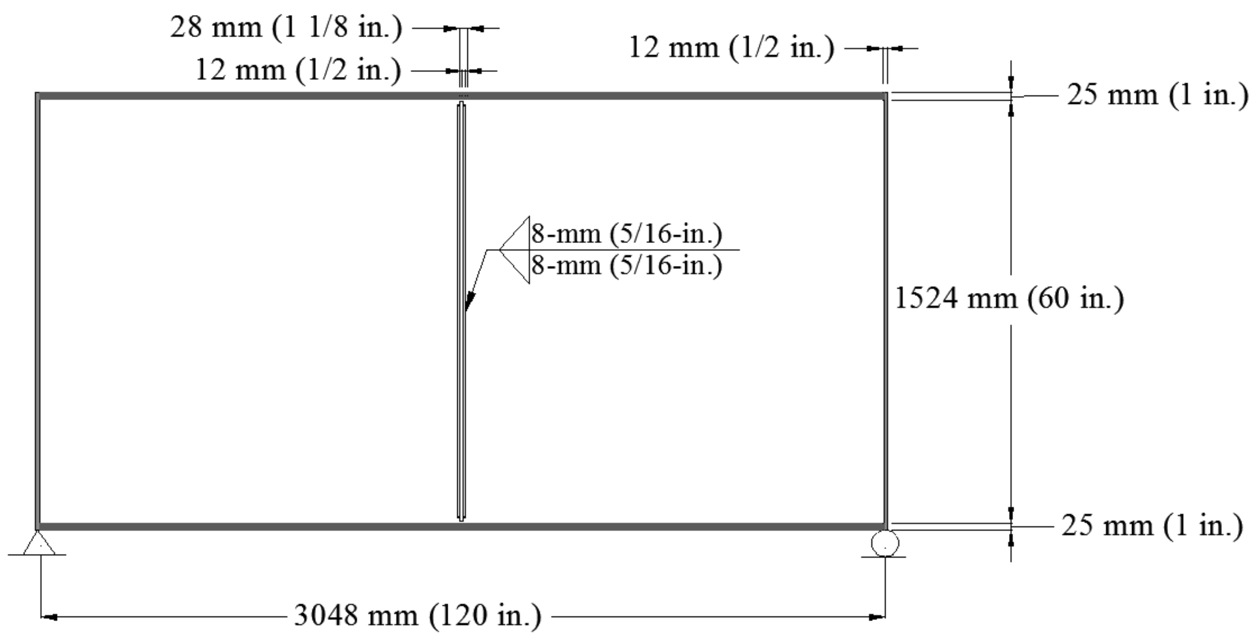

Figure 2: Plan view of girder section

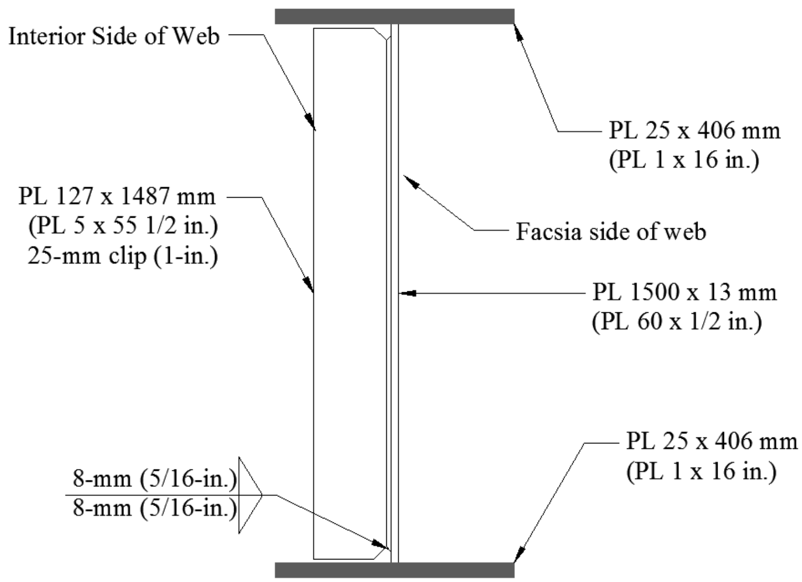

Figure 3: Girder cross section

Parameters Considered

The effects of cross-frame loading and bending moment on the stress field at the web gap were analyzed separately. Cross-frame forces were modeled as point loads placed at mid-thickness of the connection plate. A 22-kN (5-kip) load was placed near both the top and bottom of the connection plate. The load near the top of the connection plate was placed in tension while the load near the bottom was placed in compression to match cross frame forces calculated using full-scale bridge models by Hassel (2011) and Roddis and Zhao (2003). In the study by Hassel (2011) the calculated compression force was approximately 1.5 times greater than the tension force. A Finite Element analysis was completed on the girder section, shown in Fig. 2, to determine the effect on the stress field due to the disproportionate loading scenario. Although stress values were slightly higher near the welds in the bottom web gap (as would be expected) there were no significant differences in the stress fields between the two models. For this reason it was decided that all analyses would be performed with cross-frame forces of equal magnitude.

The 22-kN (5-kip) forces were oriented at angles of 0, 5, 10, 15, 20, 25, 30, 35, and 45 deg. with respect to the horizontal axis. The angle with respect to the horizontal was maintained equal for the tensile and compressive force. The load placement in the vertical direction along the connection stiffener was changed in each model so that the projection of the cross-frame force would pass through the same point in the web gap for each model. This was done to ensure that the effects of forces placed at higher angles were not underestimated. The force parallel to the horizontal was placed 13 mm ($^{1}/_{2}$ in.) from the top (or bottom) of the connection stiffener. For each increment in angle with respect to the horizontal axis of 5 degrees, the load was moved approximately 12 mm (0.45 in) toward the neutral axis of the girder section. Fig. 4 shows a schematic of the load placements.

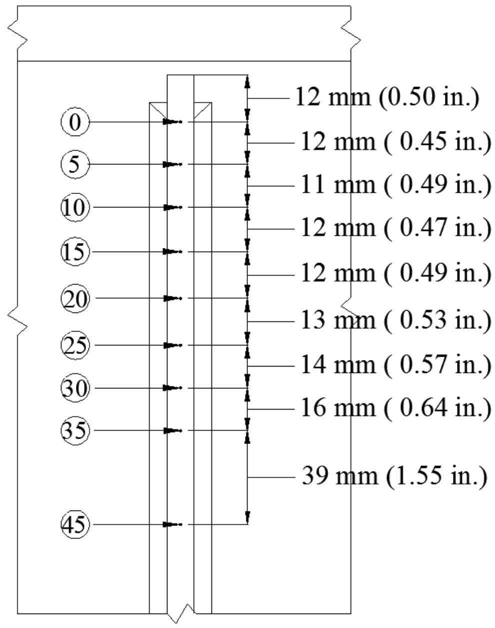

Figure 4: Placement of loads at varying degrees from horizontal

The bending stress demand was simulated by applying a uniform pressure load to the top flange of the girder. Initially the pressure load was applied to the entire surface of the top flange; however, this caused the ends of the top flange to bend downward in a manner that would not occur in a bridge because of the attachment of the top flange to the bridge deck. To avoid this distortion, the pressure load was applied along the full length of the top flange but was concentrated along the width of the web. This load distribution produced a more reasonable bending shape. Two different gravity loads were compared. The first induced a 35 MPa (5 ksi) longitudinal stress in the top flange, which would be expected under typical truck loads in a long span bridge. The second gravity load induced a 138 MPa (20 ksi) longitudinal stress in the top flange, which represents an extreme and live load level.

The effects of combined in-plane bending and out-of-plane cross-frame loading were then evaluated using the combinations given in Table 1. This was done to determine if one parameter dominated the behavior when applied simultaneously.

Table 1: Load combinations used to test effect of cross-frame force and bending

Load Combination	Angle of Cross-Frame Force with Respect to the Horizontal	Longitudinal Bending Stress
1	0 degrees	35 MPa (5 ksi)
2	0 degrees	138 MPa (20ksi)
3	35 degrees	35 MPa (5 ksi)
4	35 degrees	138 MPa (20 ksi)

Finite Element Modeling

A linear-elastic Finite Element (FE) model of the 3.0-m (10-ft) bridge girder section was constructed in Abaqus v6.10.2 (Simulia, 2008) using three-dimensional elements. Meshes were assembled using 8-node brick elements for the majority of the model. Small areas of tetrahedral meshing were used near the non-square edges of the connection stiffener. All parts of the girder section were composed of steel modeled with a modulus of elasticity of 200 GPa (29,000 ksi) and Poisson's ratio of 0.3. A maximum mesh size of 6 mm ($^1/_4$ in.) was used for all steel parts. Parts were attached using surface-to-surface tie constraints. Only the weld attaching the connection stiffener to the web was modeled explicitly. All other welds were not modeled explicitly, with the corresponding elements connected directly to each other using tie constraints. A mesh size of 5 mm (0.2 in.) was used for the weld and its material properties matched those of other steel parts.

Simply-supported boundary conditions were created by applying translational restraint along the narrow bottom edge of each end stiffener. This allowed the stress demand to be transferred in such a way that the critical region of the web, at mid-span near the connection stiffener, was not affected by irregularities caused by boundary conditions. The outermost side of each end tansverse stiffener was also restrained from movement in the out-of-place direction.

Hot Spot Stress Analysis

The potential for fatigue damage of the various loading combinations and retrofit measures was evaluated in terms of the calculated Hot Spot Stress (HSS). This method was chosen as the basis of comparison because it reduces the effect of the mesh configuration in areas of high stress located near geometric discontinuities, such as the connection stiffener-to-web weld. To determine the peak HSS, maximum principal tensile stress demands were extracted along a path located half the width of the web thickness (6 mm [$^1/_4$ in.]) from the geometric discontinuity corresponding to the intersection of the weld and the web.

For each model that was analyzed, two separate HSS paths were investigated. The first HSS path was defined around the toe of the connection stiffener-to-web weld and the maximum principal stress demand extracted from that path was designated HSS#1. This stress demand would be indicative of the potential for initiation or re-initiation of fatigue cracks of types 2 and 3. The second HSS path was defined along the flange-to-web weld and the maximum principal stress extracted from this path was designated HSS#2. Both HSS paths are shown in Fig. 5, along with the mesh configuration. For loading scenarios that did not evaluate in-plane bending, HSS#1 and HSS#2 were determined for both the top and bottom web gaps on both sides of the web. Because the bending moment induced by the gravity load produced tension in the bottom web gap, HSS#1 and HSS#2 were only extracted in the bottom web gap, on both sides of the web.

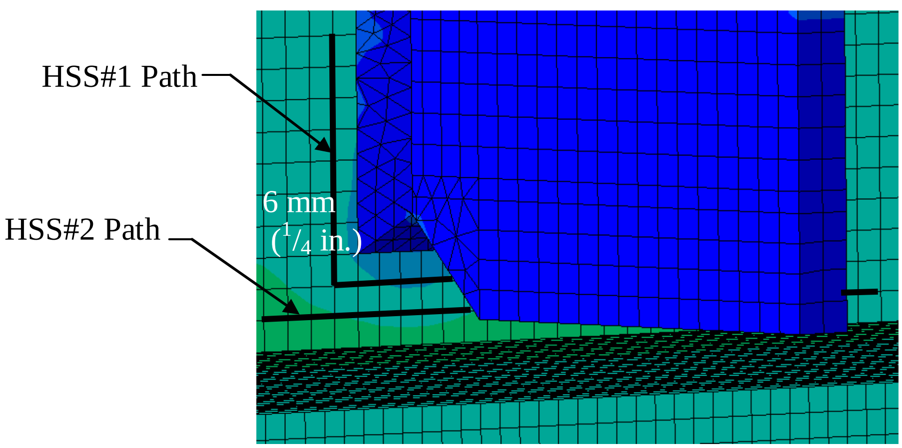

Figure 5: Schematic of hot spot stress paths

Results of Parametric Analysis

Among the FE models with various cross-frame configurations the highest web gap stress demands were found for the model in which the cross-frame force acted parallel to the horizontal. All HSS#1 and HSS#2 magnitudes decreased in both the top and bottom web gap as the angle at which the cross-frame force acted was increased. Increasing the angle to 35 degrees from the horizontal decreased HSS#1 by a maximum of 23% and decreased HSS#2 by a maximum of 15% (both in the top web gap on the fascia side of the web). Although the magnitudes of the maximum principal tensile stress changed with varying angle, no significant changes in the shape of the stress field and consequently the expected location of the fatigue cracks were found. For all variations of cross-frame force the maximum HSS was found to be HSS#1 in the top web on interior side of the web. These results indicate that under cross-frame loading only, expected to take place in regions of bridges near girder inflection points, fatigue crack initiation would be expected to occur first along the connection stiffener-to-web weld in the top web gap.

Subjecting the simply-supported girder model to pure bending caused tensile stresses in the web at the bottom web gap, and compressive stresses at the top web gap. The compressive stresses at the top web gap reduced the likelihood of fatigue damage by reducing or eliminating stress fluctuations in the tension range, making the bottom web gap the region of interest in evaluating the potential for fatigue damage. Even though in long-span bridges a large fraction of the gravity load is not cyclic in nature and consequently has no effect on the stress range, tensile stresses due to gravity do exacerbate the potential for fatigue damage by placing the web in tension prior to tensile load fluctuations caused by traffic directly in the girder and indirectly through the cross frames.

When the longitudinal bending stress in the top flange was increased from 35 MPa to 138 MPa (5 ksi to 20 ksi) the magnitude of HSS#1 and HSS#2 were both increased by approximately 300% on both sides of the web. These results clearly show that as the ratio of live to dead load increases in the bridge so does the potential for fatigue damage in the web gap regions. While the calculated change in demand constitutes a dramatic increase the increase in bending stress (or increase in the ratio of live to dead load) had a negligible effect on the shape of the stress field and consequently the locations where fatigue cracks were most likely to initiate. For models with varying bending stress, the critical location was found to be HSS#1 in the bottom web gap, on the fascia side of the web.

When the effects of bending and cross-frame loading were analyzed together, the fatigue critical location associated with bending stress controlled (HSS#1 in the bottom web gap on the fascia side of the web). This indicates that under combined loading conditions, expected to take place in positive moment regions of girders subjected to significant live loads, bending stress played a more significant role in the potential for fatigue damage. In fact, when a bending stress of 138 MPa (20 ksi) was applied, corresponding to a very high ratio of live to dead loads, the HSS in this location was comparable between models of all varying cross-frame forces and angles.

Parametric Analysis of Fatigue Repair Measures

After a fatigue crack is discovered in a steel bridge structure, it is imperative to implement some measure to repair fatigue damage and protect the structural integrity of the bridge. This study used the Finite Element models discussed above to evaluate three methods of repairing fatigue damage. The methods evaluated were: (1) drilling crack-stop holes of varying diameter, (2) applying full-girder-depth steel splice plates over the region of the web with fatigue damage, and (3) applying a carbon fiber reinforced polymer (CFRP) overlay over a localized region surrounding the fatigue crack tip.

Girder Section and Crack Geometry

All repair methods evaluated in this study were applied to the girder section shown in Fig. 2 and 3. Also, all repairs were applied to cracks of Type 2 shown in Fig. 1. If left unrepaired or repaired insufficiently, horse-shoe shaped cracks of this type have the potential to propagate deep into the girder web (Zhou and Biegalski 2010). Each repair method was implemented on a through-thickness fatigue crack that had propagated 1/8 of the depth of the web. Repair methods were also evaluated in models with simulated fatigue cracks that had propagated 1/4 of the depth of the web to determine if there were any implications of retrofitting cracks of different lengths. While in most instances regularly scheduled bridge inspections will allow finding fatigue cracks before they reach this depth, there are documented cases. Each model was loaded with 22-kN (5 kip) tension and compression cross-frame force at an angle to 35 degrees from the horizontal and a gravity load which produced a 35 MPa (5 ksi) bending stress in the top flange. Specifics about how the loading and how it was applied are discussed above. From the discussion on loading conditions given, cross-frame forces at an angle of 35 degrees from the horizontal was chosen because they represent a typical girder spacing of a multi-girder highway overpass. An induced bending stress of 35 MPa (5ksi) was chosen as it represents the induced bending that would be expected in a long-span bridge from typical truck loads.

For this pre-determined fatigue crack type, there were two possible locations for crack initiation, the top and bottom web gaps. For the reasons cited above, analyses focused on the stress demands at the bottom web gap. To reinforce that this is the location of expected fatigue damage, preliminary models were loaded with cross-frame forces acting at 35 degrees from the horizontal and an applied gravity load inducing a longitudinal stress of 138 MPa (20 ksi) in the top flange. The XFEM modeling technique was used to simulate pre-existing horse shoe cracks in the bottom web gap. This modeling technique allowed simulating crack propagation following paths of high stress demand. A refined mesh with a maximum mesh size of 1 mm (0.05 in.) was used in a region near the crack. A 25-mm (1-in.) length of tetrahedral meshing was used to transition between mesh sizes.

Significant crack propagation was not observed in the XFEM models under the prescribed loading conditions. The stresses demands at the ends of the horse-shoe crack were found to be higher in the bottom web gap region than in the top web gap. Fatigue cracks of this nature, in the bottom web gap of the positive moment region, were found to be most likely to occur in a bridge configuration with staggered cross frames in the study by Hartman et al. (2010). If a segment of bridge girder between two adjacent cross-frames of a full bridge model is considered (Fig. 6), the ends of the girder segment are pulled by cross-frames in one direction while the middle of the segment is pulled in the opposite direction by the staggered cross-frame (Hartman et al. 2010). The simply-supported model used in this study behaved in a similar manner. Each end of the girder segment was restrained from out-of-plane motion while the center of the girder segment was pulled in the out-of-plane direction by the simulated cross-frame forces. For the evaluation of three different repair techniques, cracks of pre-defined length were placed in the bottom web gap.

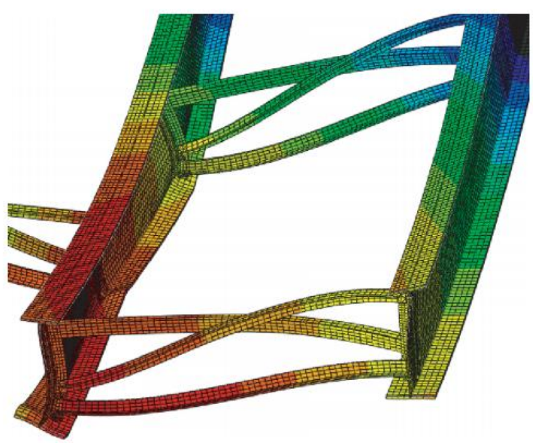

Figure 6: Schematic of staggered cross-frame bridge configuration (Hartman et al. 2010)

Repair Methods Evaluated

Currently, the use of crack-stop holes is a common method to repair fatigue damage in older steel girder bridges that experience distortion induced fatigue damage. As previously discussed, expressions like Eq. 1 were derived based on experimental data from fatigue specimens subjected to fracture mode 1 displacements. To gain a better understanding of the effect of crack-stop holes on the potential for crack re-initiation under the stress conditions in the web gap region, models with pre-defined cracks and various crack-stop hole diameters were evaluated. A test matrix for all models with crack-stop holes is presented in Table 2. Those models listed in Table 2 that do not have a crack-stop hole are the un-retrofitted cracked models which were used as basis of comparison between different repair methods. The reduction in stress demand for each repair method was calculated based on the maximum HSS demand extracted from each of the models.

Expressions to calculate the minimum crack-stop hole diameter such as Eq. 1 were developed based on tensile fatigue tests, therefore, an evaluation of the effect of crack-stop hole diameter on stress demand was also performed using a girder web under pure tension loading. The girder web dimensions were consistent with those shown in Fig. 2 and 3. The left end of the girder was restrained against translational motion while a distributed load of 207 MPa (30 ksi) was applied to the other end, placing the web in pure tension. Both a horse-shoe shaped crack and a straight vertical crack were tested under pure tension for completeness, however, only one crack geometry was evaluated per model. Fig. 7 shows boundary conditions, crack locations, and loading for models tested under pure tension loading.

Table 2: Test matrix for models testing effect of crack-stop holes

	Crack Size Hole Diameter mm (in.)					
	None	12 ($^1/_2$)	19 ($^3/_4$)	25 (1.0)	51 (2.0)	102 (4.0)
Horse-Shoe Crack 1/4 depth of web Combined Loading	x	x	x	x	x	
Horse-Shoe Crack 1/8 depth of web Combined Loading	x	x	x	x	x	
Horse-Shoe Crack 1/4 depth of web Pure Tension Loading	x		x		x	x
Straight Crack 1/4 depth of web Pure Tension Loading	x		x		x	x

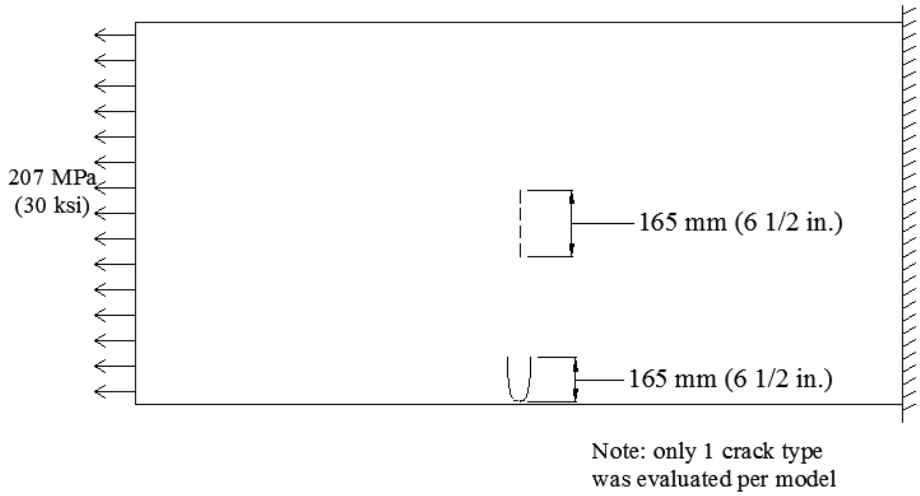

Figure 7: Boundary conditions and loading for models evaluating effect of crack-stop holes under pure tension loading

The second repair method evaluated was the attachment of 13-mm ($^1/_2$-in.) thick steel splice plates along the full depth of the girder, as shown in Fig. 8. Because crack-stop holes are an accepted and widely used fatigue repair technique, the system included the drilling of a 19-mm ($^3/_4$-in.) crack-stop hole in the web at each tip of the fatigue crack. Two splice plates measuring 127 x 1473 mm (5.0 by 58.0 in.) were attached to the interior side of the web, one on each side of the stiffener. Because there was no transverse stiffener on the opposite side of the web, a single splice plate measuring 283 x 1473 mm (11.1 x 58.0 in.) was attached there. Each splice plate was terminated at a distance of 25 mm (1.0 in.) from the adjacent flange to prevent the splice plate from restraining the motion of the flange. Splice plates were attached using high-strength 19-mm ($^3/_4$-in.) tensioned bolts spaced at 102 mm (4.0 in.). The horizontal spacing of bolts is shown in Fig. 8. Each bolt was tensioned to 125 kN (28 kip) following the stipulations in ASSHTO Table 6.13.2.8-1 (ASSHTO, 2010). When attached to the web, the steel splice plates completely covered all the fatigue damage, except for the initiation site. They also covered the area where any further crack propagation would occur, making inspection impossible without removal and reattachment of the repair.

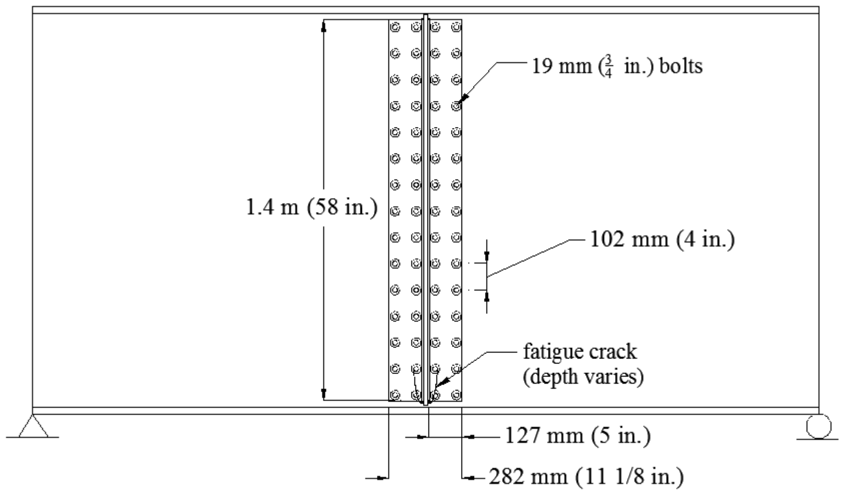

Figure 8: Full-depth splice plate fatigue damage repair

The CFRP repair assemblage evaluated in this study was created to be representative of fabrication methods under field conditions. The use of CFRP overlays to repair fatigue damage in steel structures has not been widely tested on full-scale models. Research at the University of Kansas has evaluated the use of adhesively bonded CFRP overlays to reduce the fatigue-crack propagation rate in tensile specimens with pre-existing fatigue cracks (Alemdar 2011; Gangel 2012). The experiments showed that for a given stress range, an optimized thickness could be found for the CFRP overlay based on the ratio of the axial stiffness of the CFRP overlay to the axial stiffness of the underlying steel. Because the stress demand in the web gap region is difficult to define and because an additional steel plate was used over the CFRP to prevent debonding of the repair, an optimized thickness for the CFRP overlay could not be determined based on the previous experimental research. Although the results were not directly comparable, they did provide a useful frame of reference. Based on the observed performance of the tensile specimens with overlays (Alemdar 2011; Gangel 2012) a CFRP overlay thickness of 6 mm (0.25 in.) was adopted in this study.

As with the full-depth splice plate repair, the system included the drilling of a 19-mm ($^3/_4$-in.) crack-stop hole in the web at each tip of the fatigue crack. The assemblage then consisted of a 6-mm ($^1/_4$-in.) thick CFRP overlay adhesively bonded to the web. A 13-mm ($^1/_4$-in.) steel cover plate covering the CFRP overlay was bolted to the web, as shown in Fig. 12, to provide a uniform compression force on the overlay and prevent debonding under cyclic loading. 19-mm (3/4 in.) bolts were used to bolt the steel cover plate. Each bolt was tensioned to 125 kN

(28 kips) following the stipulations in ASSHTO Table 6.13.2.8-1 (ASSHTO, 2010). A 13-mm ($^1/_2$ -in.) thick cover plate was chosen because the thickness was sufficient to evenly distribute the force from the tensioned bolts without damaging the CFRP overlays. A very thin steel cover plate could result in an uneven distribution of the bolt force, damaging the CFRP layer and greatly decreasing the effectiveness of the repair. The adhesive bond layer between the steel and CFRP overlay was a 0.6-mm (25-mil) resin layer

Dimensions of both the CFRP overlay and steel cover plate (Fig. 10 and 11) were chosen as 127 x 267 mm (5.0 x 10.5 in.). A repair system of this size would cover a large portion of the damaged web and the region with the highest stress demand. If for any reason the repair would not perform adequately and allowed crack re-initiation to occur, this type of repair would allow increased fatigue damage to be detected during inspection. A repair of this size was placed on each side of the welded stiffener on the interior face of the web. On the opposite side of the web, the repair system consisted of a single CFRP overlay and cover plate with dimensions of 267 x 283 mm (10.5 x 11.1 in.).

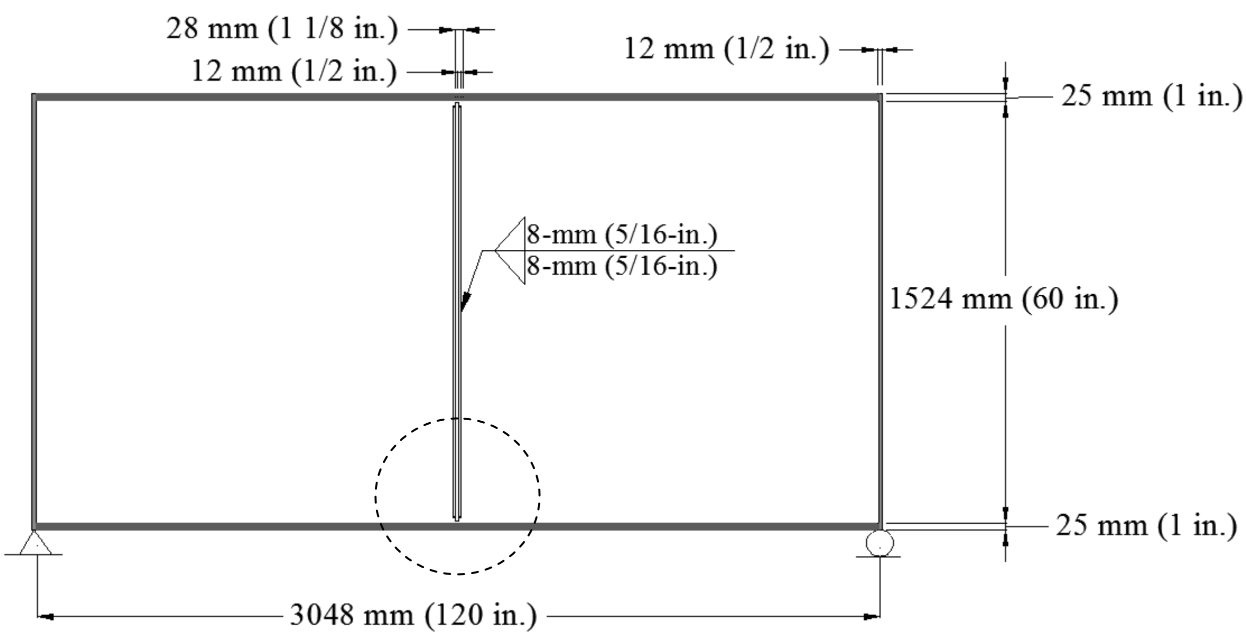

Figure 9: Circled region shows area of probable fatigue damage and repair

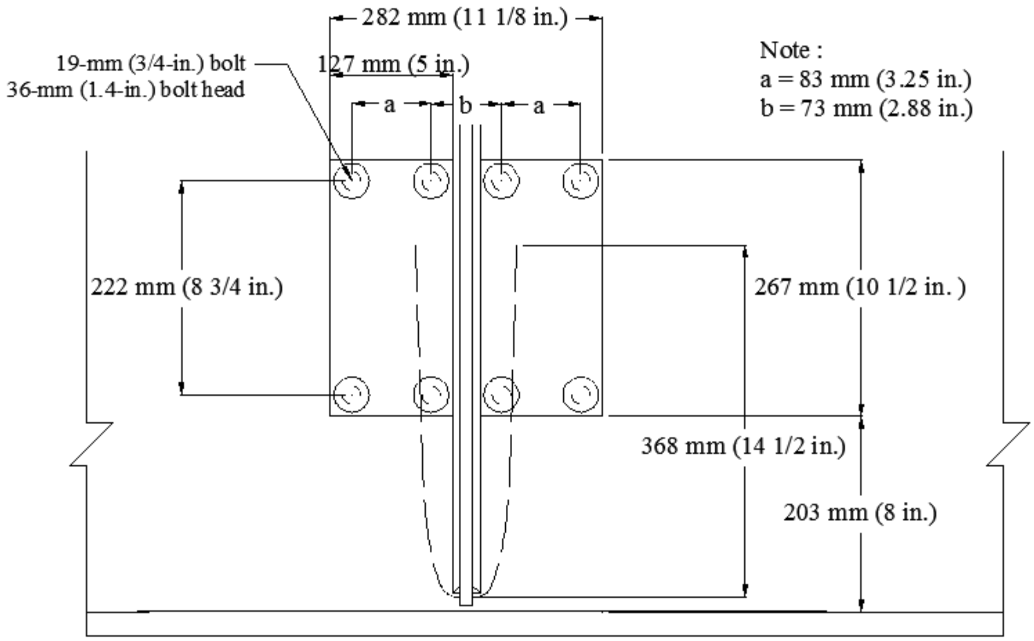

Figure 10: Repair dimensions for crack length equal to ¼ of the web depth

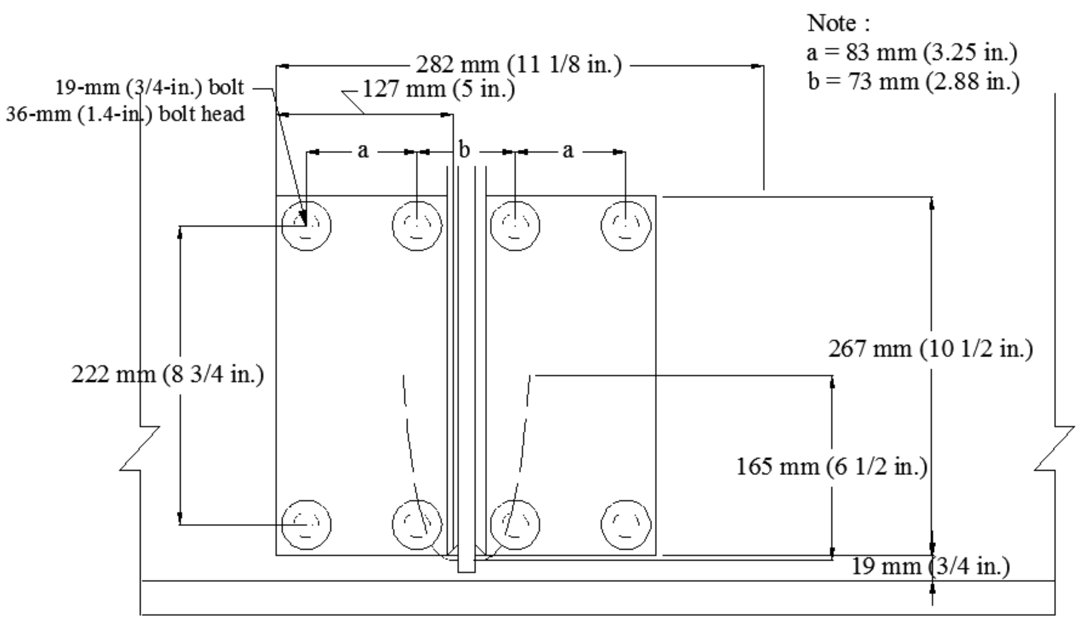

Figure 11: Repair dimensions for crack length equal to $^1/_8$ of the web depth

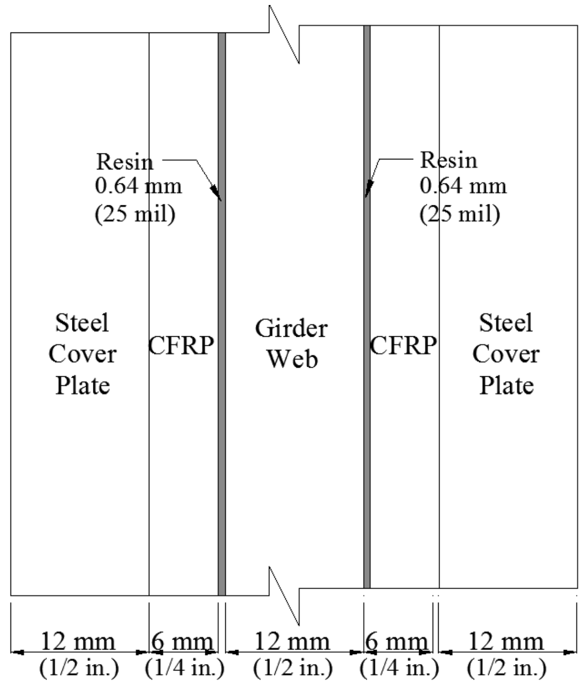

Figure 12: Cross section of CFRP repair

Finite Element Modeling

The Finite Element (FE) models of the segment of bridge girder developed in ABAQUS v6.10.2 (Simulia 2008) and discussed above were used to evaluate the expected performance of the three repair methods. The model remained linear-elastic and was constructed using three-dimensional elements. Meshes were assembled using 8-node brick elements for the majority of the model, except near regions of fatigue cracking, crack-stop holes, and bolt holes. In these regions a sweep mesh was used to encompass the geometric discontinuities. Each layer of resin, CFRP, and steel cover plate was meshed completely using a sweep mesh. In each model all edges of the girder web were seeded using a uniform size of 6 mm ($^1/_4$ in.). A 25-mm (1-in.) region of tetrahedral meshing was used to transition between sweep and structured meshing in the web. Fatigue cracks were modeled by removing part of the web via cuts and extrudes. The XFEM modeling technique was not used in this part of the study. Instead, fatigue cracks were created by cutting away the web material.

As with previous models, all parts of the girder section that were composed of steel were modeled with a modulus of elasticity of 200 GPa (29,000 ksi) and Poisson's ratio of 0.3. The same material properties were used for both the steel splice and cover plates. Resin layers were modeled with a modulus of elasticity of 207 MPa (300 ksi) and CFRP layers with a modulus of elasticity of 82 GPa (12,000 ksi), each with Poisson's ratios of 0.1. Parts were attached using surface-to-surface tie constraints. Only the weld attaching the connection stiffener to the web was modeled explicitly. A mesh size of 5 mm (0.2 in.) was used for the weld and its material properties matched those of other steel parts. Boundary conditions for these models were consistent with those described previously.

Material characterization tests of CFRP overlays used in the experimental studies showed large scatter in the modulus of elasticity of the CFRP, and a dependency between the modulus of elasticity and the number of plies used in fabricating the CFRP coupons (Alemdar 2011). For this reason, two additional models were produced with modulus of elasticity 25% above and below the modulus of elasticity of CFRP modulus specified above. This produced models with moduli of elasticity of CFRP of 103 GPa (15,000 ksi) and 62 GPa (9,000 ksi).

Hot Spot Stress Analysis

The Hot Spot Stress method was again used to compare and evaluate the reduction in stress demands associated with each of the three fatigue damage repair methods. However, the Hot Spot Stress paths used in this evaluation were different than those discussed previously. The introduction of a fatigue crack into the girder section created two regions of high stress demand, as will be discussed further in the following sections.

The first region of high stress demand occurred near the tip of the crack or the top outside edge of the crack-stop hole on the web face, where crack re-initiation would be most likely to occur. At this location a horizontal path was defined either 6 mm ($^1/_4$ in.) from the tip of the fatigue crack or 6 mm ($^1/_4$ in.) from the outermost edge of the crack- stop hole, depending on whether the model included a crack-stop hole. The maximum principal stress extracted from this path was designated HSS#3. Reductions in HSS#3 were adopted as an indicator of the effectiveness of the various repair techniques.

The second region of high stress demand occurred in the bottom web gap region at the point of maximum curvature in the horse-shoe shaped crack. This is the location at which crack initiation is expected to occur and where a crack of Type 1 (Fig. 1) would be expected to initiate. A path was defined at a distance of 6 mm ($^1/_4$ in.) from the curved edge of the fatigue crack. The maximum principal stress demand extracted from this path was designated HSS#4. HSS#3 and HSS#4 were determined on both the interior and fascia surfaces of the web.

The extraction of the HSS was complicated by the sweep type mesh used in critical regions. Sweep meshes do not produce a horizontal path at the desired location from which a maximum principal tensile stress could be determined. It was for this reason that HSS#4 (Fig. 13) was extracted from a curved path, because the sweep mesh in this region did produce a fairly uniform curve around the fatigue crack. HSS#3 (Fig 13) was extracted from points located closest to a horizontal line located at 6 mm ($^1/_4$ in.) from the tip of the crack or edge of the crack-stop hole. Although this resulted in a somewhat uneven path, stress magnitudes in the critical locations of high stress demands were available at the desired distance from either the end of the crack or edge of the crack-stop hole. If no points were available near the intended location of the extraction path, the magnitude of the tensile principal stress was interpolated at the desired location from two adjacent paths. Results for the reduction in HSS#3 and HSS#4 are reported for all repairs, however, HSS#3 is the most important to this study as it indicates the potential for crack re-initation and further damage.

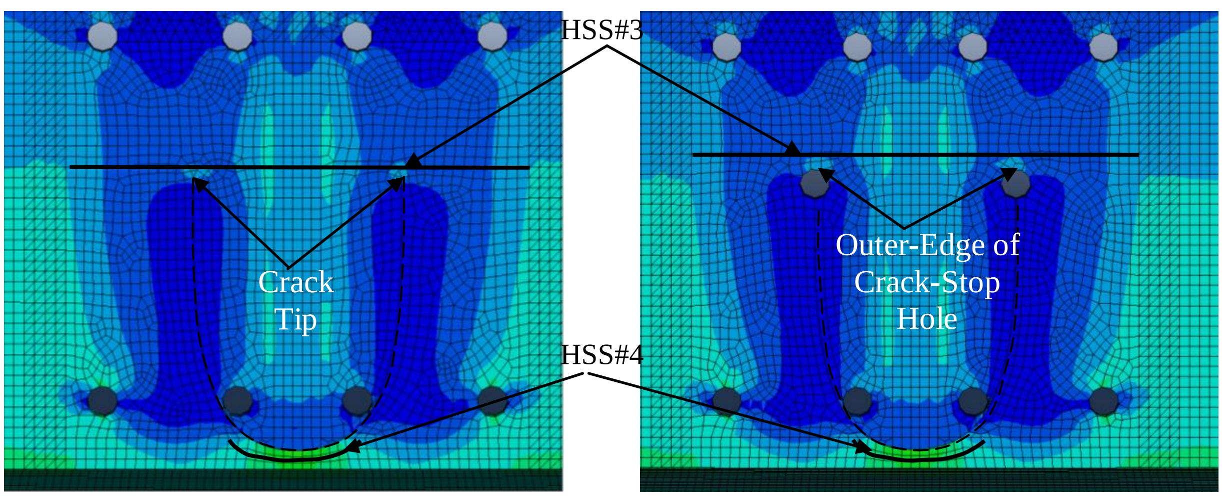

Figure 13: Hot spot stress paths used to evaluate fatigue damage repair methods

Results

Evaluation of Crack-Stop Holes

In the un-retrofitted base models without crack-stop holes listed in Table 1, large maximum tensile principal stress demands were observed at four separate locations near the crack. The regions where high maximum stress demands were observed were consistent in all models regardless of crack length. The first region of high stress demands was located in the girder web, at the tips of each end of the crack, on the interior side of the web where the connection stiffener was welded (Fig. 14). High stress demands at this location were expected because of the sharp discontinuity imposed by the tip of the crack (Barsom and Rolfe 1999). On the fascia side of the girder, high stress demands were also found in the web, at each tip of the crack. The main difference between the stress field at the two critical locations was that at the former the high stress demands were localized in the vicinity of the crack tips, and at the latter the high stress demands were not localized and were instead spread along the length of the web, between the two legs of the crack (Fig. 14). The difference in stress distribution between the two faces of the girder can be attributed to the placement of the connection stiffener, which stiffens the interior face of the web and reduces stress demands in that region. Both of these stress demands were captured by the HSS#3. The third and fourth peak stress locations occurred on both faces of the web in the web gap region, as shown in Fig. 14. The high stress demands at locations 3 and 4 were caused by the combined effects of geometric discontinuities and bending stresses induced in the web gap by the cross frame. These areas of high demand were captured by HSS#4.

While crack-stop holes greatly increase the radius of the crack tip, and should consequently reduce the stress demand at that point (Barsom and Rolfe 1999), the evaluations in this study indicated that in the web gap region the presence of crack-stop holes did not have a significant effect on the maximum stress demands for diameters lower than 51 mm (2.0 in.). The use of a 19-mm (3/4-in.) crack-stop hole resulted in small reductions in HSS#3 and HSS#4, as shown in Fig. 15a and 15b, compared to other retrofit techniques. Even for the model with a 51-mm (2.0-in.) crack-stop hole, the only meaningful reduction in stress demand occurred on the interior side of the web, at the crack tips, as shown in Fig. 15c. The high stress demands at all other critical locations remained unchanged or decreased by a small amount. The introduction of a 51-mm (2.0-in.) crack-stop hole at the tip of the crack with a length equal to $^{1}/_{8}$ of the girder depth resulted in reductions in HSS#3 of approximately 17% on the interior face of the web and 12% on fascia side of the web. With the deeper crack, propagating $^{1}/_{4}$ of the depth of the web, the 51-mm (2.0-in.) crack-stop hole resulted in higher reductions in peak stress demand (40% and 27% on the interior side and fascia side of the web, respectively). While the magnitude of HSS #3 did in fact decrease with the introduction of a large crack-stop hole, the area of high stress demands on the fascia side of the web increased greatly as the diameter of the crack-stop hole increased (Figs. 15b and 15d). There was no reduction in HSS#4 observed in models with either crack length.

Models subjected to tensile loading also had large maximum principal stress demands at each tip of the crack. For models with a horse shoe shaped crack, high stress demands were found in the same four regions discussed for models under combined loading. As shown in Fig. 16 the introduction of crack-stop holes did not significantly reduce or alter the stress distribution near the cracked region. High stress demands were still present, even when the crack-stop hole diameter was increased to 102 mm (4.0 in.), a diameter much larger than what could be practically drilled in the field. With this size of crack-stop hole drilled at the tip of the horse shoe shaped crack, HSS#3 decreased by approximately 12% while HSS#4 actually increased by approximately 18%, indicating that drilling large crack-stop holes in the web gap region may have detrimental effects. For a straight crack subjected to pure tension, the condition for which Eq. 1 was intended, the reduction in peak stress demand was approximately 8% for a 102-mm (4.0-in.) crack-stop hole.

Based on the results from all the FE models with crack-stop holes it is concluded that while drilling of crack-stop holes may be effective in reducing the peak demand at the tip of the crack by removing damaged material from the fracture process zone, this type of repair is not effective in mitigating stress demands induced by out-of-plane forces in web gap regions, and should be used in combination with other retrofit measures intended to reduce large stress demands induced by geometric discontinuities in the web gap region. Because the primary benefits of drilling crack-stop holes are the removal of the sharp crack tip and fracture process zone, the drilling of large-diameter crack-stop holes is unjustified, and was shown to be detrimental in some instances.

Evaluation of full-depth steel splice plates

Repairing the girder web with full depth steel splice plates did provide an alternate load path and reduce HSS#3 demands on both sides of the web, as shown in Fig. 17. Effectiveness of this repair method also increased as the length of the crack increased from $^1/_8$ of the depth of the web to $^1/_4$ of the depth of the web. Reductions in HSS#3 for the model with the shorter crack length were 56% and 78% on the interior and fascia side of the web, respectively. When the crack length was increased to $^1/_4$ of the depth of the web, larger reductions in HSS#3 of 77% and 89% on interior and fascia side of the web, respectively, were observed. Reductions in stress demands of this magnitude are a positive indicator that the potential for crack re-initiation is greatly reduced when this repair method is implemented. Stress reductions in HSS#4 of approximately 30% were found on the interior side of the web for both crack lengths; however, the magnitude of HSS#4 actually increased on fascia side of the girder for both crack lengths.

Evaluation of CFRP overlay and steel plate retrofit measure

The use of adhesively bonded CFRP overlays in combination with a 19-mm (3/4-in.) crack-stop hole and bolted steel cover plates showed drastic reductions in stress in the cracked region of the web when compared with simulation results from un-retrofitted models, models repaired with crack-stop holes, and models repaired with full-depth splice plates (Fig. 18).

With a crack length equal to $^1/_8$ of the depth of the web, the introduction of the CFRP steel plate repair measure decreased HSS#3 by 83% and 92% on the interior and fascia sides of the web, respectively. Decreases in HSS#4 were 59% and 23% on the interior and fascia sides of the web, respectively. Of all the repair methods evaluated, this was the only one that produced a significant decrease in HSS#4. The use of a resin layer between the steel web and the CFRP layer was shown to be effective in transferring the high stress demands in the web gap to the CFRP and the steel plate. Bonding the CFRP layer had the effect of distributing the stress over the entire area covered by the repair, eliminating the presence of small regions with highly concentrated stress demands. This smoothing effect is the main benefit of this retrofit measure with respect to the others discussed.

The FE model with a crack length 1/4 the depth of the web and the CFRP repair also showed positive results. HSS#3 decreased by 95% and 96% on the interior and fascia side of the web, respectively. The reduction in HSS#4 was not as significant as in the case of the shorter crack configuration because the CFRP overlay and steel plates only covered approximately 50% of the length of the horseshoe-shaped crack. These results suggest that the effective crack length, defined as the length of crack not covered by the retrofit measure, seems to be a driving factor in the magnitude of the reduction in HSS#4. For this reason, an additional CFRP retrofit configuration was evaluated for the model with the longer crack (1/4 depth) so that the CFRP and steel plates covered the majority of the crack. In this extended configuration, shown in Fig. 19, the length of all layers of the retrofit assemblage was increased from 267 mm (10.5 in.) to 444 mm (17.5 in.). The increased dimensions of this retrofit measure made the effective crack length approximately equal for the two crack configurations evaluated. A comparison between the calculated stress demands for the models with a crack length equal to 1/4 of the depth of the girder showed that HSS#4 on the interior side of the web was 43% lower for the configuration with the shorter overlays and 61% lower for the configuration with the longer overlays. On the fascia of the web, the reductions in HSS#4 were 7% for the model with the shorter overlays and 33% for the model with the longer overlays. These results are consistent with the results from the models with the full-depth splice plate repair in that if the effective crack length was kept approximately constant, the effectiveness of the repair increased as the crack length increased. The decrease in stress demand produced by each retrofit method is shown in Fig. 20.

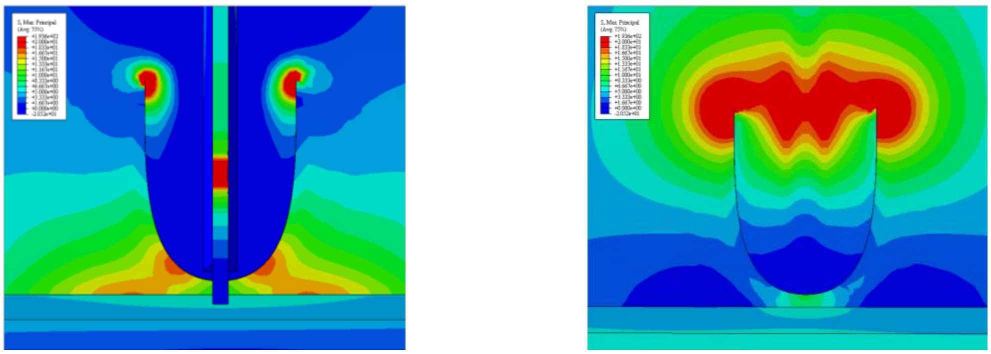

(a) No retrofit – interior **(b) No retrofit – fascia**

Figure 14: Maximum principal tension stresses in unrepaired models

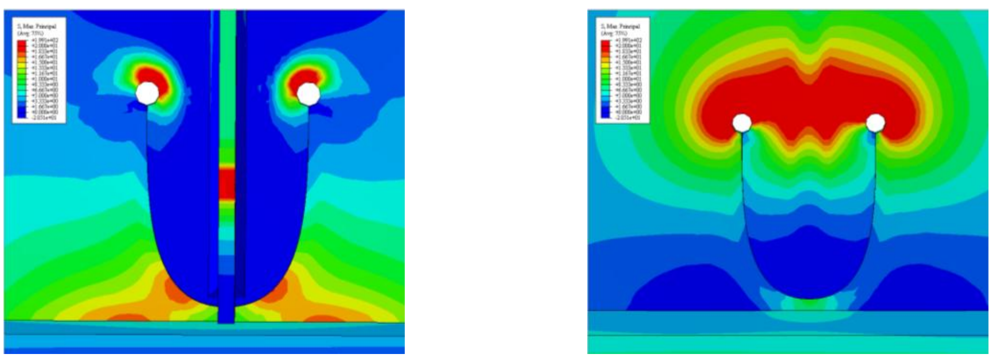

(a) 19-mm (0.75-in.) CSH– interior **(b) 19-mm (0.75-in.) CSH– fascia**

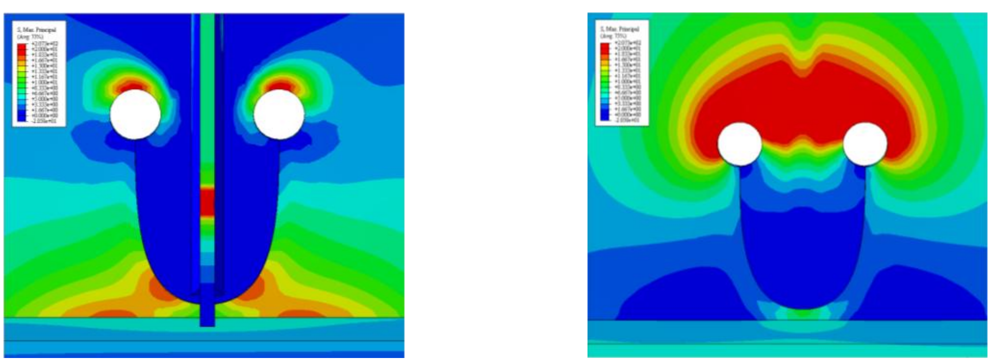

(c) 51-mm (2.0-in.) CSH – interior **(d) 51-mm (2.0-in.) CSH – fascia**

Figure 15: Maximum principal tension stresses in models repaired with crack-stop holes under combined loading conditions

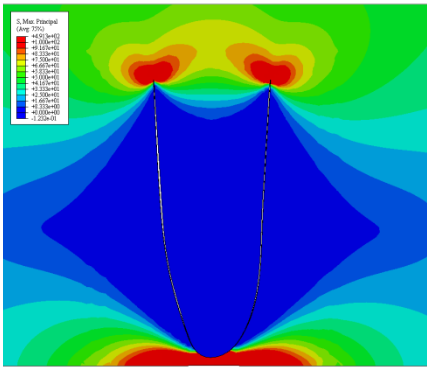

(a) Tension loading – no retrofit

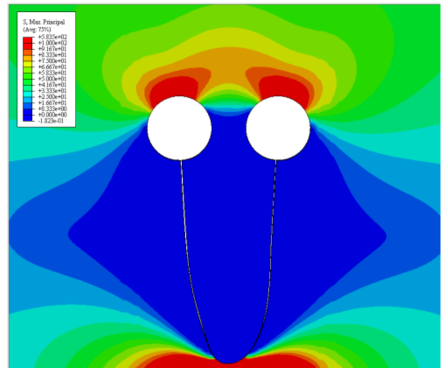

(b) Tension loading – 102-mm (4.0-in.) CSH

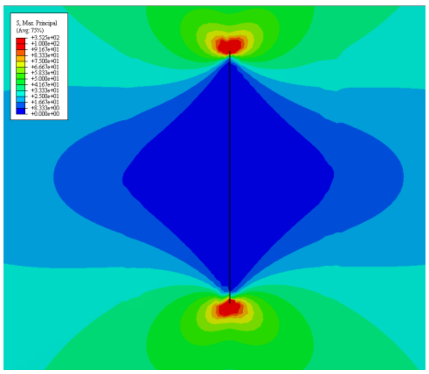

(c) Tension loading – no retrofit

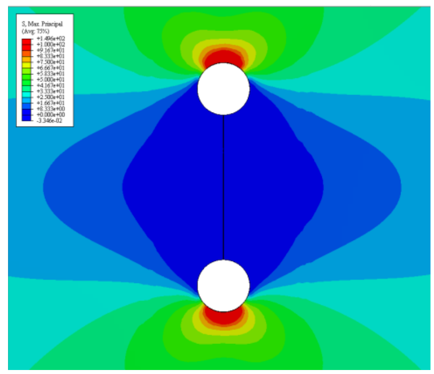

(d) Tension loading – 102-mm (4.0-in.) CSH

Figure 16: Maximum principal tension stresses in models repaired with crack-stop holes under pure tension loading conditions

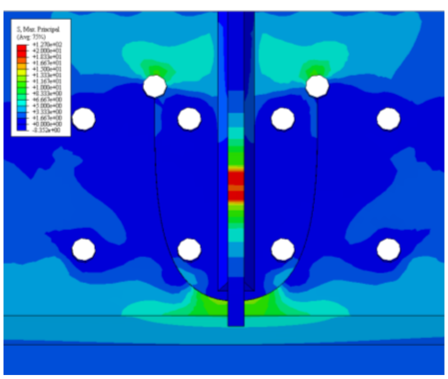

(a) Full-depth splice plate –interior

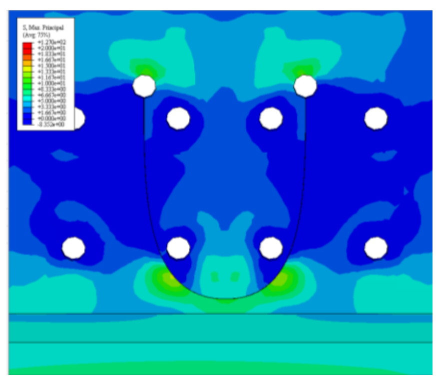

(b) Full-depth splice plate –fascia

Figure 17: Maximum principal tension stresses in models repaired with full-depth splice plate

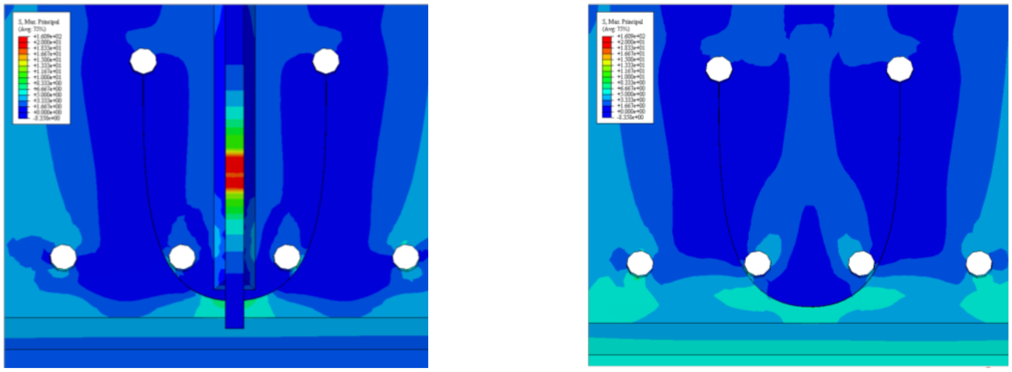

(a) CFRP retrofit system – interior (b) CFRP retrofit system – fascia

Figure 18: Maximum principal tension stresses in model repaired with CFRP

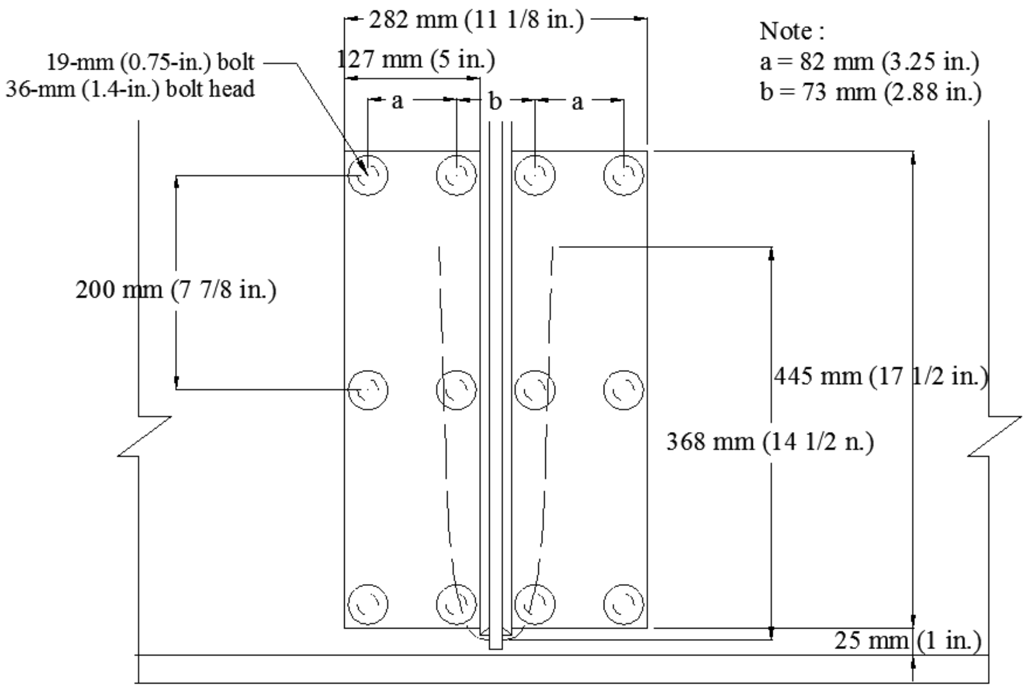

Figure 19: CFRP repair measure with increased length of repair

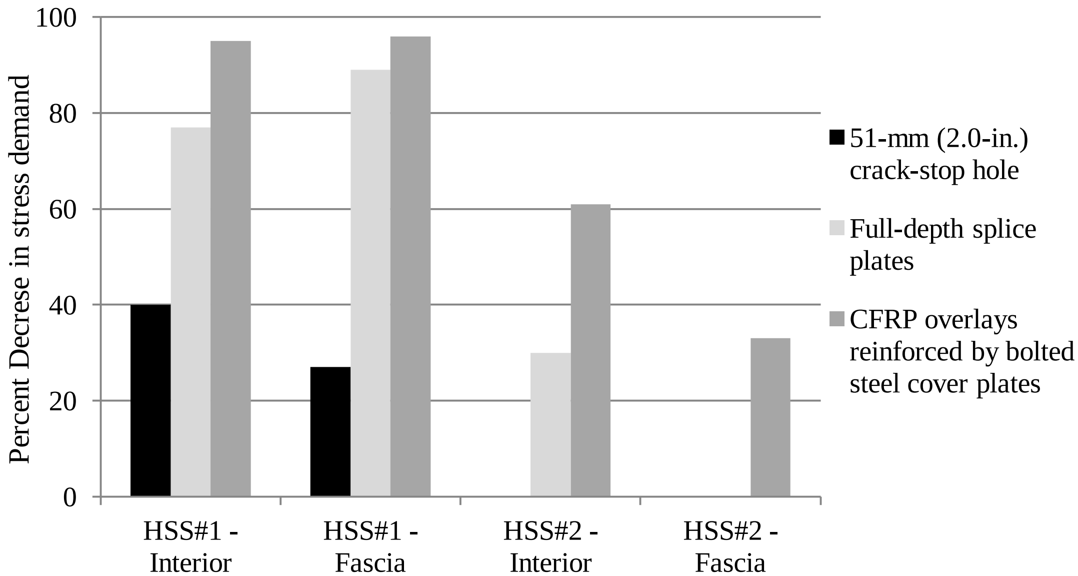

(a)

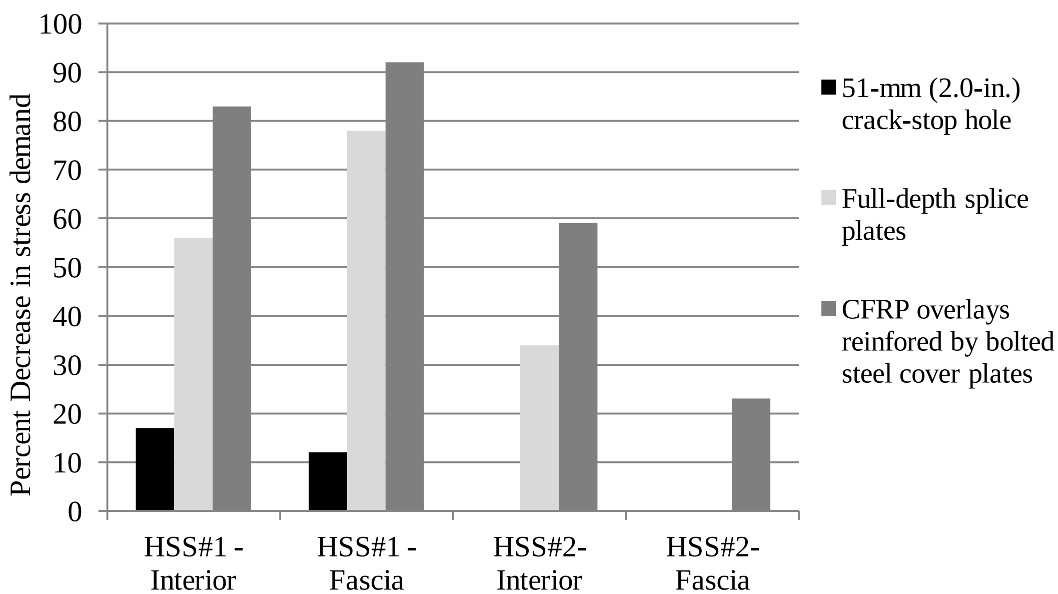

(b)

Figure 20: Comparison of decrease in stress demand for model with crack length equal to (a) 1/4 the depth of the web and (b) 1/8 the depth of the web

As discussed in the section on finite element modeling, the modulus of elasticity of the CFRP was varied as a parameter because previous research has shown that the stiffness of the CFRP may have a significant effect on the effectiveness of the repair (Alemdar 2011). For the range of elastic moduli and overlay thickness evaluated in this study it was found that changes in the modulus of elasticity of the CFRP did not have a significant effect on HSS#3 nor HSS#4.

This behavior can be attributed to the fact that the layer of CFRP was relatively thin compared with the thickness of the web and the steel cover plates, causing the stiffness of the repair to be dominated by the steel.

The increased effectiveness of the CFRP repair with respect to the bolted splice-plate repair can be attributed to the bond provided by the layer of resin used to attach the CFRP overlay to the web. This layer introduces an alternate load path which allows stresses to transfer between the two sides of the fatigue crack through shear. If bond is lost between the web and the CFRP overlay at localized areas of high peel or shear stress demand the repair is designed to remain effective due to the effect of the tensioned bolts, which are intended to limit the amount of debonding. Although the compression force is likely to keep the overlay in place, it is also possible that the effectiveness of the repair could decrease as a consequence of partial debonding of the overlay. This type of behavior is very difficult to evaluate through computer simulations and should be quantified through physical simulations.

Within the resin layer, the highest shear stress demand in the vertical direction was found to take place at the corner adjacent to the bottom flange and opposite the connection stiffener, where the greatest geometric discontinuity occurs. In the horizontal direction, the largest shear stress demands were found to follow the path of the existing fatigue where the relative motion between the two faces of the fatigue crack is restrained by the repair. Further analytical and physical testing is needed to determine if the shear stress demand at the critical locations in the resin layer is high enough to cause de-bonding of the CFRP. As previously discussed, the compressive stress imposed by the bolts is intended to limit the potential for debonding of the CFRP overlay. Another measure that could reduce the potential for debonding is the fabrication of resin pools extending beyond the edges of the CFRP overlays, which would allow a more gradual transition of stresses by staggering the geometric discontinuities induced by the edge of the overlay and the edge of the resin layer. This technique was shown to drastically increase the number of cycles prior to debonding in three-point bending tests (Kaan et al. 2012).

Conclusions

The effect of in-plane bending and out-of-plane cross-frame forces on the potential for distortion-induced fatigue damage in the web gap region of steel girders was studied, and the following conclusions were drawn:

- As the angle between the cross-frame force and the horizontal increased, the magnitude of maximum principal tensile stress at the connection stiffener-to-web weld and web-to-flange weld (HSS#1 and HSS#2 respectively) decreased. The highest stress demands were found when the cross-frame force was placed parallel to the horizontal.
- As longitudinal bending stress in the top flange increased from 35 MPa to 138 MPa (5 ksi to 20 ksi), magnitudes of HSS#1 and HSS#2 were greatly increased, indicating that in girder segments away from inflection points the potential for fatigue damage is expected to increase as the ratio of live to dead load increases.
- For models in which the gravity load was small relative to the cross-frame load, the highest stress demand was found in the top web gap, on the interior side of the girder. For models in which the stress fluctuations induced by live loads were significant and the cross-frame forces negligible, the highest stress demand was found in the bottom web gap, on fascia side of the web.
- In bridges for which the stress fluctuations due to bending and out-of-plane forces were both significant, the location of maximum stress demand was found to be similar to the case in which the effect of cross-frame forces was negligible, signifying that the potential for fatigue damage was most sensitive to fluctuations in in-plane stress due to live loads that produce bending.

Three different methods to repair severe fatigue damage were evaluated: drilling of crack-stop holes, attaching full-depth steel splice plates, and attaching of CFRP-steel plate assemblages. The effectiveness of the three methods was quantified in terms of the maximum principal stress demands and the following conclusions were made:

- Crack-stop holes implemented as the only repair method were deemed to be ineffective in preventing crack re-initiation regardless of crack length.
- Bolted full-depth splice plates were effective in reducing the magnitude of HSS#3. The maximum stress was reduced by 78% for models with a crack length of $^{1}/_{8}$ the depth of the web and by 89% for models with a crack length of $^{1}/_{4}$ of the depth of the web. The change in the magnitude of HSS#4 for either crack length was negligible.

- The CFRP-steel plate retrofit measure resulted in the greatest reductions in stress demand. The magnitude of HSS#3 was reduced by 92% for a crack length of $^{1}/_{8}$ of the depth of the web and 96% for a crack length of $^{1}/_{4}$ of the depth of the web.
- The CFRP-steel plate repair resulted in the most significant reduction of HSS# 4 with a maximum reduction of 61% was found.
- The effectiveness of the retrofit measure increased with the length of the crack for both the full-depth bolted splice plate and the CFRP-steel plate repairs.

Three methods to repair distortion-induced fatigue damage were evaluated through computer simulations. Of the methods evaluated the most effective was found to be the CFRP-steel plate assemblage. The reduction of stress demands in the web caused by this type of repair is attributed to both the increased stiffness of the strengthened cross section and the transfer of shear stresses through the resin layer. Because the transfer of stresses through the resin layer is of critical importance to the effectiveness of this repair method, more analytical and physical testing is recommended to evaluate the susceptibility this type of repair to debonding. However, the use of CFRP overlays to repair fatigue damage in steel bridge girders has great potential and can be an asset to the field of bridge engineering.

References

AASHTO 2010. “AASHTO-LRFD Bridge Design Specifications: 5th." *American Association of State Highway and Transportation Officials (AASHTO)*, Washington D.C.

Alemdar, F. (2011). "Repair of bridge steel girders damaged by distortion-induced fatigue," thesis, presented to University of Kansas, at Lawrence, KS, in partial fulfillment of the requirments for the degree of Doctor of Philosophy in Civil Engineering.

Barsom, J.M., and Rolfe, S.T. (1999). “Fatigue and fracture behavior of welded components.” Fracture and Fatigue Control in Structures, 3rd ed., (10), American Society for Testing and Materials, West Conshohocken, PA, 35-53.

Denney, J.J., and Mall, S. (1997). “Characterization of disband effects on fatigue crack growth behavior in aluminum plate with bonded composite patch.” *Engineering Fracture Mechanics*, 57(5), 507-525.

Fisher, J. W. and Mertz, D. R. (1984). “Fatigue and Fracture in Steel Bridges.” *The Conference on Bridges*, Pittsburgh, PA, 10-21.

Gangel, R.E. (2012). “Use of CFRP Overlays to Repair Fatigue Damage in Steel Bridge Girders and Components,” thesis presented to University of Kansas, at Lawrence, KS, in partial fulfillment of the requirements for the degree of Master of Science in Civil Engineering.

Hassel, H.L. (2011). "An analytical evaluation of distortion-indiced fatigue in steel bridges," thesis, presented to University of Kansas, at Lawrence, KS, in partial fulfilment of the requirements for the degree of Master of Science in Civil Engineering.

Hartman, A., Hassel, H., Adams, C., Bennett, C., Matamoros, A., and Rolfe, S. (2010). “Effects of Cross-Frame Placement and Skew on Distortion-Induced Fatigue in Steel Bridges.” *Transportation Research Record* (TRR), 2200, 62-68.

Kaan, B.N., Alemdar, F., Bennett, C.R., Matamoros, A., Barrett-Gonzalez, R., and Rolfe, S. (2012). "Fatigue enchancement of welded details in steel bridges using CFRP overlay elements". *Journal of Composites for Construction,* in press.

Liu, H. B., Al-Mahaidi, R., and Zhao, X.L. (2009). "Experimental study of fatigue crack growth behaviour in adhesively reinforced steel structures." *Composite Structures,* 90(1), 12-20.

Mall, S., and Conley, D.S. (2009). "Modeling and validation of composite patch repair to cracked thick and thin metallic panels." *Composites Part A: Applied Science and Manufacturing,* 40(9), 1331-1339.

Roddis, W. M., and Zhao, Y. (2003). “Finite-Element analysis of steel bridge distortion induced fatigue.” *Journal of Bridge Engineering,* 8(5), 259-266.

Roddis, W. M., and Zhao, Y. (2001). "Out-of-Plane Fatigue Cracking in Welded Steel Bridges: why it happened and how it will be reapired." *Welding Inovation,* 27(2) , 2-7

Sabelkin, V., Mall, S., Hansen, M.A., Vandawaker, R.M., and Derriso, M. (2007). “Investigation into cracked aluminum plate repaired with bonded composite patch.” *Composite Structures,* 79(1), 55-66.

Zhou, Y., and Biegalski, A.E. (2010) “Investigation of large web fractures of welded steel plate girder bridge.” *Journal of Bridge Engineering,* 15(4), 373-383.

APPENDIX A: MANUFACTURE AND ATTACHMENT OF CFRP DOUBLERS

A.1 RELEVANCE

The following procedure is the procedure developed at the University of Kansas to manufacture carbon fiber reinforced polymer (CFRP) patches and adhesively bond them to steel component specimens. This procedure will need to be altered slightly if the specimen the CFRP doublers are being attached to changes. The following procedure can only be followed step for step when the CFRP doublers are being attached to component specimens.

A.2 SAFETY PRECAUTIONS

Many of the chemicals used in the composites lab are carcinogenic and teratogenic. The Hysol resin used in the following procedure should be treated as both; therefore, it is EXTREMELY IMPORTANT for everyone, especially women, to follow these safety measures when working in the lab.

1. Protecting rubber gloves must be wore at all times during the manufacture and attachment of CFRP doublers.
2. Hands must be washed thoroughly whenever gloves are removed… then repeat washing
3. When cutting the cured CFRP doublers a face mask should be wore to protect against airborne carbon particles.
4. Safety goggles must be worn when cutting the cured CFRP doublers and the entire time the CFRP doublers are being attached.
5. Protective lab coats should be worn while CFRP doublers are being attached to avoid chemicals coming into contact with skin and clothes.
6. DO NOT TOUCH HYSOL RESIN and never rub eyes or face when you have been working with this chemical.

A.3 MANUFACTURE OF CFRP DOUBLERS

1. Determine number of CFRP single plies and Scotch-Weld Epoxy adhesive bond layers needed to manufacture the CFRP doublers.
    a. Two single ply doublers are needed for every 1.6 mm (0.0625 in) of CFRP doubler thickness.

b. Place Scotch-Weld Epoxy adhesive layers evenly throughout thickness of doubler. Once adhesive layer is needed at least every fourth layer, or more frequently for thinner doublers.

2. Cut CFRP and Scotch-Weld Epoxy adhesive layers into 508 x 152.4 mm (20 x 6 in) strips. These measurements will make two doublers, one for each side of the steel specimen. They will be cut in half after curing.
3. Carefully stack CFRP and Scotch-Weld Epoxy adhesive layers into desired configuration on top of steel plate of the mold, shown in Figure A.1. Try to line up edges of all layers as much as possible.

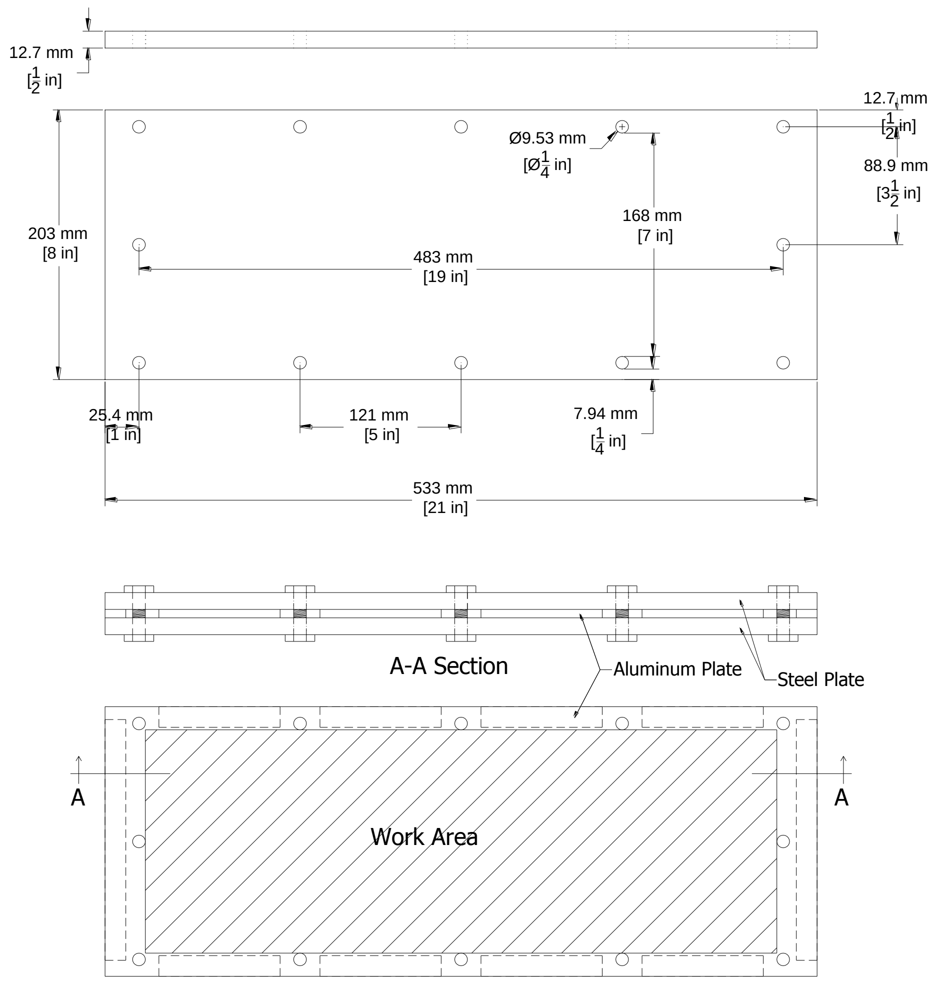

Figure A.1 : Steel plates for making CFRP doubler

4. Place second steel plate of mold on top of CFRP layers.

5. Place ten aluminum spacers between the two steel plates to give doublers desired and uniform thickness.
6. Clamp the steel mold to the table and tighter the bolts around the perimeter.
7. Remove the clamps. Place the mold under load and tighten the bolts fully until target thickness is reached.
8. Preheat curing oven to 175 C (347 F).
9. Place mold in curing oven for three hours.
10. Remove mold from curing oven and cool to room temperature for 48 hours.
11. After 48 hours of curing, remove CFRP doublers from mold.
12. Cut to final dimensions of 457 x 64 mm (18 x 2.5 in) using a diamond saw.
13. Rinse doublers to remove any loose carbon. Pat dry.
14. Check for compactness. There should be no visible voids between the individual plies.
15. Smooth all edges with grade 400 sand paper.

A.4 ATTACHMENT OF CFRP DOUBLERS

1. Roughen the each surface of the steel specimen with a hand grinder to achieve a surface roughness of approximately 0.8 mm (30 mils).
2. If the specimen name or other label information is present near the grips, cover the area with painter’s tape to protect the labels.
3. Take one doubler and place a long strip of painters tape along each edge of the doubler so that it overhangs about an inch (Note: If a thick steel specimen is being used in combination with a thick CFRP overlay the tape may need to be doubled to create a longer overhang length).

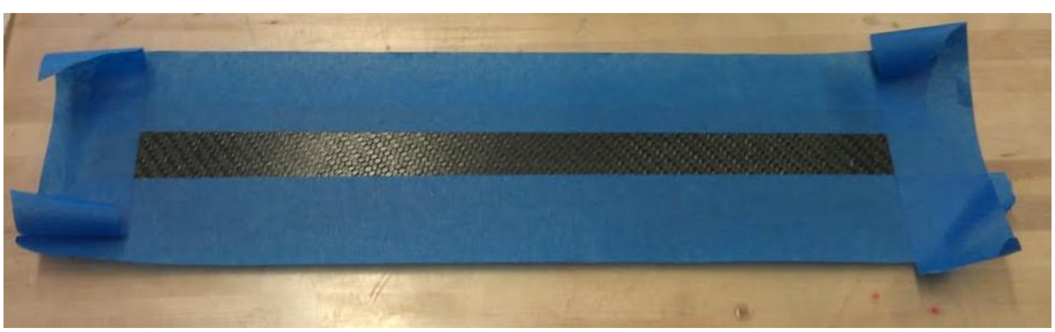

Figure A.2: Tape Overhang

4. Press the tape up along each edge to create a barrier or bowl shape.

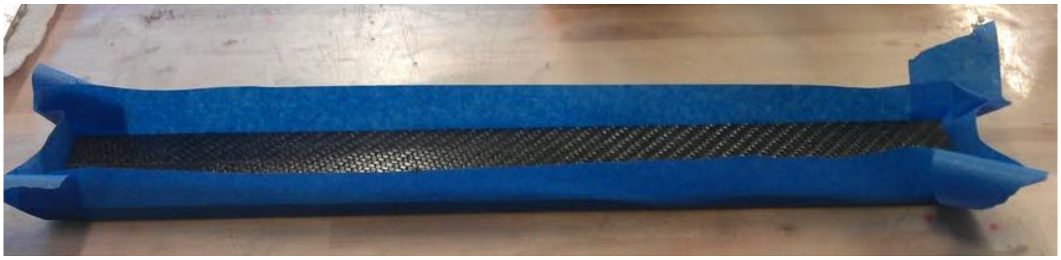

Figure A.3: Tape Barrier

5. Take other doubler and completely cover one longitudinal face with painter's tape. Do not create an overhang.
6. Lay the doubler prepared in step 3 on an elevated block like the one shown in Figure A.4. The barrier or bowl shape should be facing upward as shown in Figure A.3 .

Figure A.4: Elevated block

7. Clean steel thoroughly with Acetone and paper towels. Repeat cleaning process with Methanol and paper towels.
8. Clean side of each doubler that will be bonded to the steel with methanol and paper towels.
9. In cup mix Hysol resin.
    a. Put cup on scale and zero out.
    b. Scoop approximately 120 g of Hysol resin into cup.
    c. Multiply exact weight of Hysol resin by 1.25 to get total mass.
    d. Add the activating liquid until total mass is reached.
10. Thoroughly mix resin and activating liquid.
11. Place six 2-56 (25 mils) washers along the length of the CFRP doubler. These act as spacers so the thickness of the resin layer stays consistent.

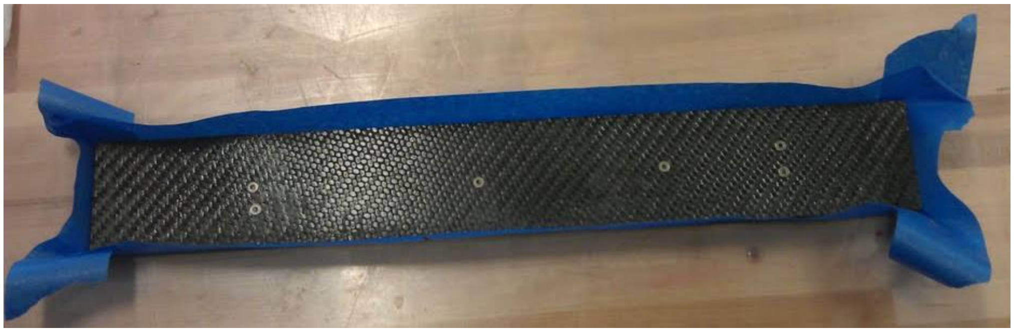

Figure A.5: Placement of spacers to control thickness of resin layer

12. Pour a layer of resin onto doubler. Use a tool with a flat edge to spread resin to edges of doubler. Make sure entire doubler face is covered.
13. Lay steel specimen on top of doubler so that the center of the steel specimen lines us with the center of the doubler.
14. Fold piece of painter’s tape around end of steel specimen to prevent Hysol resin from spilling out.
15. Place six 2-56 (25 mils) washers along the length of the steel specimen. These act as spacers so the thickness of the resin layer stays consistent.
16. Pour another layer of resin on top of steel. Use a tool with a flat edge to spread resin to edges of doubler. Make sure entire face of the steel specimen is covered.
17. Place second doubler on top of steel, painter’s tape side up.
18. Fold tape overhangs from bottom doubler up around both the steel and the second doubler to create barrier for the ysol resin.
19. Take a 2x2 block of wood and cover one face with painter’s tape.
20. Place the block on top of the specimen, tape side down.
21. Clamp entire system with four c clamps or bar clamps.
22. Leave remaining resin mixture in cup as an indicator of when resin has hardened
23. Clean up all materials used.
24. Allow resin to cure for 48 hours minimum.
25. Once clamps and tape have been removed, perform final preparation by removing remnant resin with a chisel and heat gun.

APPENDIX B: PROCEDURAL DOCUMENTATION FOR MTS TESTING MACHINE

B.1 RELEVANCE

The MTS testing machine was used to initiate and propagate fatigue cracks in all steel component specimens. The following is a step-by-step procedural document explaining how to use the MTS as it was used in this application. It includes how to determine the proper testing load, how to create and run a testing program, and important precautions to protect the test specimen.

B.2 DETERMINATION OF APPLIED LOAD

For this application, the applied load was determined based on the desired nominal stress range at the net cross section of the specimen. The net cross-section should be based on the actual (measured) dimensions of the specimen. The applied load was not adjusted as the cross-section was reduced due to crack propagation.

B.3 STARTING STATION MANAGER

1. Open the station manager icon on the desktop.
2. Open station "TSIIs" in the menu that appears.
3. On the left hand side of the station display, select the "MPT" display if it does not appear automatically.

B.4 STARING PUMP AND PUTTING SPECIMEN IN MTS

1. **Turn on the pump BEFORE placing the specimen in the machine**. This is to avoid damaging the specimen should the displacement of the actuator adjust (kick) when the pump is turned on.
2. To turn on the pump, first place the pump under low pressure by pushing the button in Figure B.1 (b). Once the low pressure button stops flashing, turn the pump on high pressure using the button in Figure B.1(c).

a) No pressure b) low pressure c) high pressure

Figure B.1: MTS pressure stages

3. Unlock the station manager.

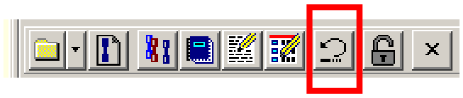

Figure B.2: Toggle execute/edit mode

4. Use the manual command (located under "station controls") to set the machine **DISPLACEMENT** so the specimen and pins fit properly. You may need to adjust it more than once (usually the starting position is about 0.1 in). Record this initial value. Do not use the slide adjustment.

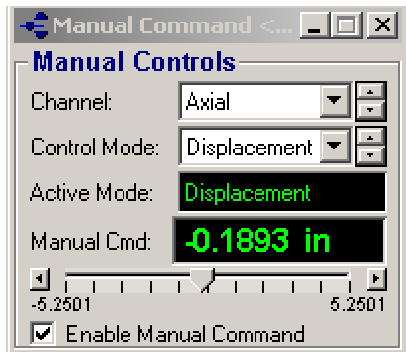

Figure B.3: Manual command

5. Once the specimen fits properly put both pins in place. Secure with a screw near the top and bottom pins.
6. Close manual command.

B.5 Creating Test Program

1. Select "New Specimen".

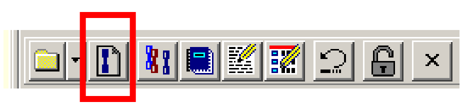

Figure B.4: New specimen

2. Name the specimen with name of specimen, test type, and stress range.
3. Open "Procedure Editor. The following is the procedure is standard for fatigue testing.

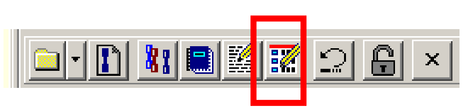

Figure B.5: Procedure Editor

   a. Ramp to 100 lb - Ramp to 0.1 kips (100 lbs) over 30 seconds.

b. Load Hold 1 – Hold load for 30 seconds.

c. Ramp to Ave Load - Ramp to half the maximum load over 30 seconds.

d. Hold Load 2 - Hold load for 30 seconds.

e. Cyclic Fatigue Testing - Oscillate between maximum and minimum load. Also set frequency.

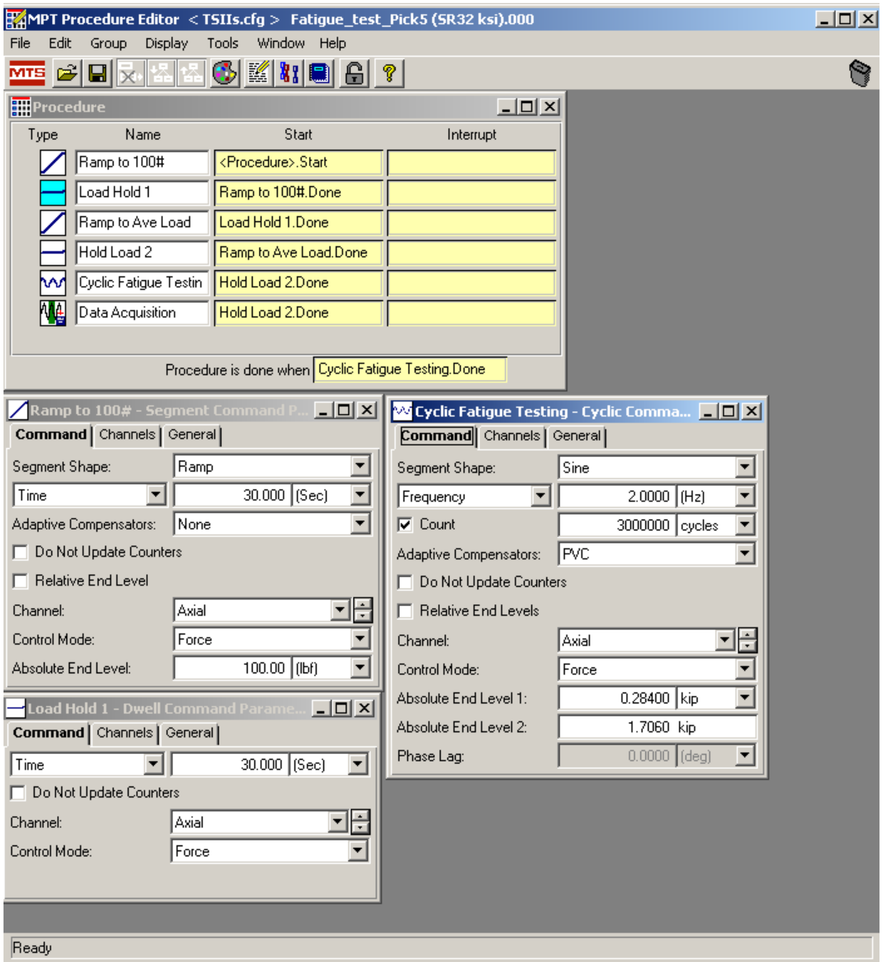

Figure B.6 Procedure editor and step examples

4. Save the procedure with the specimen name and stress range.
5. Lock the station manger using the toggle in Figure B.2.
6. To run the cyclic program, press the play button. If the test needs to be paused use the hold program button (pause button) instead of stopping the program. The program should only be stopped when the test is over or being suspended for long enough that the specimen will be removed and the pump will be turned off.

B.6 SET PROTECTION LIMITS

1. Once the test has begun to oscillate, open the detector.

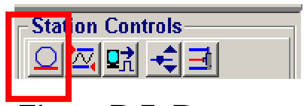

Figure B.7: Detectors

2. Change the upper axial displacement limit to 0.0127 mm (0.0005 in) above the current reading. The current reading will continue to drop and the limit will need to be readjusted as the current reading drops. Each time the limit is changed, select "disabled" as the upper action before changing the limit. When testing, the upper action should be set to "program interlock".

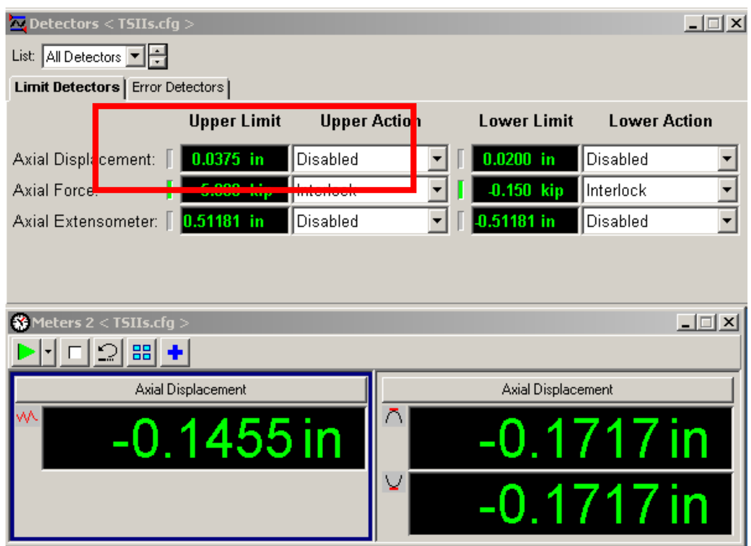

Figure B.8: Upper limit and action

3. For crack initiation – once this limit has been breached the crack has initiated.
4. For crack propagation – once this limit has been breached the crack is propagating. Increase the limit in 0.0127 mm (0.0005 in) increments until the desired crack length has been reached

B.7 TAKING SPECIMEN OUT OF MTS

1. Unlock the system.
2. Open up manual commands.
3. Change the DISPLACEMENT to the initial recorded value or take load to zero.
4. Take out screws and pins.

Appendix C: Procedural Documentation for Instron Testing Machine

C.1 Relevance

The Instron testing machine was used to test all steel component tests repaired with CFRP overlays. The following is a step-by-step procedural document explaining how to use the Instron as it was used in this application. It includes how to determine the proper testing load, how to create and run a testing program, and important precautions to protect the test specimen.

C.2 Determination of Applied Load

For this application, the applied load was determined based on the desired nominal stress range at the net cross section of the specimen. The net cross-section should be based on the actual (measured) dimensions of the specimen. The applied load was not adjusted as the cross-section was reduced due to crack propagation.

C.3 Starting WaveMaker Editor

4. Username: Falemdar Password: fa9631056
5. Open WaveMaker Editor icon on desktop.
6. Open Console icon on desktop.

C.4 Starting pump and Putting Specimen in instron

7. **Turn on the pump BEFORE placing the specimen in the machine**. This is to avoid damaging the specimen should the displacement of the actuator adjust (kick) when the pump is turned on.
8. The pump must be turned on from the computer connected to the MTS machine. To turn on the pump, first place the pump under low pressure by pushing the button in Figure B.1 (b). Once the low pressure button stops flashing, turn the pump on high pressure using the button in Figure B.1(c).

b) No pressure b) low pressure c) high pressure

Figure C.1: MTS pressure stages

9. Using the button shown in Figure C.2, apply low pressure to the Instron. This is an Instron control located near the actuator.

Figure C.2: Instron pressure and displacement

10. Open both the upper and lower clamp using the grip control located near the actuator.

Figure C.3: Grip controls

11. Use the course and fine manual displacement adjustment, shown in Figure C.2 (located to the right of the power/pressure control) to move the actuator so that both ends of the specimen fits within the two grip assemblies of the Instron. To adjust the displacement the actuator may need high pressure. If this seems to be the case give it high pressure using the bottom button on the pressure control shown in Figure C.2.
12. If specimen cannot fit between actuator heads properly using course adjustment, the height of the top grip assembly needs to be adjusted. To do this unlock the system (turn the knob to the right) and then open the valve to raise or lower the head using the controls shown in Figure C.4. Do not do this while a specimen is in the Instron. Take the

specimen out first as movement can be rapid. Close the valve to stop the head from moving and lock the system before continuing.

Figure C.4: Controls to adjust height of top head of actuator. Shown in closed positions

13. Make sure the center of the specimen grip is aligned with the center of the top Instron grip in both the longitudinal and transverse direction.
14. Close the top grip.
15. Adjust the actuator displacement until the bottom grip of the specimen is aligned with the bottom Instron grip. Do this slowly to protect the specimen. Use level to check the longitudinal placement if necessary. If the alignment is off the specimen will be damaged when the bottom grip is closed.
16. Close the bottom grip.

C.5 CREATING TEST PROGRAM

7. Create a file for the new specimen. Files for previous fatigue specimens can be found under Desktop-My Documents-WaveMaker File-tension spec.
8. Open files from a previous specimen given in the previous step to find a program file matching the desired testing stress range. Copy that file and transfer it into the file created for the new specimen.
9. Within WaveMaker Editor, open the transferred stress-range program file In WaveMaker. This will open a new window in WaveMaker Editor. Close all other windows within the program so only this one is open.

10. Select the portion of the testing sequence labeled “operator input”.

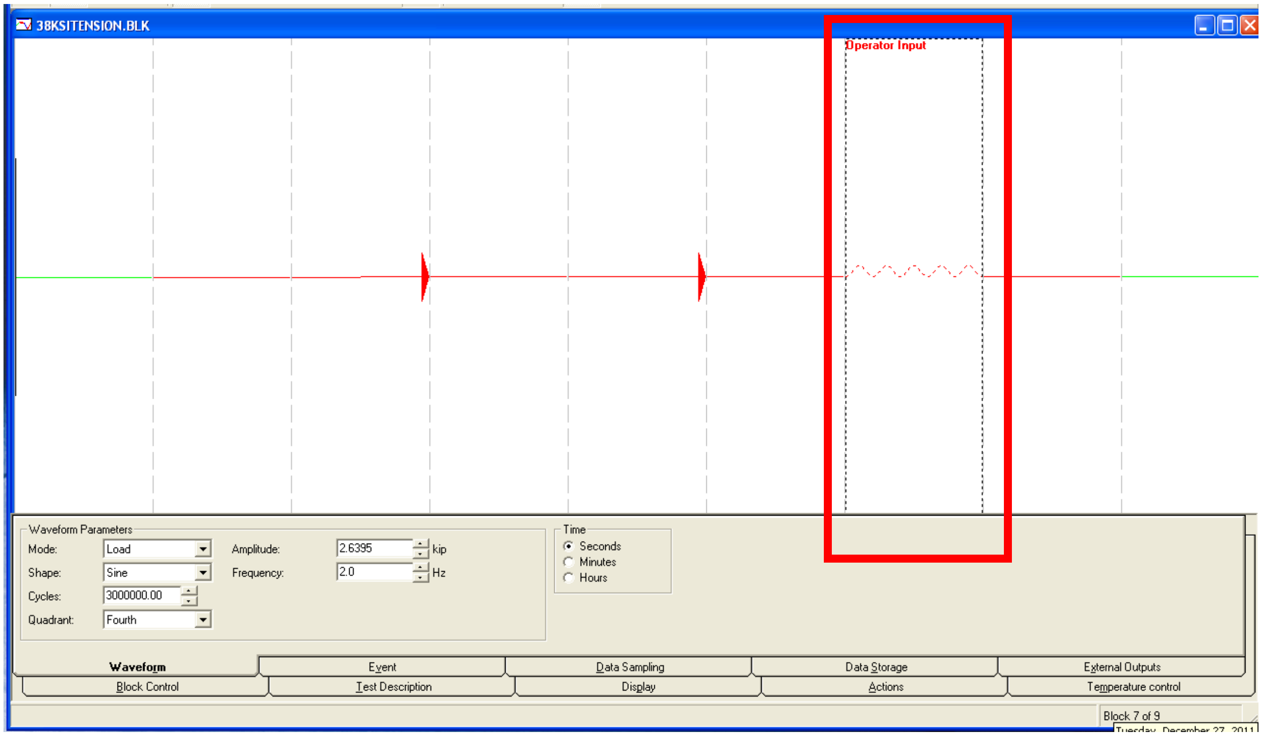

Figure C.5: Operator Input

11. Check and make necessary adjustments to the program using the tabs below the testing sequence screen. The following are the tabs that have been found to need adjustments:
    1. Waveform
        1. Mode: Load
        2. Shape: Sine
        3. Cycles: Adjust to cycle count when test should end (if you are unsure when you want the test to end set to a high value)
        4. Quadrant: 4^{th}
        5. Amplitude: Should be set for test range selected. Will equal half the maximum load determined
        6. Frequency: Set to desired frequency. 2 Hz was used most often
        7. Time: Seconds
    2. Data Sampling – Adjust sampling rate if desired. 1.0 kHz was used previously.
    3. Data Storage – Change the output file name to the name of the specimen and save to the storage file created for the specimen.

4. Test Description – Change to match accuate data for the specimen being tested.
5. In the testing sequence, select the green portion of the on the left side of the screen to make sure the test starts from the beginning. The portions in-between start and the operator input should be pre-set to ramp and hold the load in increments. If there are questions about whether these steps are correct check them against the same steps of the programs for specimens that have been tested previously.

C.6 Run Testing Program

5. In WaveMaker Editor, select the run button. If you are asked to save change, do so.

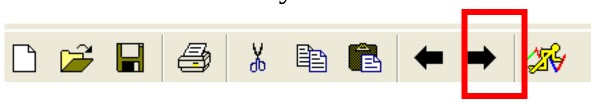

Figure C.6: Run Button

6. A new window containing the Instron WaveRunner program will open:

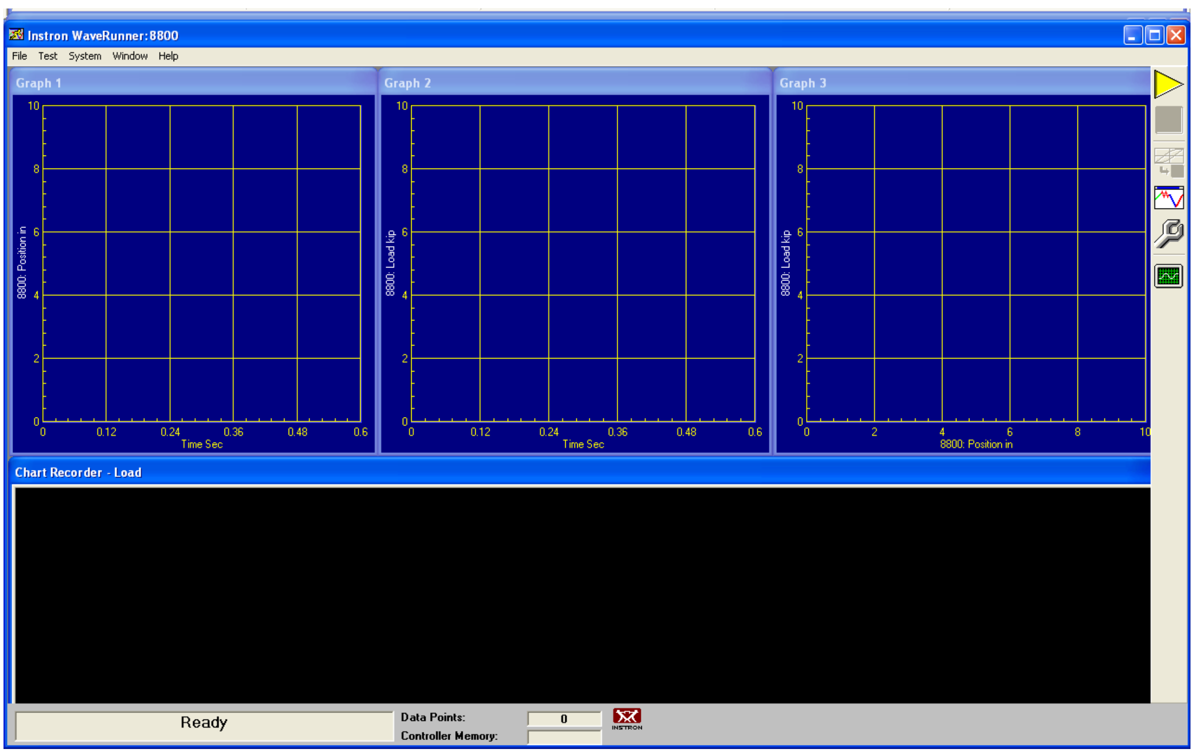

Figure C.7: Instron WaveRunner

7. Right Click in the Console Program:

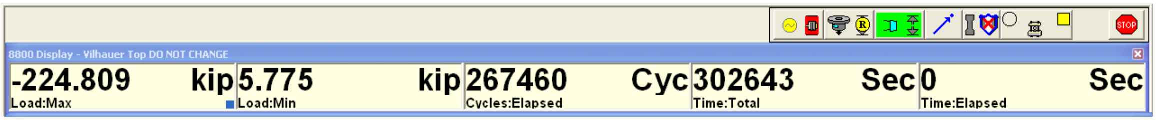

Figure C.8 Console Program

8. Select "open displays".
9. Open both "Vilhauer bottom DO NOT TOUCH" and "Vilhauer top DO NOT CHANGE". This will allow the test progression and specifics to be monitored during testing.
10. Start testing by selecting the "start test" button in WaveRunner. Pop-up screens will appear asking that information be verified and that the test may be run. Answer the pop-up screens accordingly.

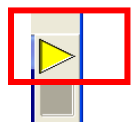

Figure C.9: Play button to begin testing

11. If the output file needs to be opened during testing to check specifics such as change in displacement, create a copy of the file and open that file. Never open the original output file during testing because the program will no longer write to the file and subsequent testing data will be lost.

C.7 TAKING SPECIMEN OUT OF INSTRON

5. Stop the program using the "stop test" button located below the "start test" button in WaveRunner, shown in Figure C.9.
6. Open the bottom grip.
7. Lower the bottom head of the actuator.
8. Open the top grip.
9. Remove specimen, actuator displacement may need to be adjusted until specimen can be taken out.

Appendix D: Creation of Clamps

D.1 Relevance

During the testing of specimen F20, significant debonding was observed near the top and bottom of the adhesively bonded CFRP overlays. Two clamps were created in order to negate the affect de-bonding might have on the fatigue life of the specimen during subsequent testing.

D.2 Attachment of clamps to steel specimen

Each clamp, as shown in Figure D.1, was created by placing an A36 steel plate measuring 19.1 mm (0.75 in) x 101.6 mm (4 in) x 228.6 mm (9 in) on either side of the adhesively bonded system. The plates were placed so that the bottom (or top) edge of the plate was flush with the bottom (or top) of the CFRP overlays and then extended 4 in over the overlays. This assured that the length affected by de-bonding would be completely covered by the steel plate.

Two A325 bolts were used to attach each clamp. The placement of the bolts is shown in Figure 1. Steel shims made of stacked steel scrap plate were used in-between the adhesively bonded system and the bolts to ensure excessive bending of the plates did not occur when the bolts were tightened. Each bolt was snug-tightened using an ordinary spud wrench before being tightened using an impact wrench until each bolt was fully tightened. After the creation and installation of the two comparable clamps, specimen F20 was placed back in the testing machine for subsequent testing.

Additional photos of the clamps placed on specimen F4-20 are shown in Figures D.2, D.3 and D.4.

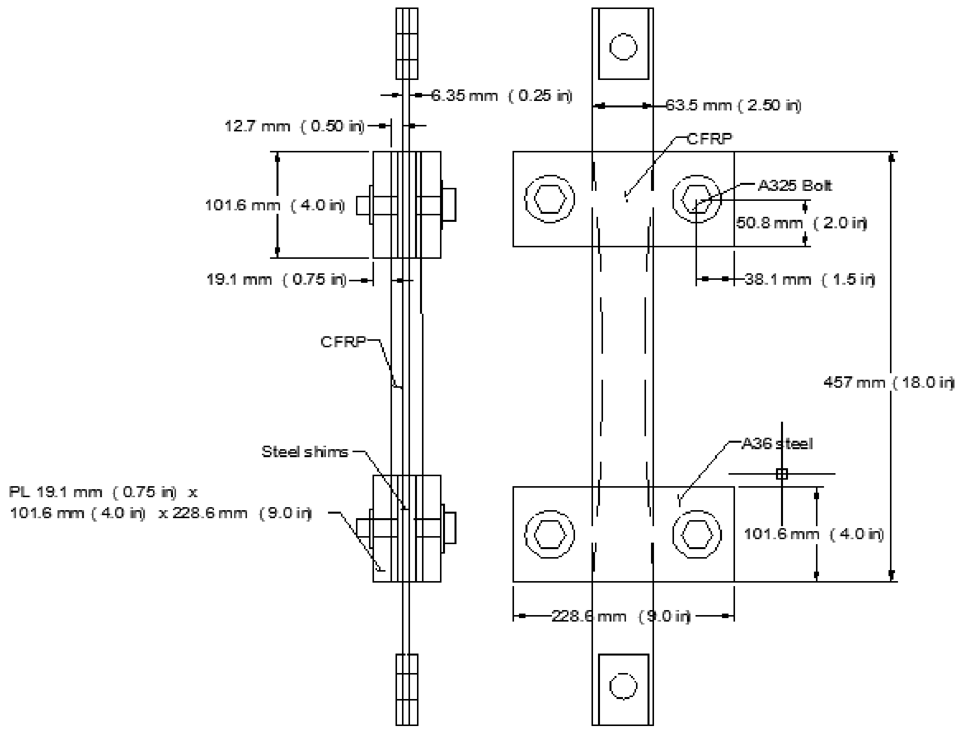

Figure D.1: Schematic of clamps created for specimen F20

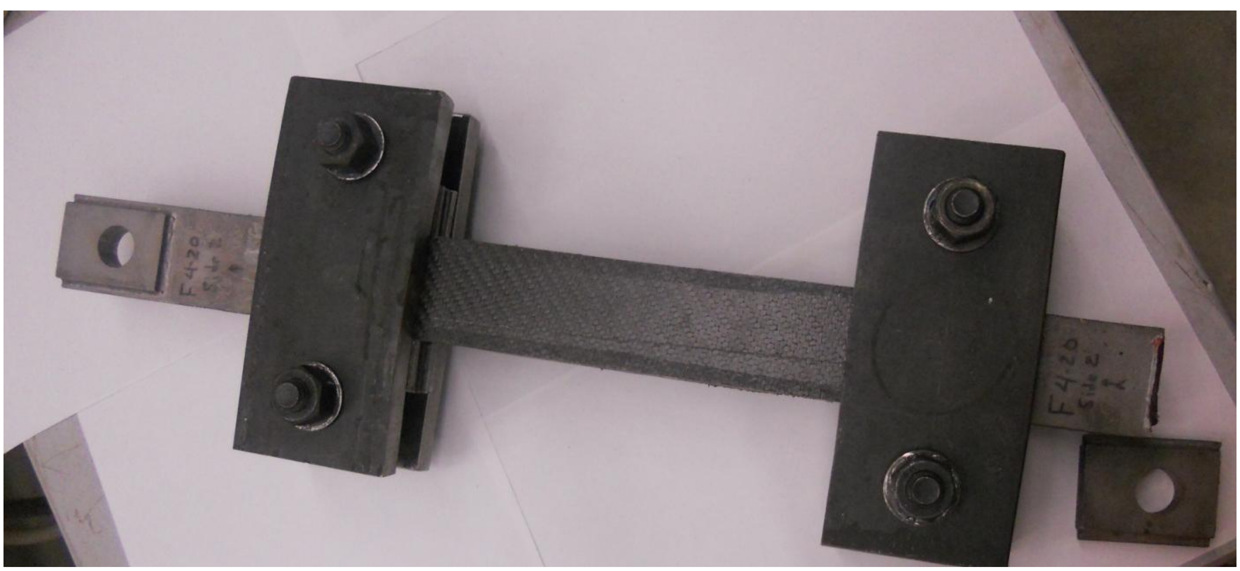

Figure D.2: Clamps placed on specimen F-20

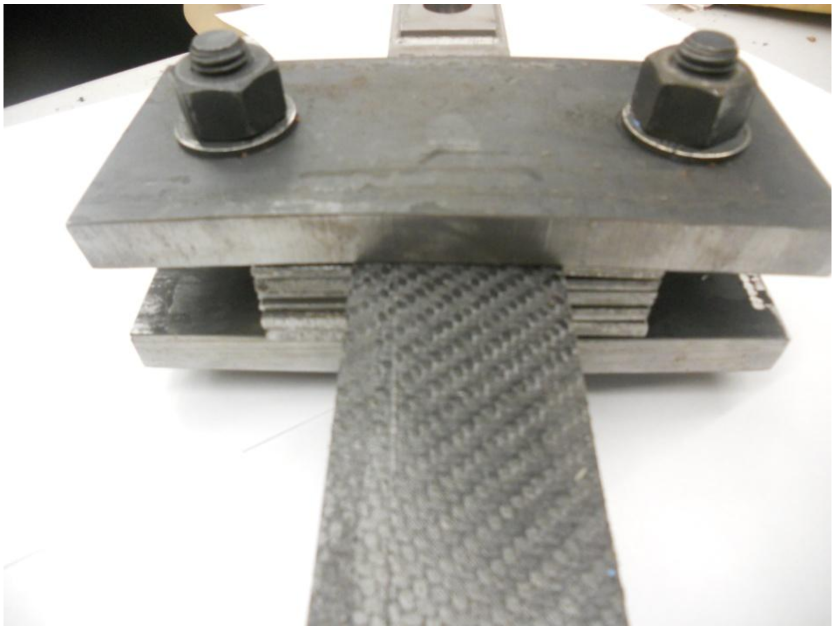

Figure D.3: Close-up of clamp and shims

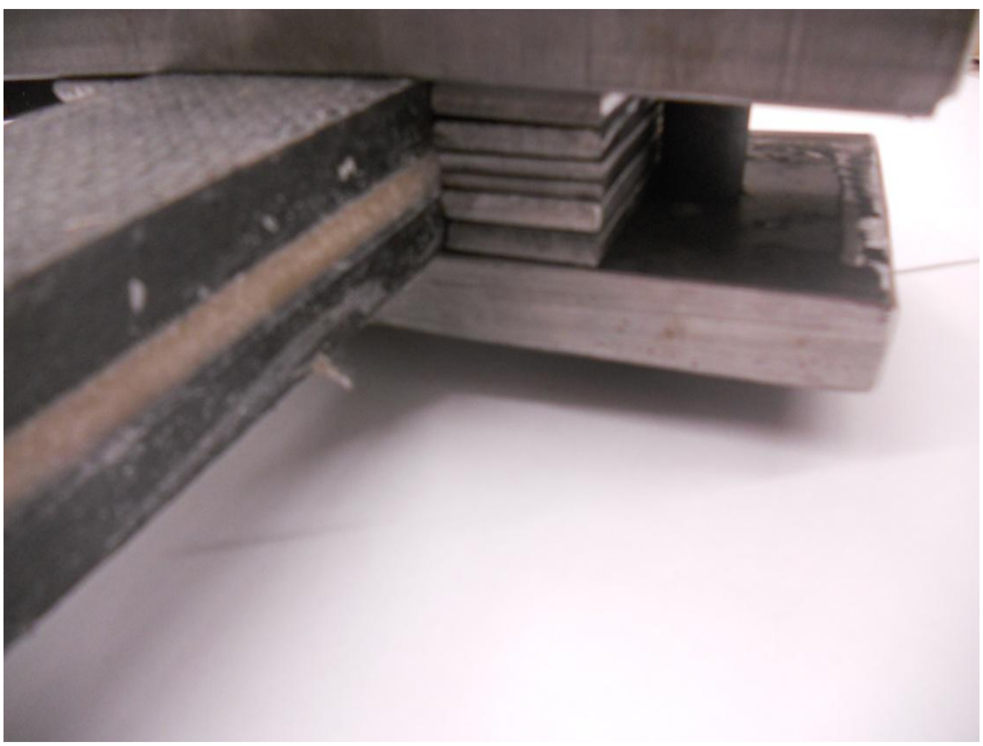

Figure D.4: Side view of specimen and clamp placement